Detecting and attributing recent warming in Europe

Irene Brox Nilsen

Thesis submitted for the degree of Philosophiae Doctor (PhD)

Department of Geosciences
Faculty of Mathematics and Natural Sciences

University of Oslo
Oslo, Norway

2017

Series of dissertations submitted to the
Faculty of Mathematics and Natural Sciences, University of Oslo
No. 1915

ISSN 1501-7710

Cover: Hanne Baadsgaard Utigard.
Print production: Reprosentralen, University of Oslo.

Abstract

Regional warming trends for Europe during the last decades have been larger than the global mean trend, especially on the seasonal scale. An improved understanding of hydroclimatic drivers of the warming is key to improve estimates of the energy balance and water balance terms. In addition to increased radiative forcing from greenhouse gases, the atmospheric circulation is the key driver of seasonal temperature trends in Europe. Of secondary importance are positive feedback mechanisms between the land surface and the atmosphere that enhance warming. For instance, partitioning of net radiation into latent and sensible heat is controlled by properties of the land surface, such as snow albedo and soil moisture content. In the first part of the thesis, monthly temperature trends and their physical drivers were explored by separating the change signal into circulation changes and other factors, so-called *within-type changes*, which may arise from local feedback mechanisms. This separation allowed identifying months and regions where temperature changes can mainly be attributed to circulation changes, and where within-type changes may also play a role. Using a novel probabilistic approach for statistical attribution, we showed that circulation changes could not account for all the observed warming in Europe over the period 1981–2010. Significant warming, such as the warming covering large parts of Europe in April, June–August, must also be caused by other factors. The second part of the thesis assessed two possible causes for this warming through a detailed study for Norway, where within-type changes were found to play a role in explaining the warming in April and July–September. This was done, first, by investigating the relationship between snow cover changes and monthly temperature trends for all of Norway (snow albedo feedback), and, second, by performing a diagnostic land surface model experiment testing the hypothesis that dry conditions may enhance the warming (soil moisture–temperature feedback). A significant decrease in snow cover was detected for most of Norway, accompanied by strong temperature trends, particularly in spring and at low elevations. Targeted model experiments with a coupled WRF–Noah-MP model for South Norway confirmed that the snow albedo feedback enhanced warming in spring, and showed that the soil moisture–temperature feedback could enhance warming during parts of the summer, provided that the soil moisture content was sufficiently low. This work has contributed to an improved understanding of the causes of recent temperature changes in Europe and Norway in particular, by assessing the relative role of circulation changes and within-type changes on regional-scale warming, through combining a statistical attribution approach and a physically-based modelling approach in a unique way.

Summary for the layperson

Europe has warmed faster than the rest of the globe during the last decades, especially when considering trends for each season separately. In addition to warming caused by greenhouse gas emissions, the atmospheric circulation is the key driver of seasonal warming in Europe. For example, westerly airflow tends to bring warmer weather in winter. Of secondary importance are climate feedbacks that may enhance warming locally. For example, snow reflects more sunlight than grass or bare ground. A retreating snow cover reveals a darker ground that allows more sunlight to be absorbed, and leaves more energy available for further melting and warming. This is the snow albedo feedback (albedo is a measure of reflectance). A different feedback, the soil moisture–temperature feedback, mainly acts during warm spells when the soil moisture may decrease to such low levels that evaporation is reduced. Since evaporation requires energy, less evaporation implies less cooling, and thus enhanced warming.

In the first part of the thesis, monthly temperature trends and their physical drivers were explored by separating the temperature trend signal into circulation changes (that is, variations in the occurrence of, for instance, westerly weather) and other factors (*within-type changes*). "Other factors" include local feedbacks enhancing the warming, but may also include warming due to greenhouse gas emissions. Note that this separation does not divide causes of warming into natural variability and anthropogenic forcing. To determine whether the warming could be attributed to circulation changes, we developed a novel statistical approach and applied it to temperature trends for Europe (Paper II). Circulation changes could not account for all the observed warming in Europe over the period 1981–2010. Therefore, other factors than circulation changes contributed; for instance, to the warming covering large parts of Europe in April, June–August. The second part of the thesis assessed the snow albedo feedback and the soil moisture–temperature feedback as possible causes of warming for Norway. Analyses over the past five decades showed strong decreases in snow mass at low elevations, accompanied by warming (Paper III). From Papers I–III, we chose South Norway as a focus region, in April and July–September, for a detailed model study because this region displayed potential for positive feedbacks (within-type changes). Last, we used a regional climate model to test the contributions of the snow albedo feedback and the soil moisture–temperature feedback (Paper IV). The snow albedo feedback contributed to enhanced warming in spring. Further, the positive soil moisture–temperature feedback could enhance warming in summer, provided that the ground was sufficiently dry. It is important to study these feedbacks to correctly predict temperatures, and other variables, in climate models.

Acknowledgments

Completing a PhD is like climbing a mountain; you have to hike a long way to get a good view. In the beginning, you look in one direction and you don't see the rest of the landscape, much like the start of a PhD project. You see from the map (the literature) that a whole landscape exists, but you don't appreciate the full view (the body of knowledge) until you are at the peak. And then, you still have a long way down. During the journey, you have to stick to your chosen path (follow the theme of the thesis). I'd like to thank my main supervisor, Lena Tallaksen, for giving me the map and leading me towards the right path up and down the mountain. She could not join me all the way, but she made sure I had the right travelling companions who could point me in the right direction. Thanks for all your support, for being available for discussions, and teaching me how to write science papers. A big thank you to my co-supevisors, Frode Stordal and Chong-Yu Xu, and co-authors for your help. All of you have included me into your scientific life, and you have always introduced me to your scientific colleagues and their PhDs. Keep doing that, your network has been very helpful for me. For example, Paper II would not have developed if it wasn't for the conference hosted by IAHS FRIEND-WATER in October 2014. Thanks to IIASA in Laxenburg for hosting the annual Young Scientist's Summer Programme, which I attended in 2014. Last, but not least, many thanks to Helene for guiding me through the recesses of WRF and Noah!

Team Nilsen *et al.* has consisted of more people than my supervisors and co-authors. I'd like to thank all my fellow collagues, PhD-students, and my own students in hydrology. The IT section at has always been supportive, especially when I needed it the most (when WRF segfaulted, and when I haphazardly deleted my home directory). A special thanks to Hege Hisdal and Stein Beldring for everything you have taught me, and for giving me so much flexiblility in my new job. Thanks to Trine and Helga for the moral support towards the end of my PhD; to the University Library's Academic Writing Centre for guiding my writing; to Biørneblæs brass and barbeque club (Nedre Blindern rytmeegg- og kremfløyte-kjøkken) for the social support; to Climabyte; to the Lund Prestrud family for having me at Lyngør two weeks every summer; to the bug in the webplayer of my favourite radio channel that allowed me to listen to the commercial-free night broadcasts during daytime; to Turid for reading draft upon draft, and Sarah for consulting services on commas and parentheses.

Last, but not least, I would like to thank mom, dad, Turid, and Audun for your everlasting support, for your patience, and for being there for me. I couldn't have done this without you. Thank you very much!

Contents

List of papers

Paper I
Nilsen, I.B., Fleig, A.K., Tallaksen, L.M., and Hisdal, H. (2014): Recent trends in monthly temperature and precipitation patterns in Europe. *Hydrology in a Changing World: Environmental and Human Dimensions. Proceedings of FRIEND-Water 2014, Montpellier, France, October 2014* IAHS Publ. 363.

Paper II
Nilsen, I.B., Stagge, J.H., and Tallaksen, L.M. (2017): A probabilistic approach for attributing temperature changes to synoptic type frequency. *International Journal of Climatology* 37(6): 2990–3002, DOI: 10.1002/joc.4894.

Paper III
Rizzi, J. **Nilsen, I.B.**, Stagge, J.H., Gisnås, K., and Tallaksen, L.M. (2017): Five decades of warming: impacts on snow cover in Norway. *Hydrology Research* (in production). DOI: 10.2166/nh.2017.051. Reproduced from Hydrology Research with permission from the copyright holders, IWA Publishing.

Paper IV
Nilsen, I.B., Erlandsen, H.B., Stordal, F. Xu, C-Y., and Tallaksen, L.M. (2017): Diagnosing land–atmosphere coupling in a seasonally snow-covered region (South Norway). *Manuscript prepared for submission to Journal of Hydrometeorology*.

For Papers I, II and IV, I was responsible for the programming, modelling, analyses, and writing. P. James provided the SVG data and revised the paragraph about SVG in Paper II. For Paper III, J. Rizzi performed the analyses and drafted the initial version of the paper, whereas I drafted the introduction and discussion sections of the manuscript, and reviewed the manuscript, in addition to performing initial analyses of temperature trends in SeNorge that the current analyses are based on.

List of symbols and abbreviations

α, albedo

CTR, control run in the model diagnostic study

ERA-Interim, global, gridded climate reanalysis dataset

GWB, Gridded Water Balance model

LE, latent heat [W m^{-2}]

LSM, land surface model

m_{WFDEI}, WFDEI temperature trend

m_{SC}, median of the distribution of circulation-induced trends

NAO, North Atlantic Oscillation

Noah-MP, land surface model

NVE, the Norwegian Water Resources and Energy Directorate

P, precipitation

$\rho(SM, LE)$, terrestrial leg of land–atmosphere coupling

$\rho(LE, T)$, atmospheric leg of land–atmosphere coupling

r_{circ}, trend ratio

R_n, net radiation

SCE, snow cover extent

SeNorge, a high-resolution, gridded reference dataset for Norway

SH, sensible heat [W m^{-2}]

SM, soil moisture [%]

SM_{crit}, a soil moisture content below which LE is limited [%]

SP, snow-poor run in the model diagnostic study

SR, snow-rich run in the model diagnostic study

ST, synoptic type

SVG, SynopVis Grosswetterlagen, a classification of synoptic types

SWE, snow water equivalent

T, air temperature [$^{\circ}C$]

t_{obs}, observed trend

t_{circ}, circulation-induced trend

WFDEI, Watch Forcing Data ERA-Interim, a gridded, global hydroclimatic dataset

WRF, Weather Research and Forecasting model

WRF–Noah-MP, coupled atmosphere and land surface model

Chapter 1

Introduction

1.1 Motivation

The last decades have experienced strong warming globally, with each decade after 1970 being warmer than the previous (Hartmann *et al.*, 2013). This warming has implications for the water balance, for instance: changed precipitation patterns, altered evapotranspiration, a shorter snow season and less snow cover (Hartmann *et al.*, 2013; Vaughan *et al.*, 2013). The warming is partly caused by increased radiative forcing from anthropogenic greenhouse gases emitted since the industrial revolution. Besides the direct influence of increased radiative forcing, the atmospheric circulation is a main driver of hydroclimatological change on the regional scale, through advection of energy and water fluxes. In addition, feedbacks between the land and the atmosphere may lead to warming that is independent of atmospheric circulation changes.

Variations in the atmospheric circulation have been highlighted as the main driver of temperature variability in Europe, especially in winter (e.g. Corti *et al.*, 1999; Vautard and Yiou, 2009; Hoy *et al.*, 2013b; Fleig *et al.*, 2015; Saffioti *et al.*, 2015). In these studies, the large-scale circulation is characterised by synoptic types (STs) which are used to separate climatic trends into those caused by circulation changes, and those caused by other factors (Beck *et al.*, 2007; Cahynová and Huth, 2009; Jones and Lister, 2009; Küttel *et al.*, 2011). Changes in the atmospheric circulation cannot explain all the observed warming, however (Barry and Perry, 1973; Beck *et al.*, 2007; Cahynová and Huth, 2009). The part of the temperature trend that cannot be attributed to *circulation changes* (or more specifically, changes in the frequency of synoptic types) is called *within-type changes* (or more specifically, changes within the synoptic types). Within-type changes imply that the air masses change (warm) over time (Beck *et al.*, 2007). Within-type changes may arise from different sources, including radiative for-

cing from greenhouse gases and positive feedback mechanisms between the land surface and the atmosphere that enhance the warming regionally (Küttel *et al.*, 2011).

Another driver of warming is land-atmosphere interactions. The land surface controls the surface energy balance, for instance through the partitioning of net radiation into latent and sensible heat. This partitioning depends on the reflectivity of the land surface (albedo), which is high for snow and low for soil and vegetation. Strong declines in the snow cover are detected in seasonally snow-covered regions in the Northern Hemisphere, especially during the melt season (Derksen and Brown, 2012; Thackeray and Fletcher, 2016). The snow albedo feedback (Figure 2.2a) is initiated by warming that reduces the albedo and increases the amount of net radiation available on the ground, which enhance temperatures (e.g. Dickinson, 1983; Groisman *et al.*, 1994b; Chapin *et al.*, 2005; Hall and Qu, 2006).

During dry periods, a positive feedback between soil moisture and temperature may arise when warming reduces the soil moisture content, which reduces the latent heat as the soil dries out and leaves more energy available for sensible heat. This can ultimately enhance the initial warming. The soil moisture–temperature feedback is well-studied for transitional zones between dry and humid climates (Koster *et al.*, 2004; Dirmeyer *et al.*, 2013, e.g.), but less so at higher latitudes with a moist climate. In seasonally snow-covered regions, such as in Norway, the snow cover in spring influences the soil moisture storage at the start of summer. A small snow storage or early snowmelt leaves less water available to replenish the soil moisture storage (Wilson *et al.*, 2010; Xu and Dirmeyer, 2013b). Snow cover anomalies may therefore influence soil moisture anomalies at high latitudes.

Identifying regions and time periods where the temperature trend is influenced by circulation changes or within-type changes is a first step towards understanding the detailed mechanisms leading to temperature trends. The importance of within-type changes relative to circulation changes varies depending on the region and time of year (Jones and Lister, 2009; Küttel *et al.*, 2011; Cahynová and Huth, 2016; Fleig *et al.*, 2015). Different feedback mechanisms act at specific times of year and in specific regions. For instance, the snow albedo feedback is limited to snow-covered regions, and is strongest in the melting season, when the incoming sunlight is strongest (Callaghan *et al.*, 2012). Detection of trends on the monthly scale can therefore help explain the driving mechanism. The goal of this thesis is to detect recent trends for Europe on the monthly scale, and to improve our process understanding of key drivers of change. An improved understanding of local processes enhancing warming is key to improve estimates of the energy balance and water balance terms correctly. Because recent seasonal temperature trends in Europe have been accompanied by large changes in

the snow cover and summer drying, we focus on the snow albedo feedback and the soil moisture–temperature feedback.

Last, a word about terminology. The terms ”detection” and ”attribution” used in this thesis are not to be confused with the scientific field of ”detection and attribution” that seeks to explain climate change either by anthropogenic forcing or natural variability (e.g. Stott *et al.*, 2004; Stone *et al.*, 2009; Pall *et al.*, 2011). In this thesis, ”detection” or ”attribution” refer to the common uses of the words: to detect – calculate – changes in a variable and to attribute – find a cause – of those changes. Note also that we do not separate temperature trends into anthropogenic forcing and natural variability, but rather into circulation changes and within-type changes.

1.2 Objectives

The main objective of this thesis is to detect monthly hydroclimatic trends in Europe and explore their physical drivers through statistical attribution and through a model diagnostic study. In particular, the importance of land–atmosphere interactions in Norway is explored. Four research questions are defined:

1. Which regions and months have experienced significant trends in hydroclimatology in Europe?

2. Can the detected trends for Europe be attributed to circulation changes or within-type changes?

3. How do snow cover changes influence warming in a region with seasonal snow cover?

4. For regions with within-type changes, can the detected trends be attributed to the snow albedo feedback (in spring), and the soil moisture–temperature feedback (in summer)?

1.3 Study design

This work combines traditional statistical methods with model diagnostic studies. Temperature and precipitation trends were detected on the monthly scale for Europe to address research question 1, in Paper I (Nilsen *et al.*, 2014) and Paper II (Nilsen *et al.*, 2017b). Because of the noisy trend patterns for precipitation, we continued

with temperature only. Research question 2 was addressed by statistical attribution methods commonly used in synoptic climatology. The method of hypothetical trends (Leathers and Ellis, 1996) was used in combination with trend ratios (Cahynová and Huth, 2009) in Paper I, whereas Paper II provides a probabilistic expansion of trend ratios. This novel probabilistic approach improves unpon the trend ratio method by evaluating the statistical significance of synoptic circulation changes on observed climate trends.

Land surface models (LSMs) are useful tools for detailed process studies of what drives changes in hydroclimatic variables. For that purpose, a smaller target region in Europe was selected for high-resolution model diagnostic studies. South Norway was identified as a region where trends could be attributed to within-type changes in April and July–September. With its complex topography, South Norway spans different climate zones, ranging from a maritime moist and temperate climate in the western part, to a dry inland climate in the eastern part. A detailed dataset of estimated observed hydroclimatic variables is available for Norway (SeNorge), which allows for evaluation of the model results. The influence of a changing snow cover on temperatures was investigated for this dataset (research question 3, Paper III; Rizzi *et al.* 2017). A modelling study of the snow albedo feedback and the soil moisture–temperature feedback was performed using a regional climate model (WRF) coupled to the Noah-MP land surface model (research question 4, Paper IV Nilsen *et al.* 2017a). Although this model-diagnostic study for two summers (2006 and 2014) is not able to explain the full within-type trend over the period 1981–2010, it proves that the soil moisture–temperature feedback is one factor explaining the enhanced warming. Together, these four papers form a study of detailed mechanisms of what controls regional temperature trends. This thesis has contributed to the strategic research area LATICE (Land-ATmosphere Interactions in Cold Environments) funded by the Faculty of Mathematics and Natural Sciences at the University of Oslo (`http://www.mn.uio.no/geo/english/research/groups/latice/index.html`).

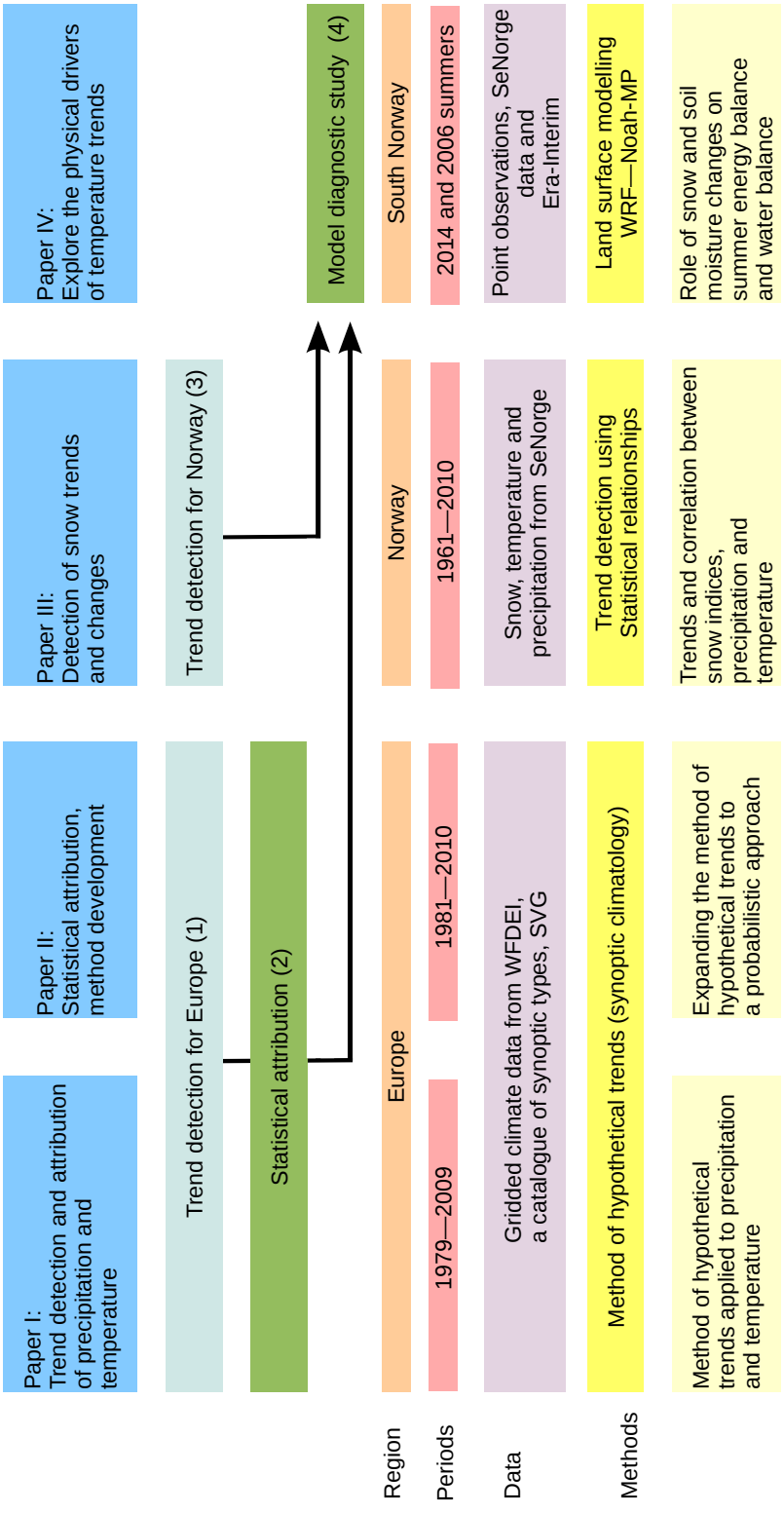

Figure 1.1: Flow chart describing the papers, including the research question numbers (in parentheses) and main methodology. 5

Chapter 2

Scientific background

This chapter presents the scientific background for the work done as a part of the thesis. First, a summary of published seasonal changes in temperature, snow, and soil moisture (relevant for reseach question 1) is presented before a review of possible processes explaining detected seasonal changes, including attribution studies (relevant for research questions 2–4).

2.1 Detected climate change in Europe and Norway

Due to a large number of detection studies, this summary is limited to i) Europe and Norway, ii) recent changes covering the past decades, iii) seasonal and monthly changes, and iv) temperature and the related variables snow and soil moisture.

2.1.1 Recent seasonal temperature changes

The temperature change for Europe has exceeded the global mean trends (Jones *et al.*, 2012; Hartmann *et al.*, 2013; EEA, 2017). Local temperature trends are sensitive to the region, season, period, method, and dataset under study. A wide range of values are therefore reported for Europe, however, clear warming signals emerge across studies. Annual temperature trends from Europe-wide studies range from 0.3 °C/decade for the period 1960–2015 at 2° spatial resolution (EEA 2017) to more than 1 °C/decade for the period 1976–2009 for point observations (Klein Tank *et al.* 2005), depending on region, time period, and resolution (Table 2.1). On the monthly scale, trend magnitudes are even higher, exceeding 3 °C/decade in northern Europe in winter (DJF) for the period 1976–2009 (Klein Tank *et al.*, 2005). Winter warming in northern Europe and

summer warming in southern and central Europe are consistent across several studies (Klein Tank *et al.*, 2005; EEA, 2008, 2017). For Norway, temperature trends for the period 1955–2014 showed warming in all seasons, most pronounced in winter and spring (Førland *et al.*, 2016) (Table 2.1).

2.1.2 Recent seasonal snow changes

The seasonal snow cover influences the climate over large parts of the globe, covering up to 30% of the global land area (Vaughan *et al.*, 2013). The snow conditions over the Northern Hemisphere have changed during the last decades (Dery and Brown, 2007). The Northern Hemisphere winter snowpack has increased over the past decades (Dery and Brown, 2007; Callaghan *et al.*, 2012) because of increased cold-season precipitation (Hartmann *et al.*, 2013). Still, a dramatic snow cover decline has been observed at the start and end of the snow season, with a stronger decline in spring than in autumn (Tedesco *et al.*, 2009). This asymmetry has been ascribed to the stronger incoming sunlight in the melting season than in autumn (Callaghan *et al.*, 2012). The early spring snow cover in the Arctic has reduced by 18% in May–June, over the period 2008–2012 (Derksen and Brown, 2012). Fennoscandia is one of the regions experiencing the strongest reduction in the snow season length (Callaghan *et al.*, 2012). Studies for Norway have detected decreasing snow water equivalent (SWE) for the periods 1931–1960 and 1991–2009 in southern Norway (Skaugen *et al.*, 2012), and decreasing snow depth for the period 1961–2010 (Dyrrdal *et al.*, 2013). Also in Norway, the strongest reductions have been found in spring (Dyrrdal, 2010). Snow depth and SWE have increased at high elevations, above approximately 1000 m a.s.l. (Skaugen *et al.*, 2012).

2.1.3 Recent seasonal soil moisture changes

Seasonal soil moisture trends are sparse. Annual soil moisture trends show significant drying in southern Europe and significant wetting in northern Europe (Sheffield and Wood, 2008; Hartmann *et al.*, 2013), confirmed by trend studies of precipitation and evapotranspiration (Becker *et al.*, 2013; Greve *et al.*, 2014). Since soil moisture is closely related to precipitation, evapotranspiration, temperature, and streamflow, these variables may be taken as proxies for soil moisture changes. Summer streamflow has decreased in large parts of Europe for the period 1963–2000, particularly for southern and central Europe, and even for parts of northern Europe in August (Stahl *et al.*, 2012). Streamflow trends for Norway decreased in summer (Wilson *et al.*,

Table 2.1: Comparison of temperature trends in regional trend studies for Europe. Seasonal trends from Jones *et al.* (2012) are averaged over months from their Table 2. The abbreviations in column Reg (for regions) indicate: Gl=Globally, NH=Northern Hemisphere (spatial average), Eur=All of Europe, Alp=The Alps, No=Norway, Fi=Finland.

Time scale and citation	Reg	Data	Period	Trend
Annual				°C/decade
Klein Tank *et al.* (2005)	Eur	185 stations	1976–1999	0–2.0
EEA (2008)	Eur	reanalysis (ECA&D)	1976–2006	0–1.2
EEA (2008)	Eur	reanalysis (ERA-40)	1958–2001	-0.2–0.4
Böhm *et al.* (2010)	Alp	gridded	1983–2008	0.48
Jones *et al.* (2012)	Gl	reanalysis (CRUTEM4)	1951–2010	0.1–0.4
Hanssen-Bauer *et al.* (2015)	No	country average	1976–2014	0.50
EEA (2017)	Eur	Gridded	1960–2015	0.1–0.50
Nilsen *et al.*, (2017)	Eur	reanalysis (WFDEI)	1981–2010	-0.3–0.9
Spring (MAM)				
Klein Tank *et al.* (2005)	Eur	185 stations	1976–1999	-0.5–2.5
Jones *et al.* (2012)	NH	reanalysis (CRUTEM4)	1979–2010	0.34
Førland *et al.* (2016)	No	4 stations in South Norway	1955–2014	0.34
Summer (JJA)				
Klein Tank *et al.* (2005)	Eur	185 stations	1976–1999	0–2.0
EEA (2008)	Eur	reanalysis (ECA&D)	1976–2006	0–1.2
EEA (2008)	Eur	reanalysis (ERA-40)	1958–2001	0–0.5
Jones *et al.* (2012)	NH	reanalysis (CRUTEM4)	1979–2010	0.32
Førland *et al.* (2016)	No	4 stations in South Norway	1955–2014	0.20
Winter (DJF)				
Klein Tank *et al.* (2005)	Eur	185 stations	1976–1999	-0.5–>3.0
EEA (2008)	Eur	reanalysis (ECA&D)	1976–2006	-0.2–2.0
EEA (2008)	Eur	reanalysis (ERA-40)	1958–2001	0.1–0.8
Tietäväinen *et al.* (2010)	Fi	country average	1979–2008	1.43
Jones *et al.* (2012)	NH	reanalysis (CRUTEM4)	1979–2010	0.32
Hanssen-Bauer *et al.* (2015)	No	country average	1900–2014	0.04
Førland *et al.* (2016)	No	4 stations in South Norway	1955–2014	0.41

2010), confirmed by (Stahl *et al.*, 2012). Projections show a continued drying trend in summer, both in Europe (Seneviratne *et al.*, 2006; Eisner *et al.*, 2017) and Norway (Hanssen-Bauer *et al.*, 2015). In particular, the variability of the summer temperatures in Europe is expected to increase, which increases the probability of dry conditions in the future (Schar *et al.*, 2004; Whan *et al.*, 2015).

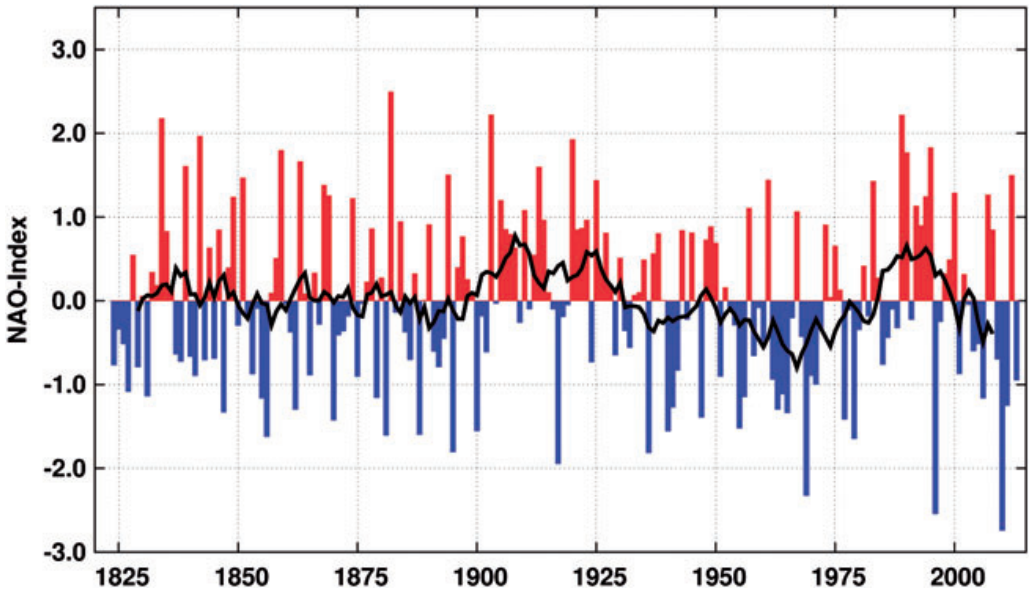

Figure 2.1: "Updated NAO Index after Jones et al. (1997) for boreal winter (DJFM) 1823/1824 to 2012/2013 re-normalized with respect to the full time period. The black line shows an 11-year running mean." (Feser *et al.*, 2015). Reprinted with permission from John Wiley and Sons.

2.2 Drivers of detected changes in the regional climate

2.2.1 Role of atmospheric circulation on the regional climate

The global oceanic and atmospheric circulation is primarily a mechanism to even out differences in the incoming energy between the poles and tropics (Lamb, 1982). In Europe, westerly airflow dominates the atmospheric circulation, advecting oceanic, mild and moist air onto northern Europe and dry air onto southern Europe (Becker *et al.*, 2013). Variations in storm tracks, pressure systems and circulation patterns in the Northern Hemisphere are often described as the North Atlantic Oscillation, NAO (Hurrell *et al.*, 2013) or as other circulation indices (Huth *et al.*, 2008, 2016). Circulation indices are useful because of their strong positive correlation to local temperature and precipitation (Hurrell and Deser, 2009; Hurrell *et al.*, 2013).

The NAO index is the difference between the normalised sea level pressure in the Iceland low and the Azores High (Hurrell *et al.*, 2013). Strong westerly airflow across the North Atlantic and toward Europe is characterised with a positive NAO index (NAO+), whereas a negative NAO index (NAO-) is associated with weaker westerlies. The NAO index increased from NAO- to NAO+ between the early 1970's and the mid-1990's (Figure 2.1), which was accompanied by an increased occurrence of westerly airflow and frontal weather during that period (Hurrell *et al.*, 2013). After the year 2000, NAO- prevailed until the winter 2012/2013, but has been positive since then (Hurrell and Staff, 2017). Numerous studies have focused on trends in the atmospheric circulation, or trends in variables that depend on the atmospheric circulation for the decades 1970, 1980 and 1990 (e.g. Klein Tank *et al.*, 2005; EEA, 2008; Cahynová and Huth, 2009; Cahynová and Huth, 2016). Due to the shift in the NAO index, these studies are, however, not representative for the most recent past.

Links between the atmospheric circulation and the local climate are studied through the old field of *synoptic climatology* (Barry and Perry, 1973). Early weather prediction, prior to the advent of numerical weather prediction models, relied on relationships between the local climate and atmospheric circulation, and assumed that local climate trends could only be explained by changes in the atmospheric circulation (Dzerdzeevski, 1963; Yarnal, 1993). However, other factors than circulation changes have also been shown to contribute to local climate trends. For example, temperature changes are to a larger degree explained by changes in the atmospheric circulation in winter than in summer, when other factors contribute to warming (Beck *et al.*, 2007; Cahynová and Huth, 2009; Fleig *et al.*, 2015). Further, the importance of circulation changes varies over multidecadal time scales (Beck *et al.*, 2007; Küttel *et al.*, 2011).

An important topic in synoptic climatology is to separate local climate changes into those caused by changes in the atmospheric circulation, and those caused by other factors (Beck *et al.*, 2007; Jones and Lister, 2009; Cahynová and Huth, 2009; Küttel *et al.*, 2011). To relate the local climate to the atmospheric circulation, the circulation patterns are classified into synoptic types (STs) describing the synoptic situation on a given day (Huth *et al.*, 2016). STs allow separating the cause of temperature trends two parts: *circulation changes* and *within-type changes*. Circulation changes refer to changes in the frequency of STs that induce a climate trend, whereas within-type changes refer to changes within the STs that induce a climate trend (Beck *et al.*, 2007). Within-type changes may include increased radiative forcing from greenhouse gases, and positive feedback mechanisms between the land and atmosphere, but may also stem from uncertatinties in the stratification of STs (Küttel *et al.*, 2011). Technically, a positive within-type change means that the STs become warmer over time. For those regions and time periods where the temperature trend is not due to more frequent warm synoptic types, possible interactions between the land surface and the atmosphere may play a role. Note that increased radiative forcing from greenhouse gases may also influence circulation changes.

Attribution studies STs are correlated with many local climate variables, which make them useful to study the physical processes controlling local climate change. Circulation changes have explained changes in a range of variables, from daily streamflow (Massei and Fournier, 2012), floods (Prudhomme and Genevier, 2011), and drought (Fleig *et al.*, 2011; Hannaford *et al.*, 2013) to ozone concentrations (Otero *et al.*, 2016).

Beck *et al.* (2007) analysed monthly temperatures for central Europe for the period 1780–1995 and found that within-type changes were present in all seasons, particularly in summer. Cahynová and Huth (2010) found circulation changes in seasons other than winter to be of minor importance for temperature trends at stations in the Czech Republic (1961–1998). Studies by Beck *et al.* (2007); Vautard and Yiou (2009); Cahynová and Huth (2010); Hoy *et al.* (2013b) conclude that within-type changes explained a large part of the observed temperature trends, especially in summer in central Europe (Beck *et al.*, 2007), though they differ slightly in their findings for other seasons. Küttel *et al.* (2011) analysed gridded temperature and precipitation time series for all of Europe and concluded that within-type changes were also important for temperature changes in winter, especially in eastern Europe and Scandinavia. One of the reasons for the different response in winter and summer is that winter weather is dominated by advective, large-scale processes, whereas summer weather is dominated by radiative, small-scale processes (Huth *et al.*, 2016).

2.2.2 Role of the land surface on the regional climate

Accurate information about properties on the land surface is a vital requirement to estimate the components in the energy and water balances correctly. The land surface controls the local climate by regulating the exchange of heat, moisture and momentum between the land surface and atmosphere (Seneviratne *et al.*, 2010). The detailed mechanisms of this coupling vary from region to region and season to season. For instance, a correct estimation of the net radiation over a given area requires an exact albedo. This is particularly important in seasonally snow-covered regions, where the albedo before snowmelt exceeds 0.5 (and may be as high as 0.9) and drops to lower values after snowmelt (0.3–0.1 in regions with forest, grasslands or bare soil) (Dingman, 2002). Through its albedo, the snow cover controls the amount of reflected shortwave radiation (Groisman *et al.*, 1994b; Betts, 2000; Dery and Brown, 2007). At other times of year, the influence of snow will be exceeded by other land surface properties. When the soil moisture content is so low that evapotranspiration becomes limited, the partitioning into latent and sensible heat fluxes is controlled by the soil moisture storage (Seneviratne *et al.*, 2010).

The soil moisture storage may be affected by the snow cover in seasonally snow-covered regions. During years with less snow in stock less water is available to replenish the soil moisture storage during snowmelt (Wilson *et al.*, 2010; Xu and Dirmeyer, 2013b). Further, a longer snow-free period means that the soil moisture storage is allowed to decline for a longer period during the summer half year. The effect of snowmelt anomalies on the water balance weeks and months after snowmelt is an emerging field of study (Wetherald and Manabe, 1995; Rowell and Jones, 2006; Rowell, 2009; Im *et al.*, 2010; Xu and Dirmeyer, 2011, 2013a,b; Saini *et al.*, 2016), and may be relevant for Norway because of the detected snow reductions in spring (Dyrrdal, 2010) and summer drying (Wilson *et al.*, 2010).

Positive feedback mechanisms Temperature changes may be modulated by feedback mechanisms between the land surface and the atmosphere that enhance or diminish the initial warming (Bony *et al.*, 2006). Many feedback mechanisms are relevant to the climate system, such as the water vapour feedback and cloud feedbacks (Held and Soden, 2000; Bony *et al.*, 2006). In this thesis, we focus on feedback mechanisms involving changes in the hydrologic cycle that can alter an initial warming, namely the snow albedo feedback and the soil moisture–temperature feedback.

The snow albedo feedback (Figure 2.2a) is initiated by warming that reduces the albedo and increases the amount of net radiation available on the ground, which leaves more energy available for further melting and warming (e.g. Dickinson, 1983; Groisman *et al.*, 1994b; Chapin *et al.*, 2005; Hall and Qu, 2006).

A feedback between temperature and soil moisture is well established for periods with a strong soil moisture limitation on evapotransporation (e.g. Koster *et al.*, 2004; Seneviratne *et al.*, 2006; Koster *et al.*, 2010; Fischer *et al.*, 2012; Miralles *et al.*, 2014). In the soil moisture–temperature feedback loop (Figure 2.2b), a spell of warm and dry weather causes an anomalously low soil moisture storage that limits evapotranspiration (evaporative cooling) and thus enhances the initial warming (Seneviratne *et al.*, 2010). This soil moisture–temperature feedback does not arise until the soil moisture has dropped below a critical point where evaportanspiration becomes limited by soil moisture (Figure 2.2c). However, a low soil moisture storage does not unconditionally feed back to temperature, as demonstrated by e.g. Quesada *et al.* (2012) for Europe, because high temperatures also depend on the atmospheric circulation situation: a blocking high pressure system favour heat waves, whereas cyclonic situations inhibit them.

A useful framework for determining if the conditions are sufficiently dry was first presented by Budyko in 1958, see a review in Greve *et al.* (2016) and Figure 2.2c. The Budyko curve defines a relationship between an evaporative index, $LE/(LE + SH)$ (or ET/ET_{max}), and a dryness index, SM, in which evapotranspiration is limited by the available water (a supply limit) and by the available energy (a demand limit) (e.g. Berghuijs *et al.*, 2014; Greve *et al.*, 2016). Three regimes exist, depending on the soil moisture's control on evapotranspiration. In humid climates, evapotranspiration is governed by other factors than soil moisture; this regime is called *energy-limited*. Below a critical soil moisture threshold, that depends on the land cover (Gallego-Elvira *et al.*, 2016), the soil moisture limits evapotranspiration. Here, a soil moisture–temperature feedback may arise (Figure 2.2) that gradually reduces the soil moisture. This stage is a transition regime between dry and humid climates. Although such transitional regimes are more common in certain geographical regions, such as southern Europe (Greve *et al.*, 2014), a humid climate may become transitional for periods without rainfall, and a dry climate may become transitional for wet periods (Zampieri *et al.*, 2009; Dirmeyer *et al.*, 2009; Seneviratne *et al.*, 2010; Halder and Dirmeyer, 2017). If the drying continues until the wilting point (which is also land cover-dependent), the evapotranspiration seizes. This characterises the dry regime. Now, the feedback stops, because there is no more water left to regulate the evapotranspiration (Seneviratne *et al.*, 2010; Gallego-Elvira *et al.*, 2016). The transitional and the dry regimes are

termed *soil moisture-limited*. Because the processes controlling evapotranspiration are so different between an energy-limited and a soil moisture-limited regime, a correct process understanding depends on a correct characterisation of the regime.

A common way of diagnosing the soil moisture–temperature feedback is to recognise that the feedback pathway consists of two segments: the terrestrial leg and the atmospheric leg (Dirmeyer *et al.*, 2006, 2014). The terrestrial leg is characterised as the correlation between soil moisture, SM, and latent heat, LE, whereas the atmospheric leg is characterised as the correlation between LE and air temperature, T (details are given in Section 4.3 and Paper IV). If both legs are present, it suggests that indeed, the land surface is contributing to the detected atmospheric change (Orlowsky and Seneviratne, 2010). It is worth noting that a correlation does not imply causality. However, it is a commonly used metric (Dirmeyer *et al.*, 2006, 2014; Halder and Dirmeyer, 2017) that points in the direction of a feedback.

Attribution studies In this paragraph, we concentrate on drivers of spring warming, as detected for Norway by Førland *et al.* (2016), and summer warming, as detected for southern and central Europe by Klein Tank *et al.* (2005) and EEA (2008). The snow albedo feedback is widely studied as a driver of spring warming (see e.g. Chapin *et al.*, 2005; Hall and Qu, 2006; Peng *et al.*, 2013). Spring snow cover reductions have accelerated over the past decades, largely driven by increasing temperatures (Brown and Robinson, 2011; Derksen and Brown, 2012), enhanced by the snow albedo feedback (Groisman *et al.*, 1994a; Dery and Brown, 2007).

Much research has dealt with the relationship between summer warming and dry soil moisture conditions in southern and central Europe, which are considered hot-spots of land–atmosphere coupling (Seneviratne *et al.*, 2006). The soil moisture–temperature feedback has been documented to drive summer warming in southern and central Europe (see e.g. Seneviratne *et al.*, 2006; Zampieri *et al.*, 2009; Orlowsky and Seneviratne, 2010; Miralles *et al.*, 2014), especially during heat waves (Schar *et al.*, 2004; Zaitchik *et al.*, 2006; Vautard *et al.*, 2013; Miralles *et al.*, 2014; Whan *et al.*, 2015). Summer warming has also been explained with drier than normal conditions in preceding seasons, such as a soil moisture anomaly in spring as documented by Whan *et al.* (2015) or earlier snowmelt due to higher temperatures, as suggested by Wilson *et al.* (2010). The soil moisture–temperature feedback has recieved little attention at northern latitudes, where the climate is usually moist.

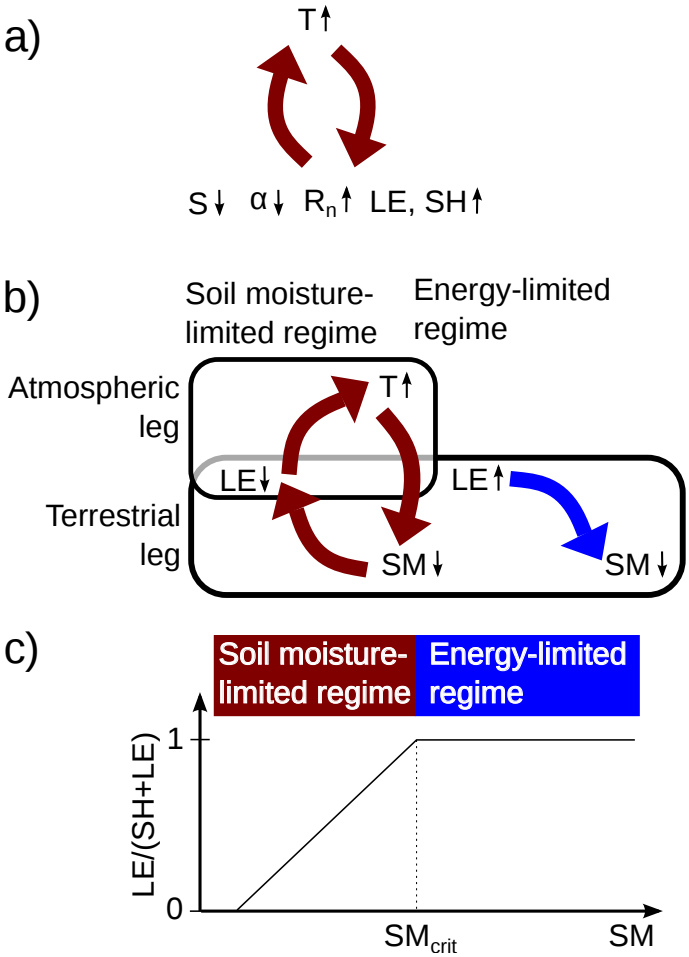

Figure 2.2: a) The snow albedo feedback. An initial warming leads to reduced snow cover, S, and reduced albedo, α, that allows more shortwave radiation to be absorbed in the ground. The result is an increase in the net radiation, R_n, that leaves more energy available for latent heat, LE and sensible heat, SH, ultimately increasing the air temperature, T. b) Soil moisture–temperature coupling. In energy-limited regimes, the soil moisture, SM, does not control the latent heat, rather, when the latent heat increases, it depletes the soil moisture storage. An initial warming that reduces the soil moisture below a critical value, SM_{crit}, shifts the regime into a soil moisture-limited regime. Here, the soil moisture limits latent heat (positive correlation; the terrestrial leg), and the warming may be enhanced by the reduced evaporative cooling (negative correlation; the atmospheric leg). c) Schematic illustration of the Budyko framework. Above SM_{crit}, latent heat is not limited by the soil moisture. Below SM_{crit}, latent heat becomes limited by soil moisture, protentially triggering a soil moisture–temperature feedback.

Chapter 3

Data

Figure 1.1 gives an overview of the data and methods used in Papers I–IV. Trends were detected for the gridded climate dataset WFDEI in Paper I (air temperature and precipitation) and Paper II (air temperature only), and for a high-resolution the gridded (1×1 km) reference dataset for Norway, SeNorge, in Paper III. Point observations as well as SeNorge data were used in the model setup and validation in Paper IV, whereas ERA-Interim reanalysis data were used to force the model. A classification of synoptic types, SynopVis Grosswetterlagen (SVG), was used for statistical attribution in Papers I and II.

3.1 Gridded hydroclimatic datasets

3.1.1 The *WFDEI* dataset

Temperature and precipitation from the a bias-corrected reanalysis dataset, i.e., the Watch Forcing Data ERA-Interim (WFDEI; Weedon *et al.*, 2014) were used for trend detection in Paper I and II. These gridded ($0.5^\circ\times\ 0.5^\circ$), daily historical data are available at 3-hourly resolution, globally (except over oceans) (`ftp://rfdata:forceDATA@ftp.iiasa.ac.at`). We used daily averages for Europe for the recent past (1979–2009 in Paper I and 1981–2010 in Paper II).

The variables making up WFDEI originate from the ERA-Interim reanalysis (Dee *et al.*, 2011). The temperature has been elevation corrected using the environmental lapse rate and bias-corrected against gridded monthly observations from the Climate Research Unit, University of East Anglia (CRU TS 3.1; Harris *et al.*, 2014). The precipitation has been corrected for undercatch and bias-corrected against Global Precipitation Climatology Centre (GPCC) data. It is worth noting that WFDEI variables

are spatially consistent after bias-correction (Weedon *et al.*, 2014), which is necessary when linking local variables to the large-scale atmospheric situation.

3.1.2 The *seNorge* dataset

We used a high-resolution dataset for Norway, the 1×1 km SeNorge dataset (Engeset *et al.*, 2004; Tveito and Roald, 2005; Saloranta, 2012, `senorge.no`). SeNorge version 1.1 contains gridded hydroclimatic data at a daily time step from 1957–today, covering mainland Norway (Engeset *et al.*, 2004).

Interpolated temperature and precipitation are produced by the Norwegian Meteorological Institute (Tveito and Roald, 2005). Interpolation is performed after subtracting a reference level of the variable, which is created by regressing physical characteristics such as latitude, elevation, distance from the coast etc. After interpolation, the reference level is added back to obtain the original physical characteristics. Monthly lapse rates are used to adjust temperature and precipitation to the terrain. Precipitation measurements are corrected for undercatch before gridding.

Hydrological variables are modelled with the GWB model, developed by the Norwegian Water Resources and Energy Directorate (NVE) (Beldring *et al.*, 2003). The model core in GWB is the commonly used HBV model (Bergström, 1995; Sælthun, 1996), forced with the interpolated temperature and precipitation. GWB is a conceptual hydrological model calibrated against runoff data for boreal conditions (shallow soils, short roots etc). Snow variables are calculated separately in a snowmap model (Saloranta, 2012).

In SeNorge, each grid cell may contain lakes, glaciers and up to two varying land use classes (”open land”, ”forest”, ”alpine”, ”heather”, or ”bedrock”). Evapotranspiration for one grid cell is modelled as a weighted average of evapotranspiration calculated for the four land cover classes, including actual evaporation and interception (over vegetation), lake evaporation (over lakes). There is no evapotranspiration over glaciers and snow (Sælthun, 1996; Beldring *et al.*, 2003). The actual evaporation is limited by soil moisture below a certain threshold (depending on the land cover class), and follows the potential evapotranspiration above the threshold. Potential evapotranspiration is a function of temperature and monthly correction factors. The correction factors are highest in June and lowest in November–March (Engeland *et al.*, 2004).

Despite being a state-of-the-art, high-resolution dataset, SeNorge is not as homogenous as it may seem at first. For instance, because most measuring stations are located at low elevations and close to settlements, the SeNorge data are most un-

certain at high elevations and remote places. The number of stations in the station network has changed over time, meaning that the uncertainty is not homogenous in time. The inconsistent number of stations may influence trend calculations.

3.2 Point observations

Station observations of snow, soil moisture, soil temperature, and air temperature were provided by NVE and were used to validate the WRF–Noah-MP model for South Norway in Paper IV. As summarised in Table 3.1, snow water equivalent, SWE and snow depth, SD, were retrieved from 12 and 11 stations, respectively. Soil mosture and soil temperature were retrieved from four stations. These 23 snow stations and four soil moisture/soil temperature stations display a range of soil and vegetation types, from lowland sites with meadows (e.g., Ås), inland sites with forests (e.g., Brunkollen) and mountain sites with birch forest (e.g., Groset) (Colleuille, 2000). A map of the stations is shown in Figure 3.1.

SWE is measured using a snow pillow, i.e., a flexible, antifreeze-filled container measuring the weight of the overlying snow (Ree *et al.*, 2011). Snow depth is measured by timing a reflected ultrasound pulse. Soil moisture is measured in six segments in the vertical, at -10 cm, -20 cm, -30 cm, -40 cm, -60 cm and -100 cm. Soil moisture is measured with Time Domain Reflectometry (TDR). Soil temperature is measured in nine segments in the vertical, 15 cm apart. Air temperature at 2 m was also provided for the stations measuring soil temperature and soil moisture (Abrahamsvoll, Kise, Groset and Ås), but due to a bias in the temperature at Groset and Ås, we used data from the Norwegian Meteorological Institute at Møsstrond (close to Groset) and Ås (in Ås).

3.3 A catalogue of synoptic types: SynopVis Grosswetterlagen (SVG)

Classifications of circulation indices aim to characterise the atmospheric circulation, based on the location of pressure patterns and storm tracks, as one categorical variable (e.g. Huth *et al.*, 2008; Cahynová and Huth, 2016; Fleig *et al.*, 2015; Huth *et al.*, 2016). Such classifications are often used to separate trends into circulation changes and within-type changes (Beck *et al.*, 2007; Cahynová and Huth, 2009, 2010; Küttel *et al.*, 2011). In Papers I and II, we used a daily catalogue of synoptic types (STs) for

Table 3.1: Point measurements used for validation in Paper IV. All data were available from the Norwegian Water Resources and Energy Directorate, except air temperature from Møsstrond, available from the Norwegian Meteorological Institute.

Var.	Station name	Municipality	[masl]	East [°]	North [°]	Station no.
Snow	Bakko	Hol	1020	8	60.68	012.142.0
depth	Brunkollen	Bærum	370	10.55	59.97	008.005.0
	Finnbølseter	Vinstra	ca. 900	9.32	61.46	002.722.2
	Grimsa	Folldal	800	9.99	62.06	002.373.0
	Groset	Tinn	950	8.31	59.83	016.232.14
	Grytå	Nissedal	645	8.34	59.17	019.078.0
	Øvre Heimdalsvatn	Øystre Slidre	1088	8.89	61.41	002.036.0
	Kyrkjestølane	Vang	953	8.11	61.2	073.011.0
	Maurhaugen	Oppdal	660	9.82	62.66	121.002.0
	Skurdevikåi	Eidfjord	1250	7.6	60.3	015.118.2
	Stenerseter rør	Trysil	ca. 600	11.88	61.41	002.716.6
SWE	Bakko	Hol	1020	8	60.68	012.142.0
	Brunkollen	Bærum	370	10.55	59.97	008.005.0
	Grimsa	Folldal	800	9.99	62.06	002.373.0
	Groset	Tinn	950	8.31	59.83	016.232.14
	Grytå	Nissedal	645	8.34	59.17	019.078.0
	Øvre Heimdalsvatn	Øystre Slidre	1088	8.89	61.41	002.036.0
	Kvarstadseter	Ringsaker	680	10.89	61.18	002.439
	Kyrkjestølane	Vang	953	8.11	61.2	073.011.0
	Lybekkbråten	Nannestad	195	11.08	60.25	002.070
	Maurhaugen	Oppdal	660	9.82	62.66	121.002.0
	Nordre Osa	Åmot	450	11.74	61.41	2.0451
	Vauldalen	Røros	840	12.03	62.64	002.072.0
SM,	Abrahamsvoll	Røros	750	11.56	62.69	2.725.1
soil T	Groset	Tinn	950	8.31	59.83	016.232.14
	Kise	Ringsaker	127	10.81	60.77	2.727
	Ås	Ås	70	10.77	59.66	5.7
air T	Møsstrond	Tinn	932	8.07	59.85	MET station
	Ås	Ås	70	10.77	59.66	5.7
P	Møsstrond	Tinn	932	8.07	59.85	MET station

Figure 3.1: Location of snow stations (measuring SWE) in blue and soil moisture stations in brown. Note that Groset is both a snow station and a soil moisture station.

Europe, the SynopVis Grosswetterlagen (SVG; provided by P. James, 2013; personal communication), based on James (2007). SVG is derived from mean sea level pressure, precipitable water, 500−1000 hPa thickness, and 500 hPa geopotential height, all taken from the Twentieth Century Global Reanalysis (Compo *et al.*, 2011) and supplemented by NCEP/NCAR reanalyses (Kalnay *et al.*, 1996) for the period after 2010 (P. James, 2016; personal communication), see details in Paper II.

Representativity of SVG for Europe The separation of trends into circulation changes and within-type changes was conducted under the assumption that SVG is able to discriminate between STs. In other words, an ST classification must be able to separate warm from cold STs. If they are mixed, a possible warming signal related to increasing warm STs would not be visible. This implies that results showing within-type changes may not explain a change in the properties of STs, but rather deficiencies related to deriving the ST classification, see Beck *et al.* (2007) for a discussion of possible factors giving rise to within-type changes. See also Sections 2.2 and 4.2.

Figure 3.2 shows the discriminative capability of SVG. The Shannon Entropy used to measure SVG's ability to separate warm STs from cold STs (described in James, 2007) is calculated using five bins of temperature data ("very cold", "cold", etc. for each grid cell) and assessing whether the temperatures for each ST are evenly distributed across the bins or are biased towards cold or warm bins. The discriminative capability drops with distance away from central Europe, which is the region that the original Hess-Brezowsky Grosswetterlagen was defined for (P. James, 2014; personal communication). Consenquently, the SVG classification is most robust for central parts of Europe. In South Norway, the discriminative capability is lower than for, for instance, Germany but we have assumed it to be sufficiently high to separate out circulation changes from within-type changes. In northern Norway, however, SVG is less reliable. Note also that the discriminative capability of precipitation is lower than that for temperature.

Frequencies and patterns of SVG synoptic types The frequency distribution of SVG synoptic types for 1948–2017 is shown in Figure 3.3a. Although this time period exceeds the one used in this thesis, it gives an impression of the relative frequencies of the different STs for each month. These frequencies vary in time, as shown in Figure 3.3b)–d) for the period 1979–2010, covering the full period used in both Paper I (1979–2009) and Paper II (1981–2010). Figure 3.3 shows smoothed values for five flow directions: "westerly" (W and SW; STs 1–6), "northerly" (N and NW; STs 7–8, 12–17), "central" (C; STs 9–11), "easterly" (E and NE; STs 18–23), and "southerly" (S and SE;

STs 24–29). The ST numbering follows the rows in Figure 3.4 (and in James, 2007), e.g., the synoptic type in the first row (Wa) is number 1. Trends in the frequency of STs are calculated using linear regression, and significance is calculated using the t-test.

When considering the whole year (Figure 3.3b), westerly STs increased significantly, whereas no other flow directions showed significant trends. Identical STs may exhibit different synoptic features in summer and winter (James, 2007). Therefore, summer trends (Figure 3.3c) and winter trends (Figure 3.3d) are shown separately. For summer, westerly types increased at the expense of northerly types. For winter, no significant trends could be detected over the period. Note that Figure 3.3 does not state whether an ST is warm or cold, which requires additional information on local temperature.

Climatological composite means for the 29 STs are shown in Figure 3.4.

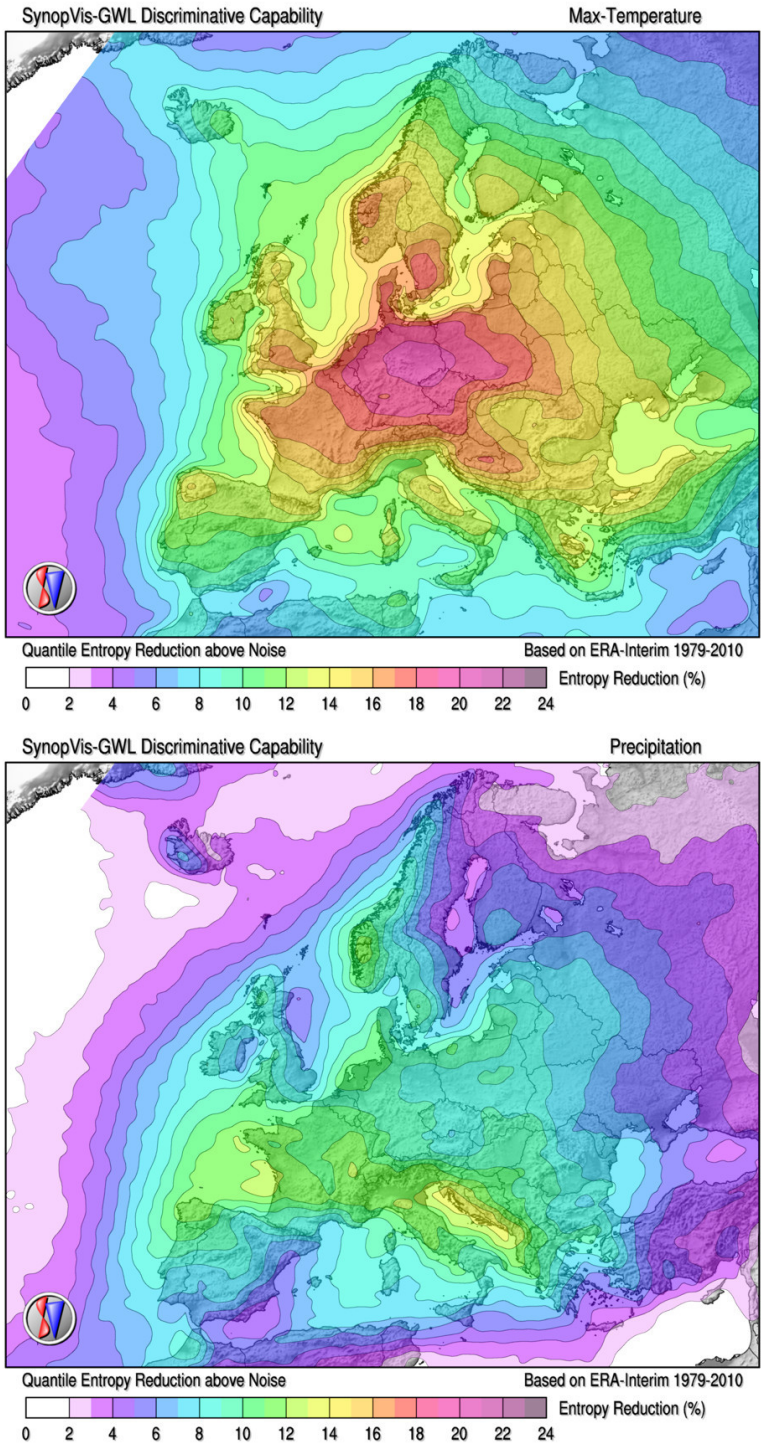

Figure 3.2: Quantile entropy reduction above noise for maximum temperature (top) and precipitation (bottom). Because some STs are colder than average and other STs are warmer than average, the distribution of quantiles for each grid cell, month and ST will be biased. The larger the bias, the higher the entropy reduction (a measure of anomalies from an unbiased ST). Even randomly generated ST classifications have an entropy reduction by chance, termed "noise". The entropy reduction above noise means that the noise is subtracted from the entropy reduction. Figures provided by P. James, 20.11.2014. Reprinted with permission from the author.

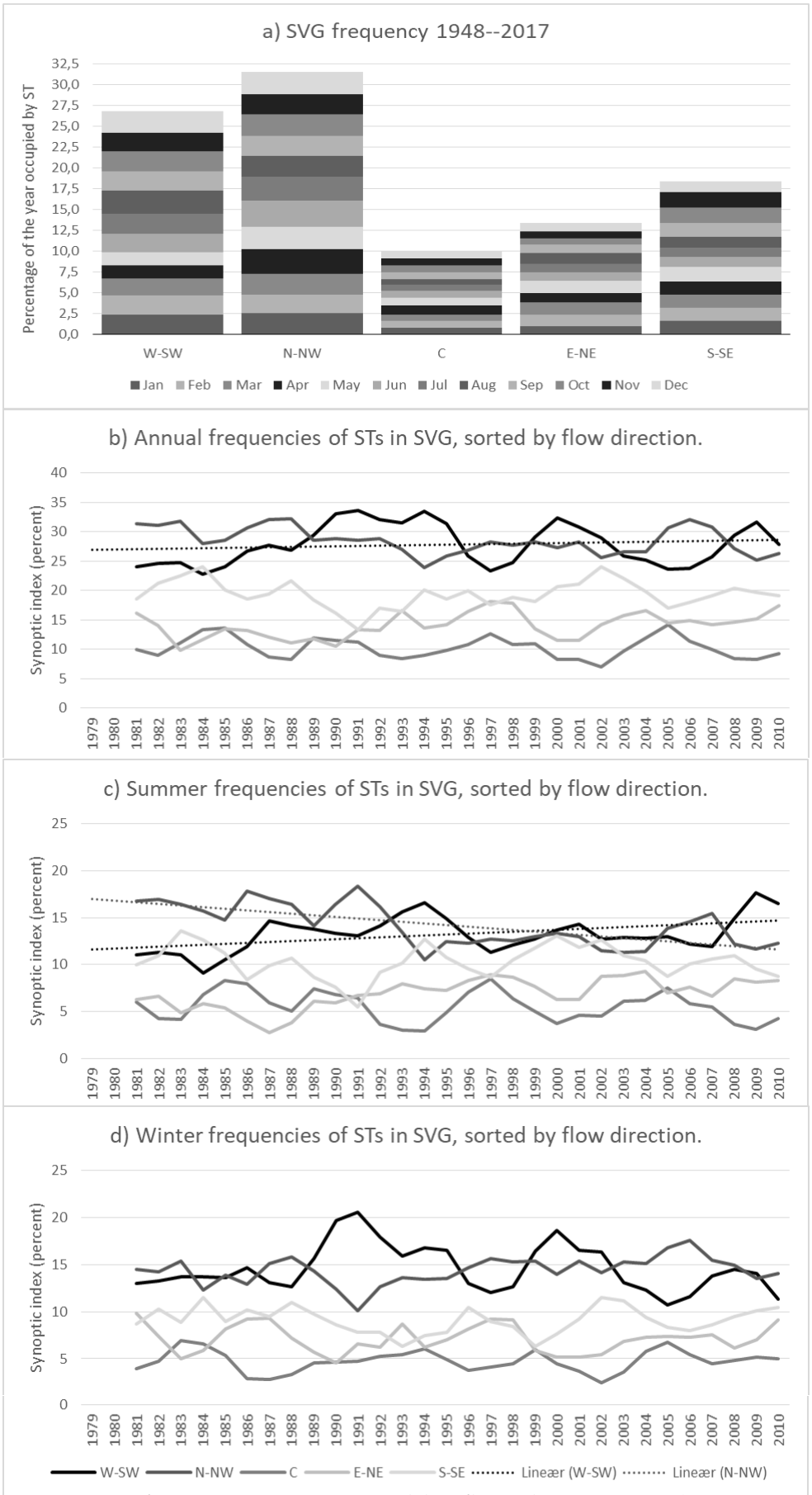

Figure 3.3: Frequencies of synoptic types sorted by flow direction as a) percentages for the period 1948–2017 (data provided by P. James, 11.10.2017), and as a 3-year moving average for 1979–2010 comprising b) all days in the year c) summer days (15 April–14 October) and d) winter days (15 October–14 April), as a percentage of the year. Significant trends at the 0.05 level are shown with a linear trendline.

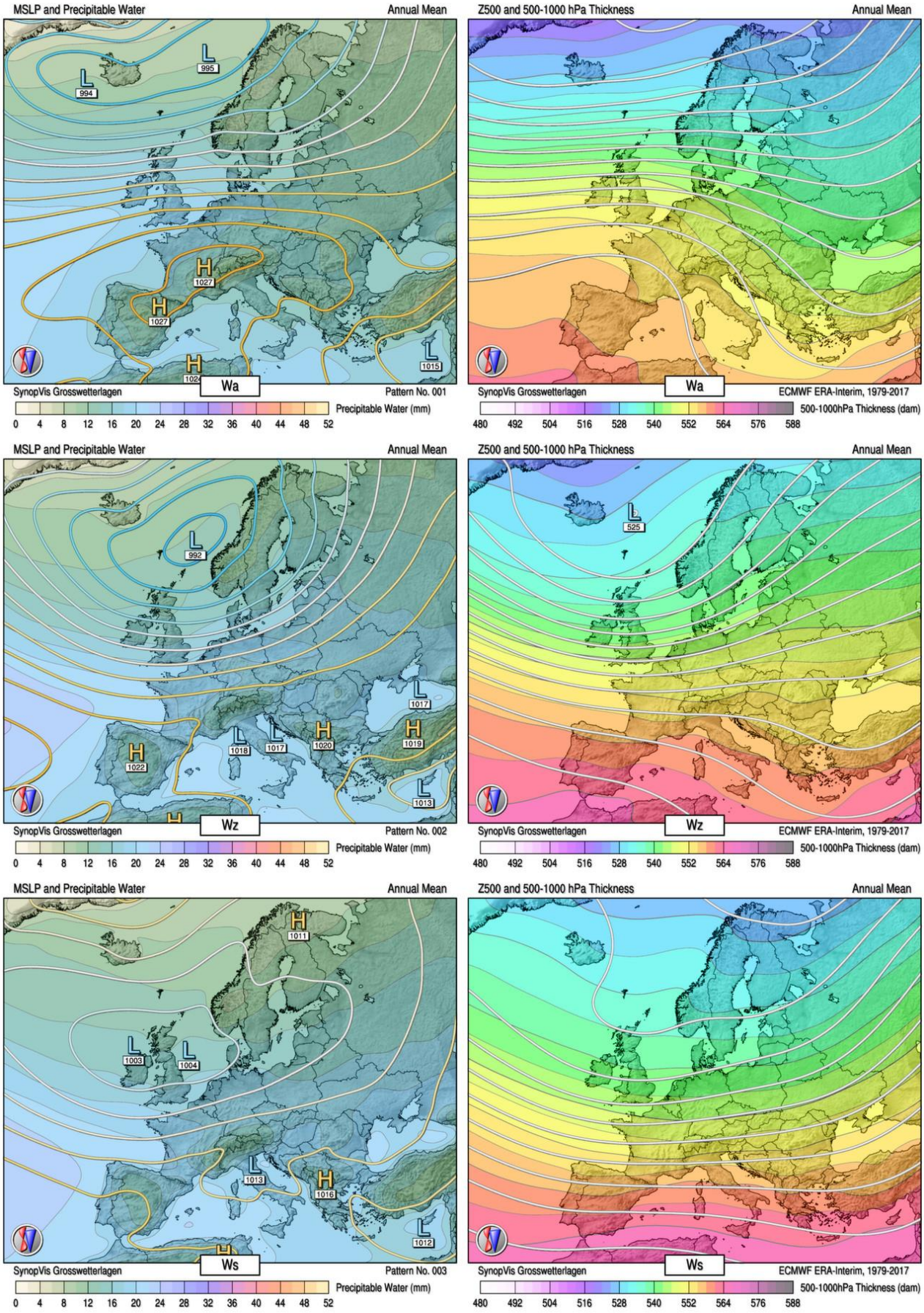

Figure 3.4: Climatological composite means for the 29 STs. Left: mean sea level pressure (contours, in hPa) and precipitable water (colours, in mm). Right: geopotential height at 500 hPa (in decametres, dam) and 500–1000 hPa thickness (in dam). Figures provided by P. James, 12.10.2017. Reprinted with permission from the author.

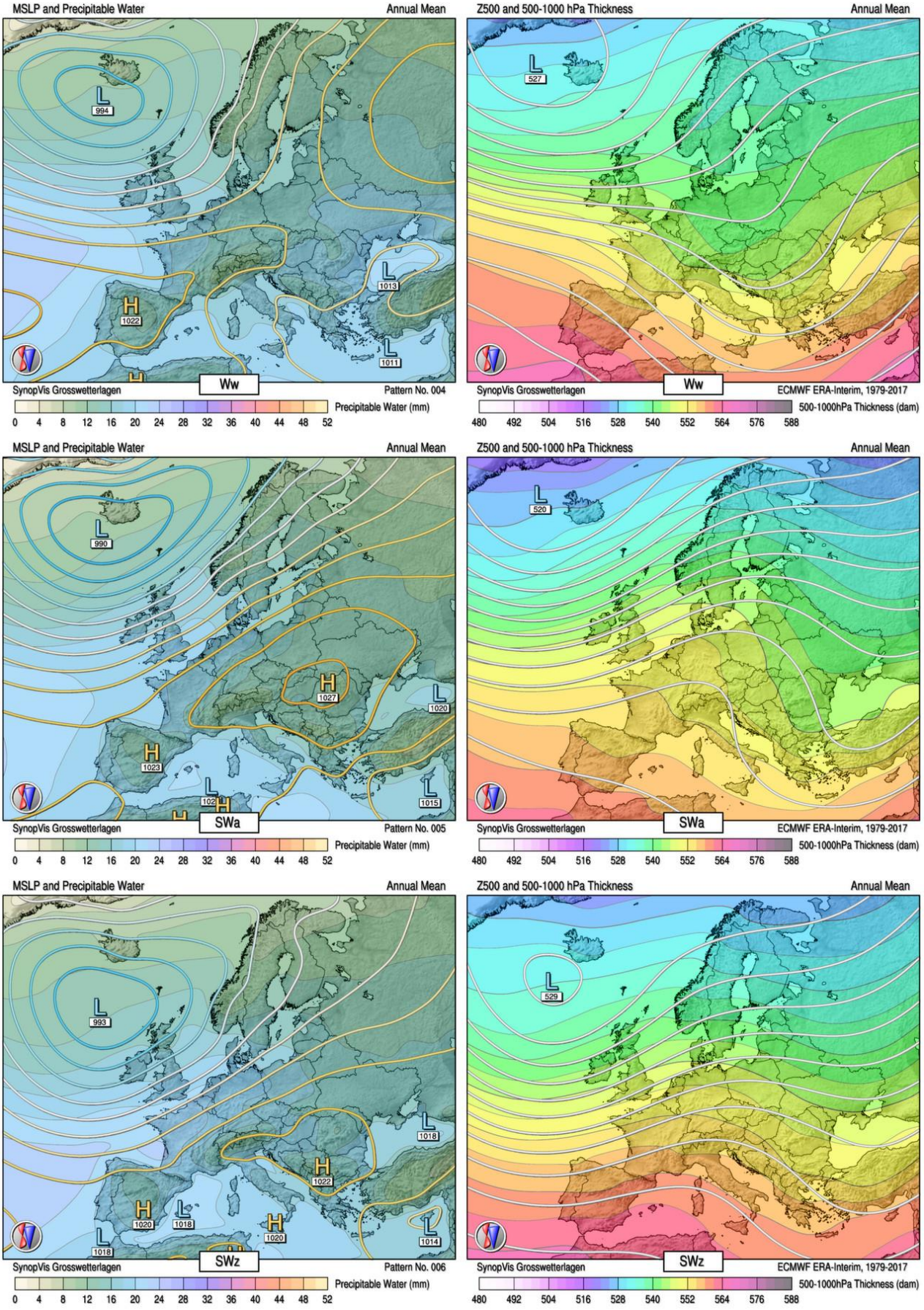

Figure 3.5: Continued from previous page.

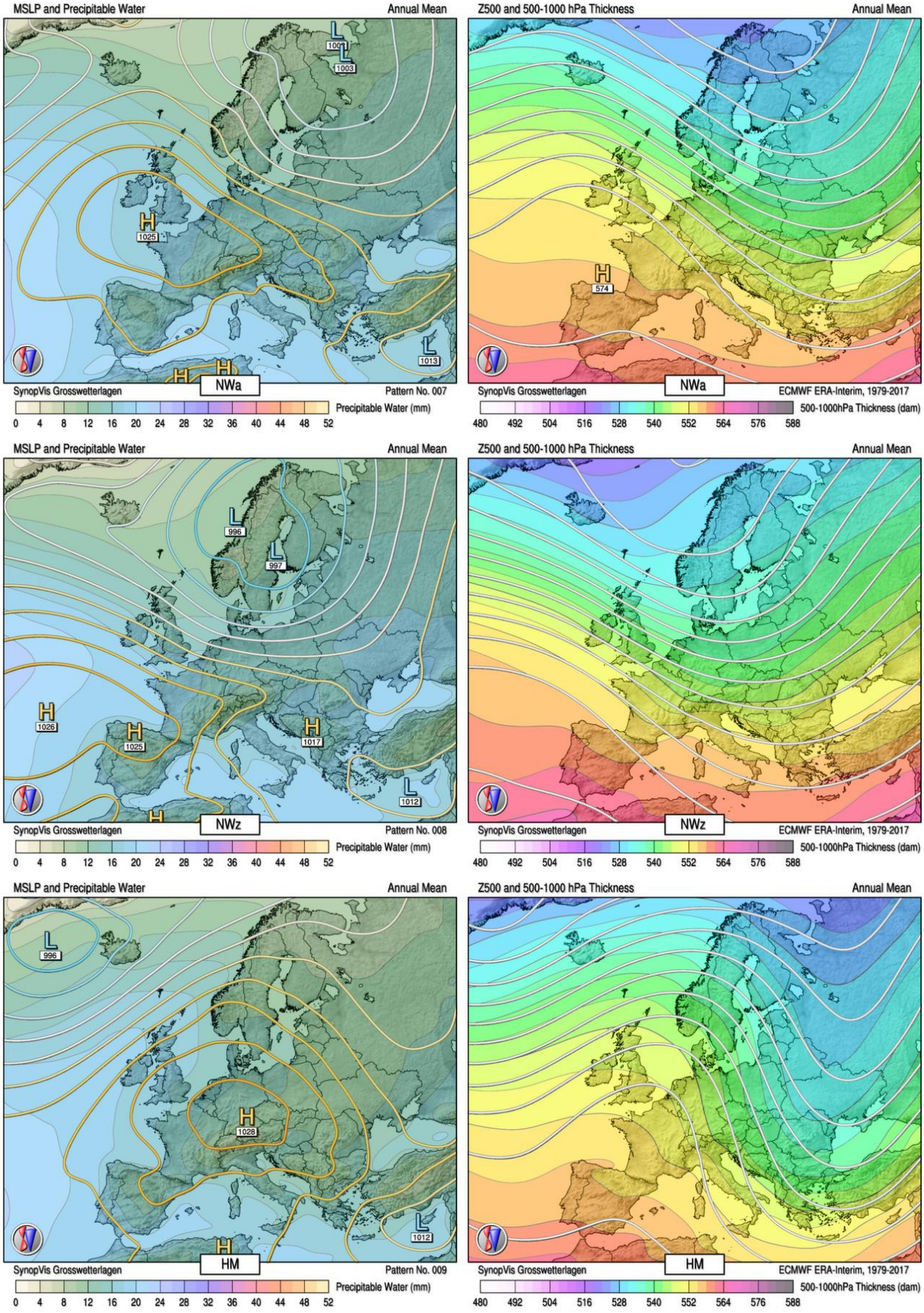

Figure 3.6: Continued from previous page.

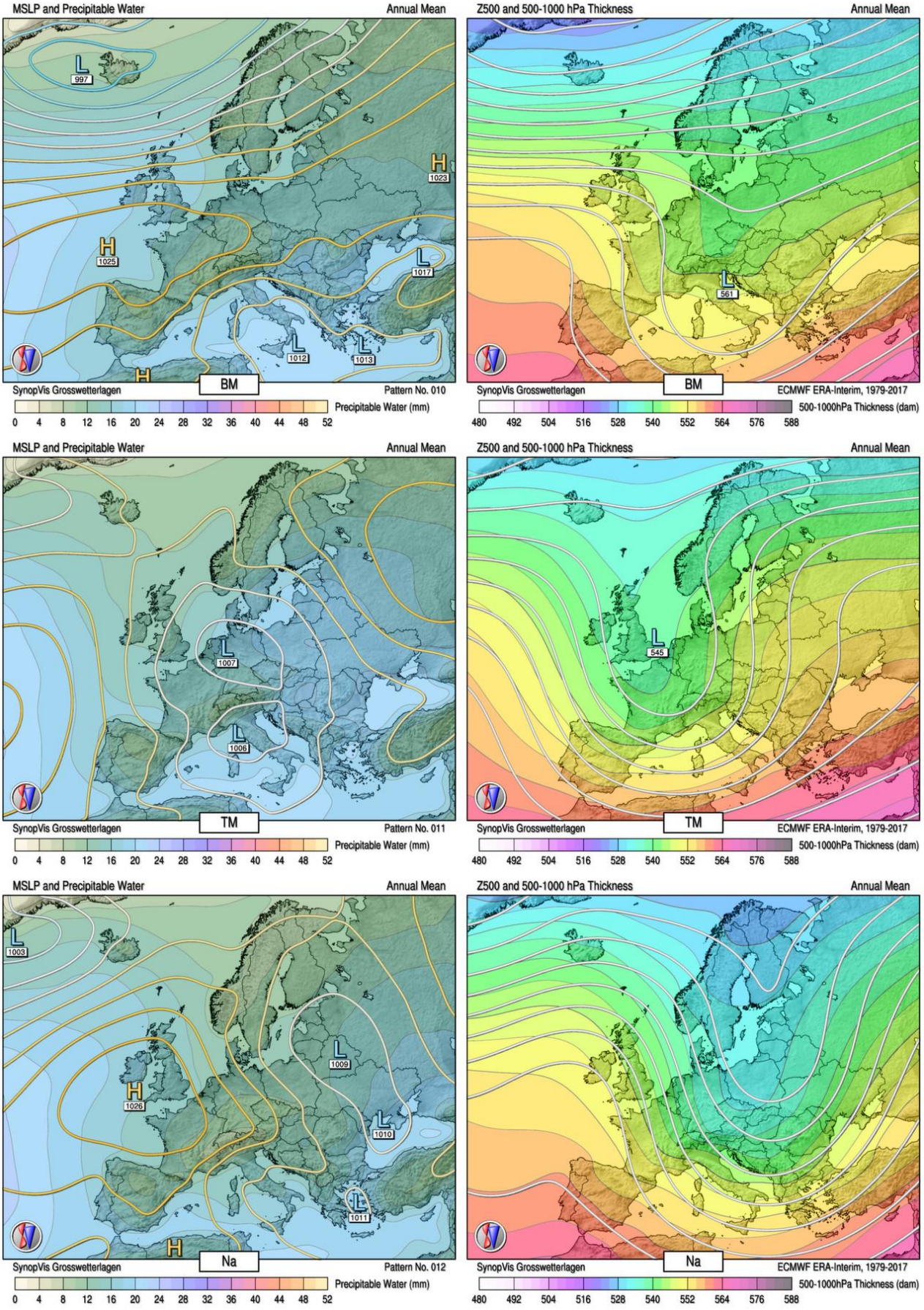

Figure 3.7: Continued from previous page.

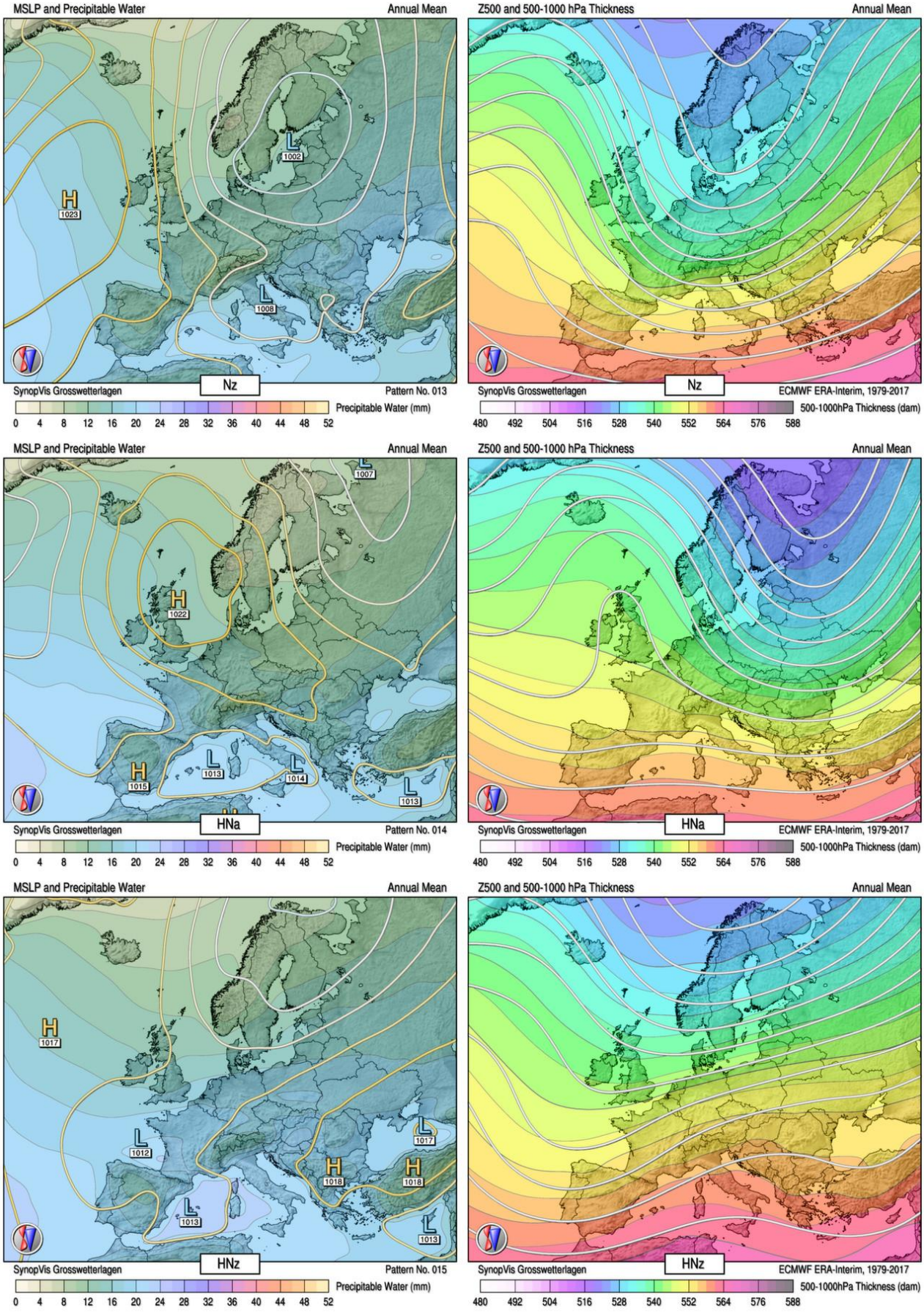

Figure 3.8: Continued from previous page.

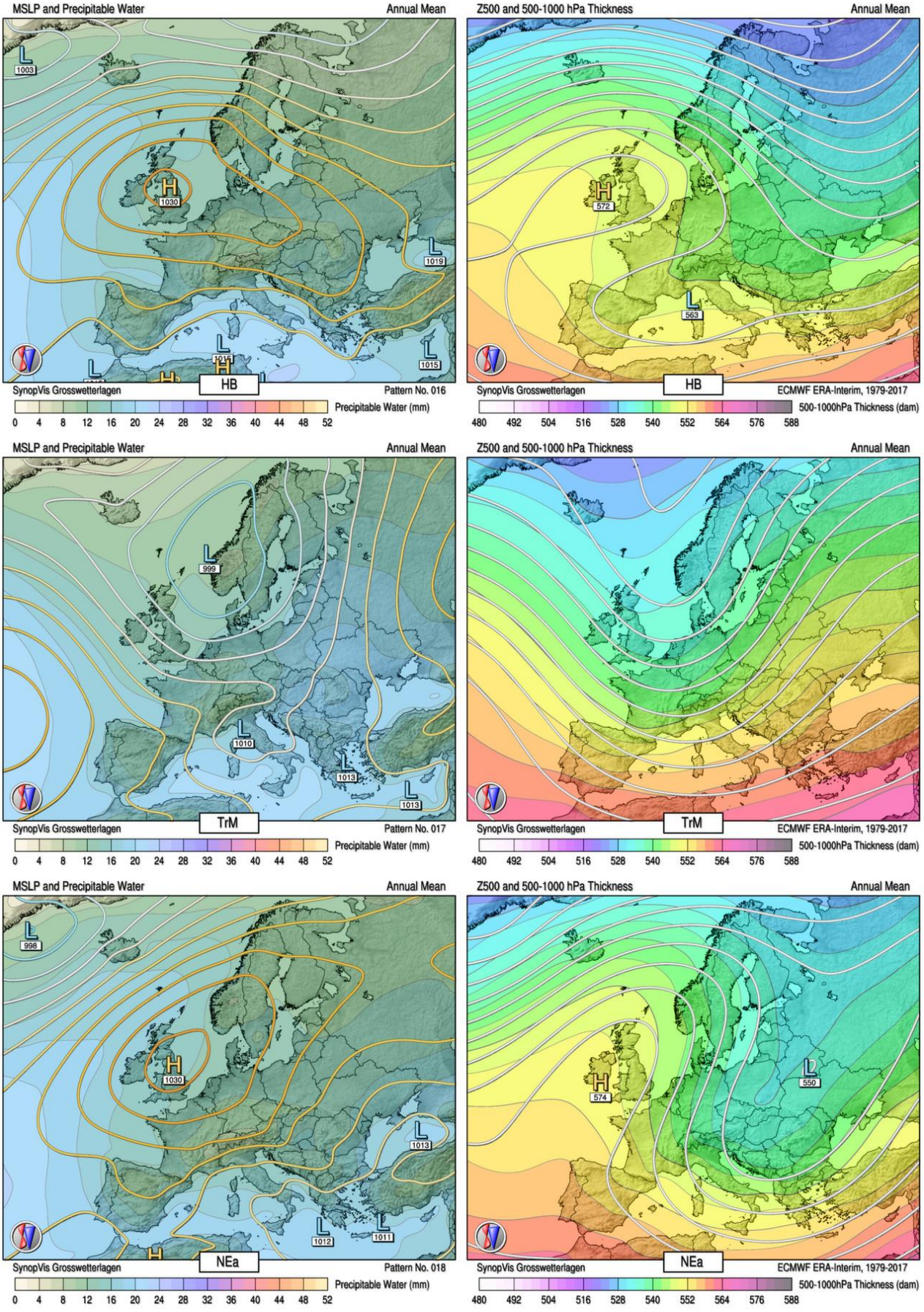

Figure 3.9: Continued from previous page.

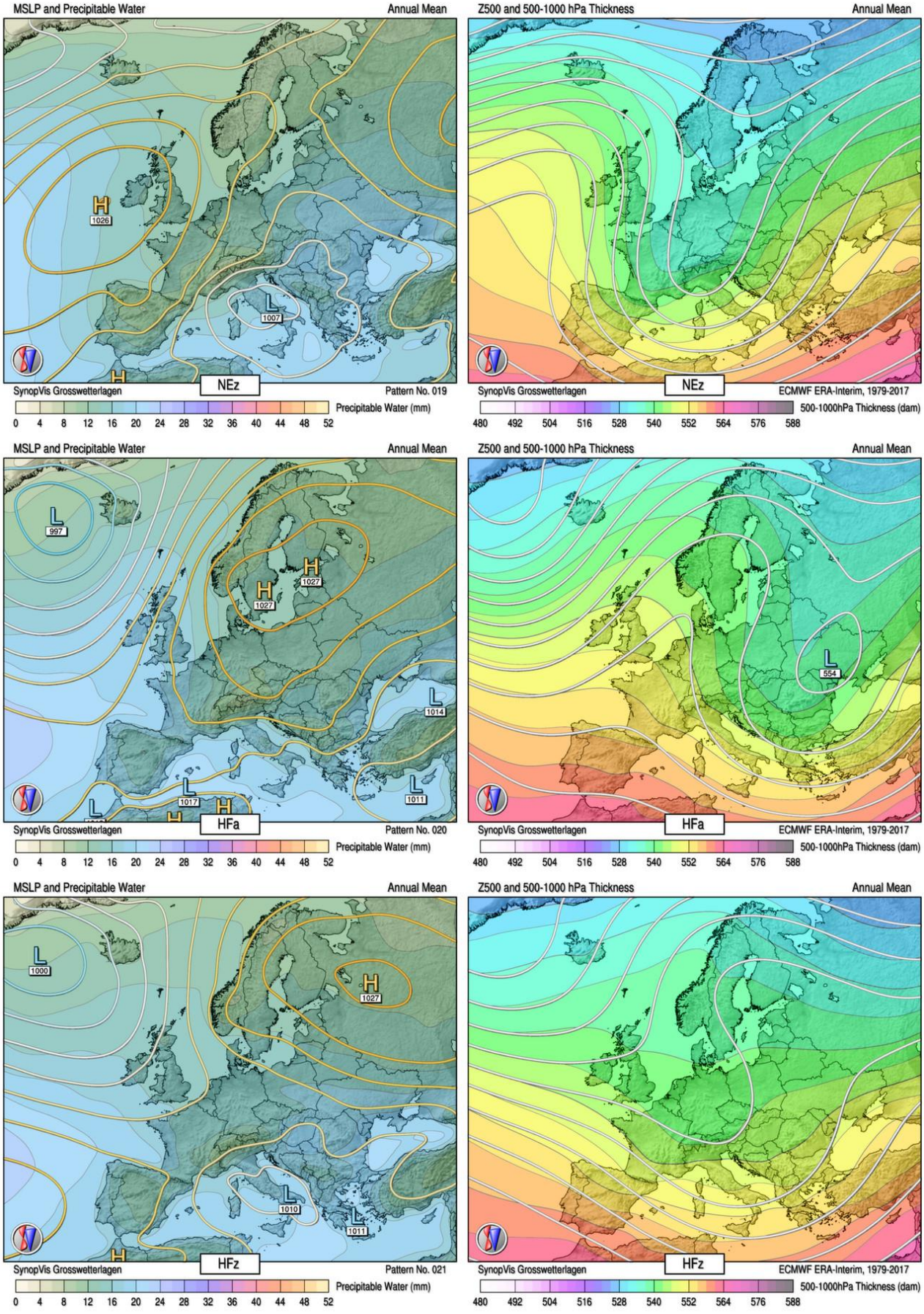

Figure 3.10: Continued from previous page.

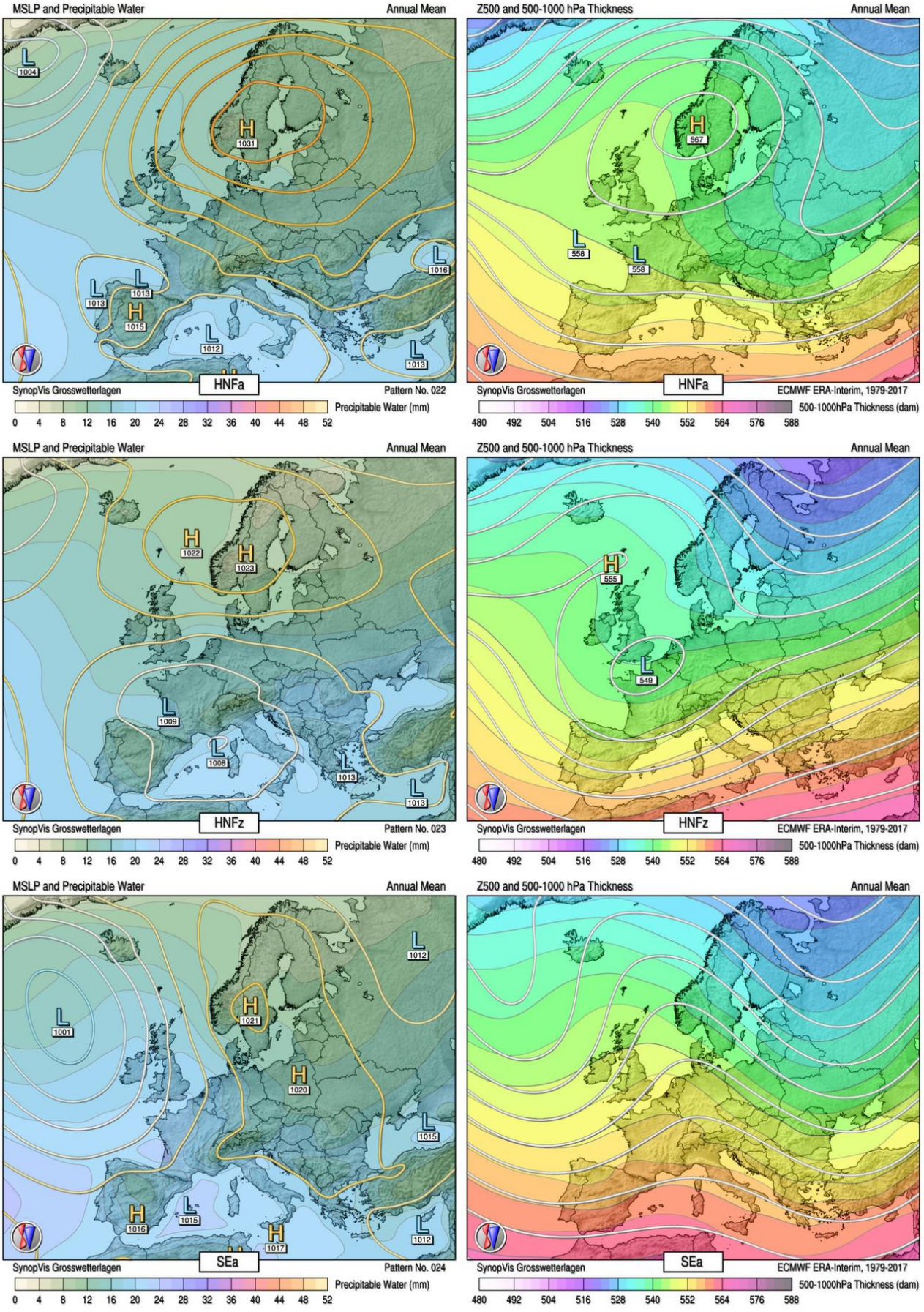

Figure 3.11: Continued from previous page.

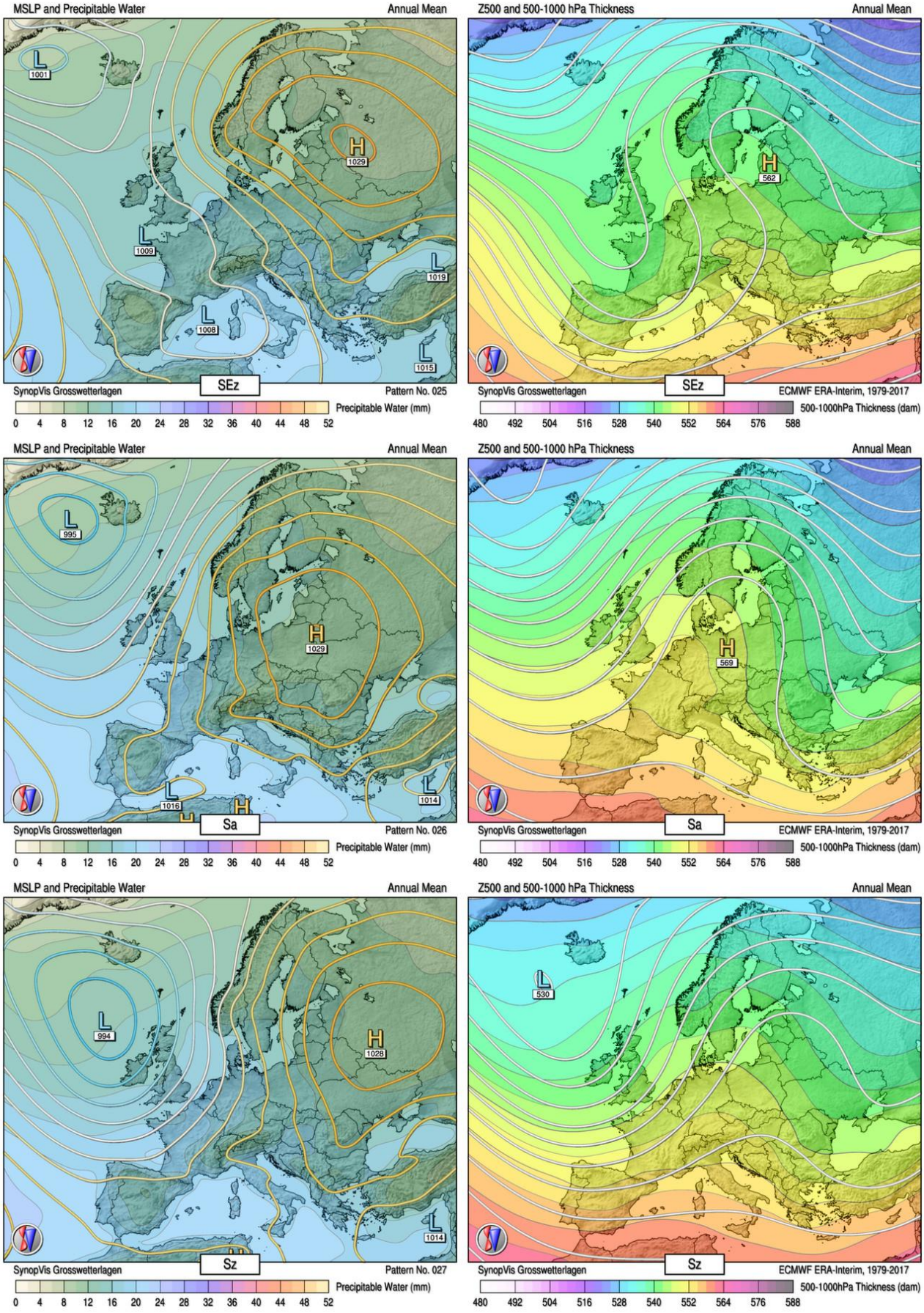

Figure 3.12: Continued from previous page.

Chapter 4

Methods

This section summarises trend detection methods, statistical attribution methods, which include the method of hypothetical trends, and a novel probabilistic approach expanding on this method, and land surface modelling performed in the model diagnostic study.

4.1 The Theil-Sen slope and Mann–Kendall trend test

Air temperature trends were calculated using the Sen slope (also called the Theil-Sen estimator or Kendall– Theil Robust Line; Theil, 1950; Dery *et al.*, 2005). The trend magnitude m is the median of the linear slopes between all pairs of values:

$$m = \text{median}\left[\frac{y_i - y_j}{t_i - t_j}\right] = \text{median}(m_k) \tag{4.1}$$

where $y_i - y_j$ is the temperature difference between all possible values in the time series, $t_i - t_j$ is the corresponding time difference between each pair of values in the time series, and m_k is a vector consisting of all possible linear slopes. A more thorough description is given in Paper II, Section 3.1. The Sen slope was selected, rather than the linear regression trend, because it is less influenced by outliers (Stahl *et al.*, 2012). However, it is still sensitive to the time period chosen (Hisdal *et al.*, 2001).

The Mann–Kendall trend test (Sneyers, 1990) was used in conjunction with the Sen slope to assess whether the estimated observed trend is significantly different from zero. When testing the hypothesis that no monotonic trend is present in WFDEI temperatures, a standard significance level of 0.05 was assumed (two-sided test). The

Mann–Kendall test statistic, Z_{MK}, is defined as (Dery *et al.*, 2005):

$$Z_{MK} = \begin{cases} \frac{S-1}{\sigma_S}, S > 0 \\ 0, S = 0 \\ \frac{S+1}{\sigma_S}, S < 0 \end{cases} \tag{4.2}$$

where S is the test statistic and σ_S is the variance of S. To calculate S, the signs of all possible trendlines m_k are summed:

$$S = \sum_{k=1}^{n(n-1)/2} \text{sgn}(m_k) \tag{4.3}$$

where $\text{sgn}(m_k)$ is 1, 0 or -1, depending on the sign of m_k.

4.2 Statistical attribution

4.2.1 Terminology

Before introducing the statistical attribution, a note on terminology is required. Paper I used terminology from Cahynová and Huth (2010) but this was not precise enough for our use of the SVG classification of synoptic types (see referee comments to Fleig *et al.* 2015). Therefore, Paper II used terminology from Fleig *et al.* (2015), who also used the SVG classification. Table 4.1 lists the terminology used in Papers I and II, and in this thesis. For instance, the term ”circulation type (CT)” was changed into ”synoptic type (ST)” in Paper II to reflect that SVG is classified based on not only sea level pressure and geopotential height, but also precipitable water and the 500–1000 hPa thickness. Further, the term ”hypothetical trend” used in Paper I is synonymous with ”synoptic-circulation-induced trend” used in Paper II. For simplicity, we use the terms ”circulation-induced trend” throughout this thesis, also for the synoptic-circulation-induced trends that result from the probabilistic approach in Paper II. Similarly, atmospheric circulation is in Paper II referred to as ”synoptic circulation” to emphasise the methodology behind SVG, but for simplicity, we use ”atmospheric circulation” throughout this thesis.

Table 4.1: Terminology in Papers I and II. Text in bold indicate the wording used in this thesis, when two terms are used synonymously.

	Term used	Definition	Reference
Paper I	Circulation type (CT)	Classified based on pressure variables	
Paper II	**Synoptic type (ST)**	Classified from more variables than pressure	
Paper I	Observed trend, t_{obs}	Climatic trend based on the WFDEI datset	
Paper II	WFDEI trend, m_{WFDEI}	The same as t_{obs}	
Thesis	**Estimated observed trend**	General term, reflecting that reanalyses are not observations	
Paper I and II	Circulation changes	Changes in the frequency of STs that induce a trend	(Beck *et al.*, 2007)
Paper I and II	Within-type changes	Changes within the STs that induce a trend	(Beck *et al.*, 2007)
Paper I	Method of hypothetical trends	Method to calculate the influence of circulation changes on a trend	(Leathers and Ellis 1996; Cahynová and Huth 2009)
Paper II	Probabilistic approach	Expanded hypothetical method	(Nilsen *et al.*, 2017b)
Paper I	Hypothetical trend, t_{circ}	Trend resulting from changed frequency of STs	(Huth, 2001)
Thesis	**Circulation-induced trend**, t_{circ}	The same as hypothetical trend	(Fleig *et al.* 2015; Cahynová and Huth 2016)
Paper II	Synoptic-circulation-induced trend	Hypothetical trend resulting from the probabilistic approach	(Nilsen *et al.*, 2017b)
Paper II	Circulation-induced component of the trend, m_{SC}	Median of the distribution of synoptic-circulation-induced trends	(Nilsen *et al.*, 2017b)
Paper I and II	Within-type trend	Component of the trend that is independen of circulation changes	

4.2.2 Method of hypothetical trends

The method of hypothetical trends (Leathers and Ellis, 1996; Huth, 2001; Cahynová and Huth, 2009) (also called method of circulation-induced trends, Cahynová and Huth 2016) provides a way to separate circulation changes from within-type changes. A new, hypothetical time series is constructed by replacing all observations in a month and ST with the long-term mean of all days having the same month and ST. The trend of the hypotetical time series is called the hypothetical trend. To assess the influence of circulation changes on the estimated observed trend, the hypothetical trend, t_{circ}, is divided by the estimated observed trend, t_{obs}, to obtain the *trend ratio*, r_{circ}. If the trend ratio is close to 1, the hypotetical trend can explain the observed trend well, and the observed trend can be attributed to circulation changes.

For trend ratios close to 1 (in Paper I, 0.5–1.5), the estimated observed trend cannot be explained by circulation changes alone, and the estimated observed trend is partly attributable to within-type changes. Small trend ratios (below 0.5) indicate within-type changes. In that case, the temperature trend could not be explained by circulation changes alone. Trend ratios exceeding 1.5 were not considered because they often stem from dividing by small estimated observed trends (Fleig *et al.*, 2015).

4.2.3 Probabilistic approach

The method of hypothetical trends and trend ratios (Section 4.2.2) does not contain any way of assigning a statistical significance to the circulation changes, nor any way of avoiding high trend ratios when dividing by a small estimated observed trend. Paper II contains an expansion of the method of hypothetical trends, denoted the *probabilistic approach for attributing temperature changes to synoptic type frequency*, or probabilistic approach, for short.

The probabilistic approach developed in Paper II provides a statistical test of whether the estimated observed trend can be explained by changes in circulation alone. First, we derived the empirical distribution of circulation-induced trends by repeated historical resampling. Building on the method of hypothetical trends by Cahynová and Huth (2009), we generated a large set of circulation-induced trends by resampling 10 000 times. Second, for the resulting distribution of circulation-induced trends, we applied a Monte Carlo test to test the likelihood that the estimated observed trend could be randomly generated from the following empirical distribution.

H_0: The estimated observed trend can be explained by changes in atmospheric circulation alone.

H_a: The estimated observed trend cannot be explained by changes in atmospheric circulation alone.

The closer the estimated observed trend is to the median of the circulation-induced trends, the more likely it is that the estimated observed trend is caused by circulation changes alone. If the estimated observed trend is significantly different from the median, it is not likely caused by circulation changes. Two requirements must be fulfilled before the temperature trend can be attributed to within-type changes: i) the estimated observed temperature trend must be statistically significant, and ii) the alternative hypothesis must be valid, see Figure 4.1, panel (b). The probabilistic approach does not quantify the magnitude of within-type trends, but tests whether within-type changes contribute to the estimated observed temperature trend or not.

4.3 Assessment of the physical drivers of temperature trends

The climatological cause of trends was assessed in a detailed study of concurrent changes in snow indices and temperature trends for Norway (focusing on the snow albedo feedback; Paper III) and through a model diagnostic study (Paper IV). This last paper explored both the snow albedo feedback and the soil moisture–temperature feedback, their sensitivity to a longer snow-free season and anomalously dry weather situations.

Many different methods of diagnosing land–atmosphere coupling exist, ranging from correlations between the land state and atmospheric state (e.g. Dirmeyer *et al.*, 2009; Halder and Dirmeyer, 2017), to running long-term climatology models (Miralles *et al.*, 2014; Walton *et al.*, 2017), and to running complex ensemble models comparing one fully coupled soil moisture (or snow) ensemble with a prescribed soil moisture (or snow) ensemble (Koster *et al.*, 2004; Seneviratne *et al.*, 2006, 2010). Many of these methods are costly in terms of computing power; running an ensemble, or running a 30-year period for climatology would increase the computation time in Paper IV by an order of magnitude. The snow albedo feedback was assessed through correlations in Paper III (see Figure 2.2a) and through comparing temperatures and radiation fluxes across different model runs in Paper IV.

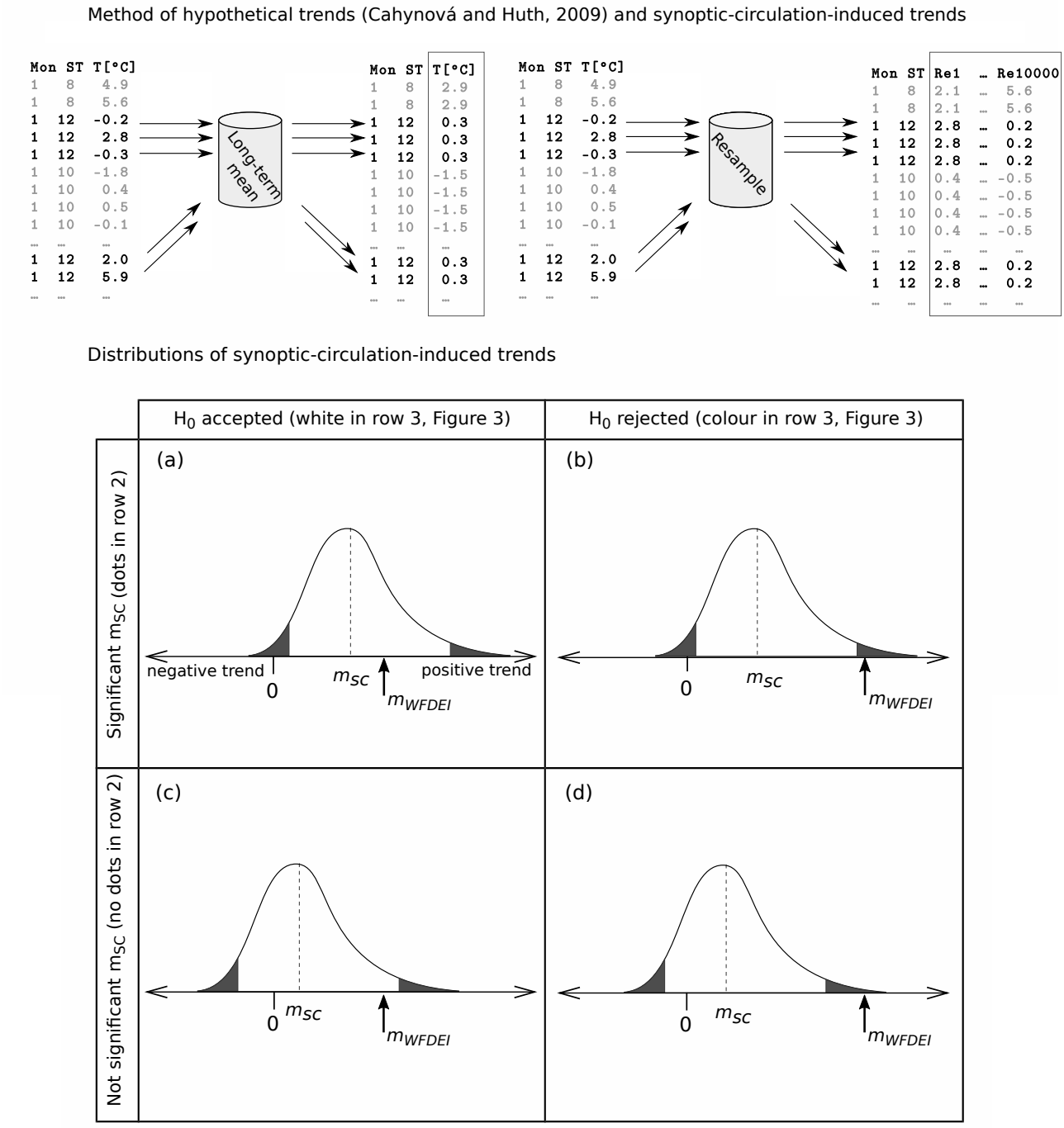

Figure 4.1: Figure 1 from Paper II, explaining the probabilistic approach. From Nilsen *et al.* (2017b).

For the soil moisture–temperature feedback, we chose the two-legged metric, consisting of correlations between the soil moisture and latent heat, $\rho(SM, LE)$ and between latent heat and air temperature, $\rho(LE, T)$. As depicted in Figure 2.2b, $\rho(SM, LE)$ reveals whether the soil moisture controls the latent heat flux, or the other way around. Coupling leading to a positive feedback occurs only if the soil moisture is low enough to control the latent heat, i.e., a positive $\rho(SM, LE)$ (see "Terrestrial leg" in Figure 2.2b). If the temperature rises as a result of reduced evaporative cooling, a negative correlation between latent heat and air temperature, $\rho(LE, T)$ indicates a soil moisture limitation on evapotranspiration (Seneviratne *et al.*, 2006; Dirmeyer *et al.*, 2009; Lorenz *et al.*, 2012) (see "Atmospheric leg" in Figure 2.2b). In that case, the reduced latent heat may accelerate warming. For land–atmosphere coupling to be present, both the terrestrial and atmospheric legs must be in place (Dirmeyer, 2011; Dirmeyer *et al.*, 2014; Halder and Dirmeyer, 2017).

4.3.1 Model diagnostic study

The regional climate model Weather Research and Forecasting (WRF) (Skamarock and Klemp, 2008), coupled to the land surface model Noah-MP (Niu *et al.*, 2011) was used to explore the physical drivers of temperature trends (Paper IV). Details of the model setup are given in Table 4.2.

Land surface models are employed to handle the land surface component of regional climate models. Noah-MP (Niu *et al.*, 2011), a multi-parameterisation development of the Noah land surface model, was created to allow for a large physical ensemble of model simulations within the same model. Noah-MP and its predecessors Noah-LSM/Noah-UA have been applied for different applications in central and northern Europe (Schwitalla *et al.*, 2011; Greve *et al.*, 2013; Gayler *et al.*, 2014; Mayer *et al.*, 2015; Rydsaa *et al.*, 2016; Aas *et al.*, 2017; Erlandsen *et al.*, 2017).

In Paper IV, we hypothesised that the warming detected for April was enhanced by the snow albedo feedback, and that the warming detected for July–September was enhanced by the soil moisture–temperature feedback (provided sufficiently dry conditions). The warm summer of 2014 was a plausible candidate for dry conditions and was chosen for control simulations with a coupled WRF–Noah-MP model. To simulate drier summer conditions, we i) increased the length of the snow-free season, and ii) introduced boundary forcing from a warm and dry summer (2006). In total, six model runs were performed (see Figure 4.2e): The first three runs differed only in their initial ground conditions (snow-poor, control and snow-rich) and used boundary forcing from the warm summer of 2014. The next three runs kept the same initial

Table 4.2: WRF–Noah-MP model configuration for Paper IV. From (Nilsen *et al.*, 2017a) (Table 2 in Paper IV).

		Reference
Atmospheric model	WRF v 3.7.1	Skamarock *et al.*, 2008
Land surface	Noah-MP with default options	(Niu *et al.*, 2011)
Microphysics	WRF Single-Moment 3-class (WSM3)	(Hong *et al.*, 2004)
Boundary layer physics	Mellor-Yamada-Janjic (MYJ)	(Janjić, 1994)
Surface layer	Eta surface layer scheme	(Janjic, 2002)
Radiation (LW & SW)	RRTMG	(Iacono *et al.*, 2008)
Cumulus	Kain-Fritsch in d01, resolved in d02	(Kain, 2004)
Simulation period	Experiments: 12 May–30 September	
Spin-up period	10.5–12.5 months (depending on run)	
Forcing data	Era-Interim; 1995, 2006, 2014	(Dee *et al.*, 2011)
Land cover	20-class MODIS 15 arc seconds	(Broxton *et al.*, 2014)
Timestep	45 s	
Nesting	Two-way nesting	
Resolution in d01	15 km (100×100 cells)	
Resolution in d02	3 km (155×185 cells)	

conditions as before and used boudnary forcing from the warm and dry summer of 2006.

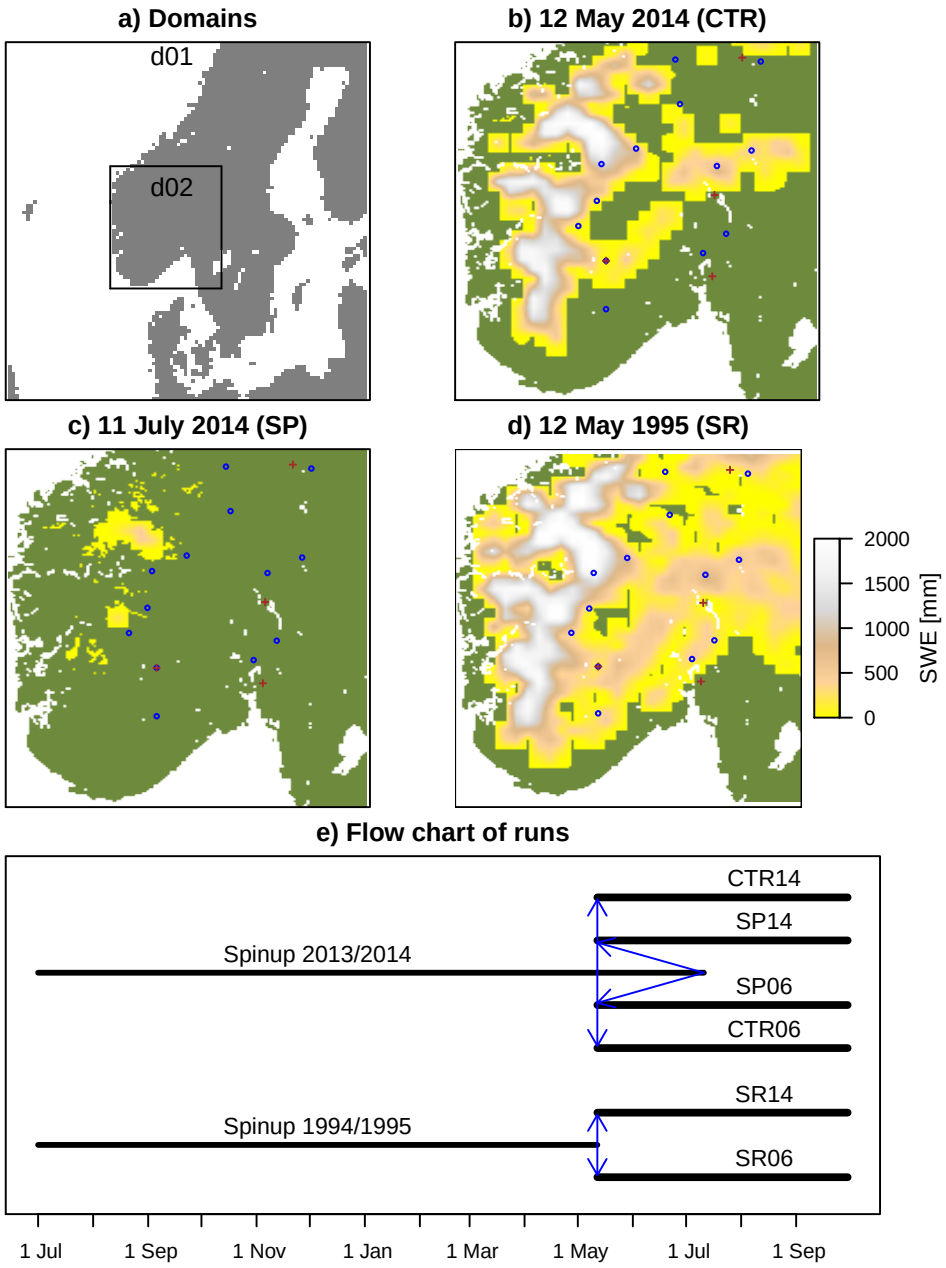

Figure 4.2: Figure 2 from Paper IV. a) Model domains, b–d) initial SWE at the start of the model run at b) 12 May 2014 (CTR), c) 11 July 2014 (snow-poor, two months earlier melting), and d) 12 May 1995 (snow-poor). e) Schematic of the different model runs. Note that in addition to SWE, we swapped snow depth, snow albedo, soil moisture, skin temperature, initial temperature, soil category fraction at the bottom and top, and an indicator function for snow. From (Nilsen *et al.*, 2017a).

Chapter 5

Findings

This section summarises the main results of the thesis, based on the four papers. A schematic of the papers is shown in Figure 1.1 and the results are further discussed in Section 6 (General discussion). Figure numbers refer to this thesis, unless stated otherwise.

5.1 Paper I: Recent trends in monthly temperature and precipitation patterns in Europe

Climate change is characterised by large spatial and temporal variations. In this study, we investigated the spatial pattern of precipitation and temperature trends in Europe for each calendar month. For this purpose, we used gridded precipitation and temperature data from WFDEI (Weedon *et al.*, 2014). The period 1979–2009 was chosen because it is a period commonly used for climate trends, and because of the availability of WFDEI data at time of the study. Further, a catalogue of synoptic types, SVG by P. James, was used in the method of hypothetical trends (Section 4.2.2) to attribute the WFDEI trends either to changing frequency of synoptic types or within-type changes. Note also that some of the terminology changed from Paper I to Paper II, as summarised in Table 4.1 and Section 4.2.1.

Main results Results were shown as "observed" WFDEI trends, t_{obs}, hypothetical trends, t_{circ}, and trend ratios, r_{circ} ($r_{circ} = t_{circ}/t_{obs}$) for the annual scale and for February in the paper. A complete figure for all months is shown in Figure 5.1, for temperature. This figure shows winter/spring and summer/autumn on two different pages.

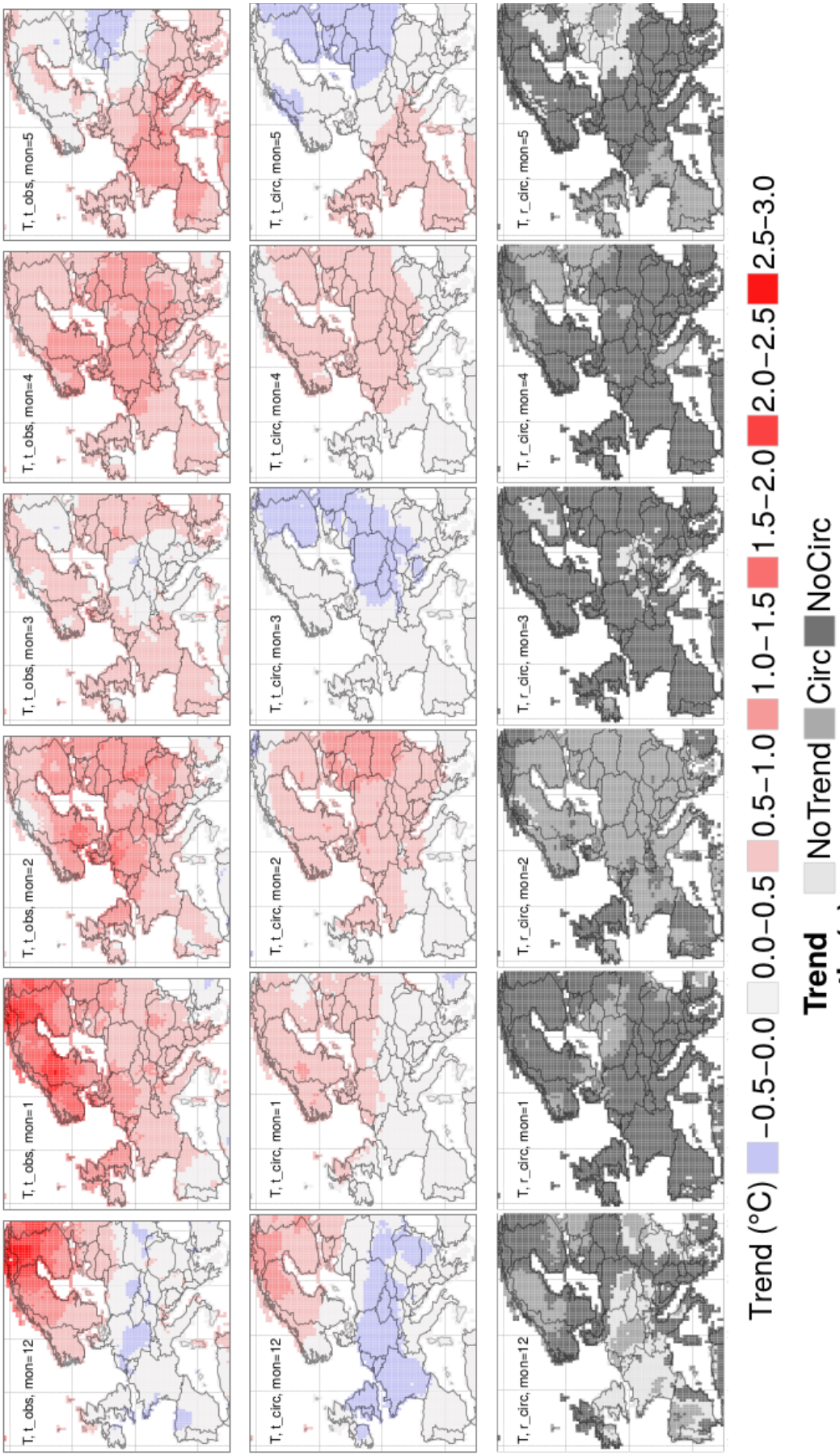

Figure 5.1: Complete Figure 2 (Paper I) of temperature, for winter and spring months (1979–2009). Left: WFDEI trend, t_{obs}, middle: circulation-induced trend, t_{circ}, right: trend ratio r_{circ}. Modified from (Nilsen *et al.*, 2014). Continued on the next page.

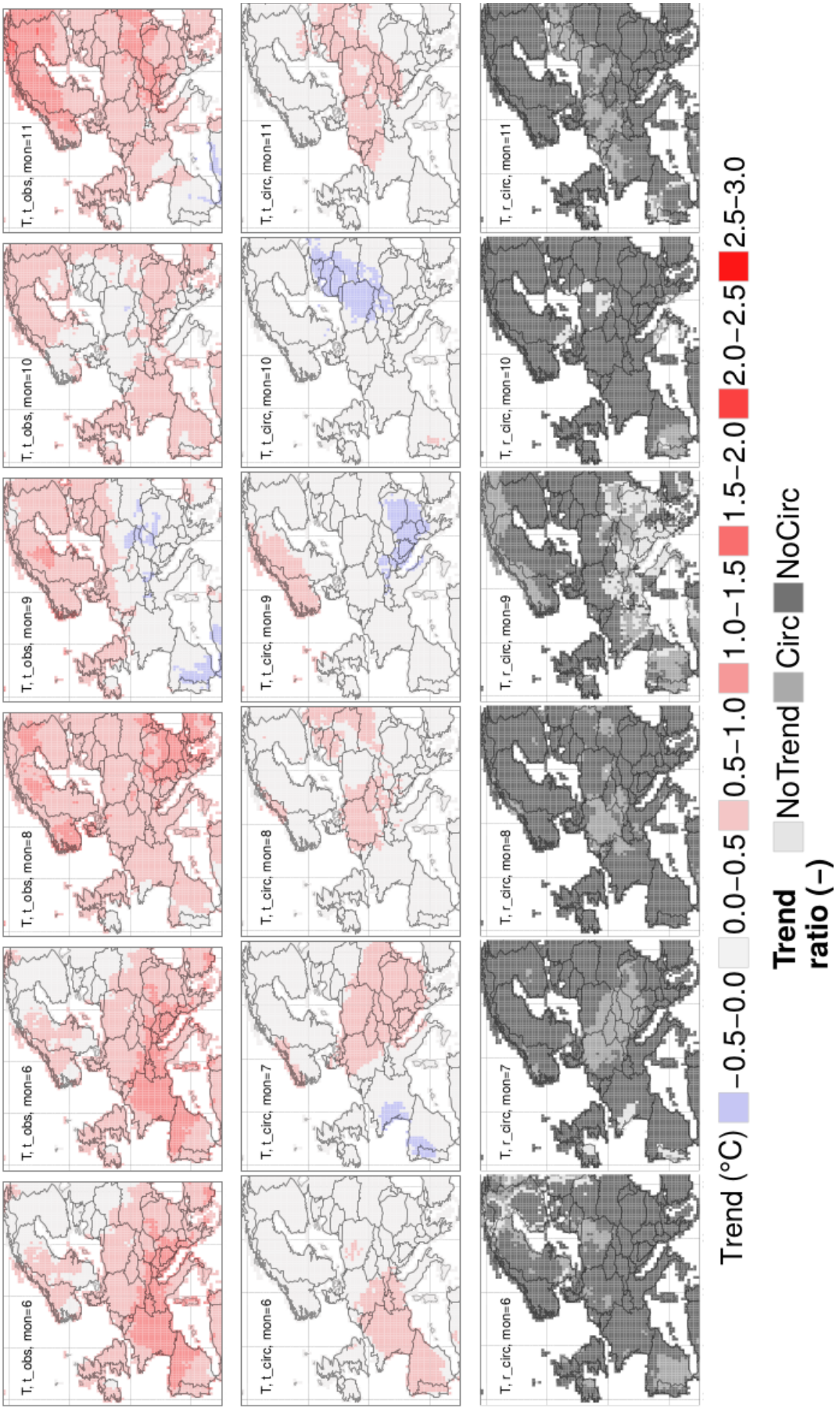

Figure 5.1: (contd.) Complete Figure 2 (Paper I) of temperature, for summer and autumn months (1979–2009). Left: WFDEI trend, t_{obs}, middle: circulation-induced trend, t_{circ}, right: trend ratio r_{circ}. Modified from (Nilsen *et al.*, 2014).

A dominant warming signal was observed in winter, spring and summer; during autumn, weak cooling trends were observed in southern Europe (Figure 5.1, upper row). Strong warming, up to 2.5 °C/decade, was seen in North Scandinavia in December and January (0.8 °C/decade on the annual scale). The summer warming occurred concurrently with negative streamflow trends for central Europe (Stahl *et al.*, 2010).

Circulation-induced trends generally resembled observed trends, but displayed a smoother spatial pattern and weaker trend magnitudes (Figure 5.1, middle row). The trend ratio highlighted regions in almost all months in which WFDEI trends could be explained by the circulation changes. The most wide-spread signal of circulation changes was found in February followed by December, September, May and April (Figure 5.1, marked as "Circ" in the bottom row). This strong influence of circulation changes in winter is consistent with an increased NAO index until the 1990s. Trend ratios less than 0.5 suggest that the trend was influenced by other factors than circulation changes (Figure 5.1, marked as "NoCirc" in the bottom row). This was found for most other months than the ones listed above. Only a few regions are marked "NoTrend", that is, where t_{obs} was so small that the resulting trend ratio exceeded 1.5.

Similar figures for precipitation (not shown) were more patchy than temperature trends. This is partly because of the more local nature of precipitation than temperature, especially in summer when convective storms dominate. Circulation-induced precipitation trends could also be influenced by the performance of the SVG, see Figure 3.2, bottom. Based on this figure, we decided not to use precipitation in the further studies.

Strong warming was detected for Scandinavia (exceeding 2 °C over the 31-year period, or 0.8 °C/decade, on the annual scale, and higher for December and January). This strong warming motivated a review of previous regional temperature trends in Europe, shown in Table 2.1. All trends are sensitive to the time period chosen, thus, other periods than the one chosen in Paper I (1979–2009) would result in different results. Comparing Figure 5.1 to Figure 5.2 shows the effect of changing the analysis period from 1979–2009 to 1981–2010. The winter 2009/2010 was very cold in Europe due to weakened westerly air flow, in fact, the NAO index was record low (Osborn, 2011). A broader picture of trends could be explored by analysing running 30-year trends, similar to Hannaford *et al.* (2013).

Unrealistically high trend ratios may result when the observed trend (in the denominator) is close to zero. In Paper I, we solved this by adding cut-off values of 0.5 and 1.5, inspired by Cahynová and Huth (2009) and Fleig *et al.* (2015). Further, the trend ratio fails to capture changes when both circulation changes and within-type changes play a role but in opposite directions. These two arguments motivated us to

extend the method of hypothetical trends in Paper II.

5.2 Paper II: A probabilistic approach for attributing temperature changes to synoptic type frequency

The probabilistic approach developed in Paper II provides an assessment of the likelihood that the estimated observed trend is attributable to circulation changes alone and allows assigning a statistical significance to the circulation changes (described in Section 4.2). The objective of Paper II was to separate the cause of temperature change into within-type changes and circulation changes (similar to Paper I), however, by applying the probabilistic approach to temperature changes in Europe (WFDEI). The period 1981–2010 was chosen so the results could be comparable with other studies using the World Meteorological Organisation's reference period.

Main results Annually, WFDEI temperature trends calculated using Sen slopes were positive for nearly all of Europe. On the monthly scale, significant temperature trends were found in large parts of Europe in April–August, and in November (Figure 5.2, upper row). The circulation-induced component of the temperature trend (median of the distribution; middle row) could explain warming trends for western Europe in May (and in the Balkans in February and Belarus in August). Here, both the WFDEI trends and circulation-induced trends were significant. Regions where the within-type changes played a role are presented in the bottom row of Figure 5.2. In the bottom row, dots are the same as in the upper row, denoting where the WFDEI trend is significant. Dots on a white background in the bottom row mean that the temperature trend can be explained by circulation changes; dots on colour mean that within-type changes are responsible for at least a part of the temperature trend. Figure 4.1 shows the difference between dots on white (panel (a)) and dots on colour (panel (b)). Overall, within-type changes could partly explain the warming in April, June–August for large parts of Europe, and in November north of the Black Sea. For South Norway, April and July–September temperature trends could partly be explained by within-type changes. Regions where temperature changes could partly be attributed to within-type changes may potentially suggest the presence of feedbacks between the land surface and atmosphere. A closer look reveals within-type changes along the coast and inland in June and along the southern coast in September.

When comparing Figure 5.2 to Figure 5.1, similarities in the WFDEI temperature trends are evident, for instance in the strong winter warming, and the cooling in

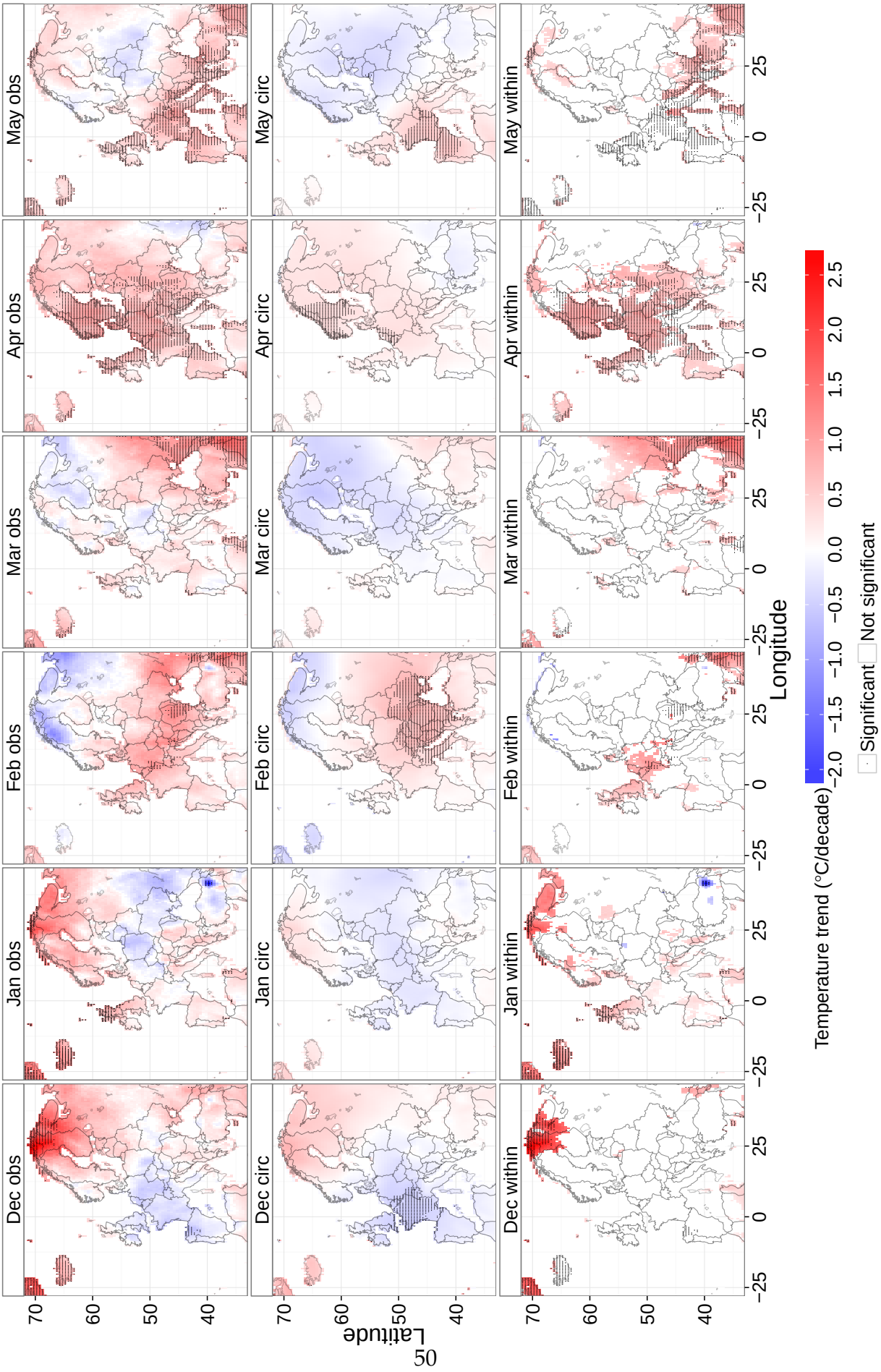

Figure 5.2: Figure 3 from Paper II. Temperature trends for winter and spring (1981–2010) for a) estimated observed WFDEI trends. b) circulation-induced component of the WFDEI trend. c) Within-type changes (in colour). Regions shaded by dots mark significant trends. From (Nilsen *et al.*, 2017b).

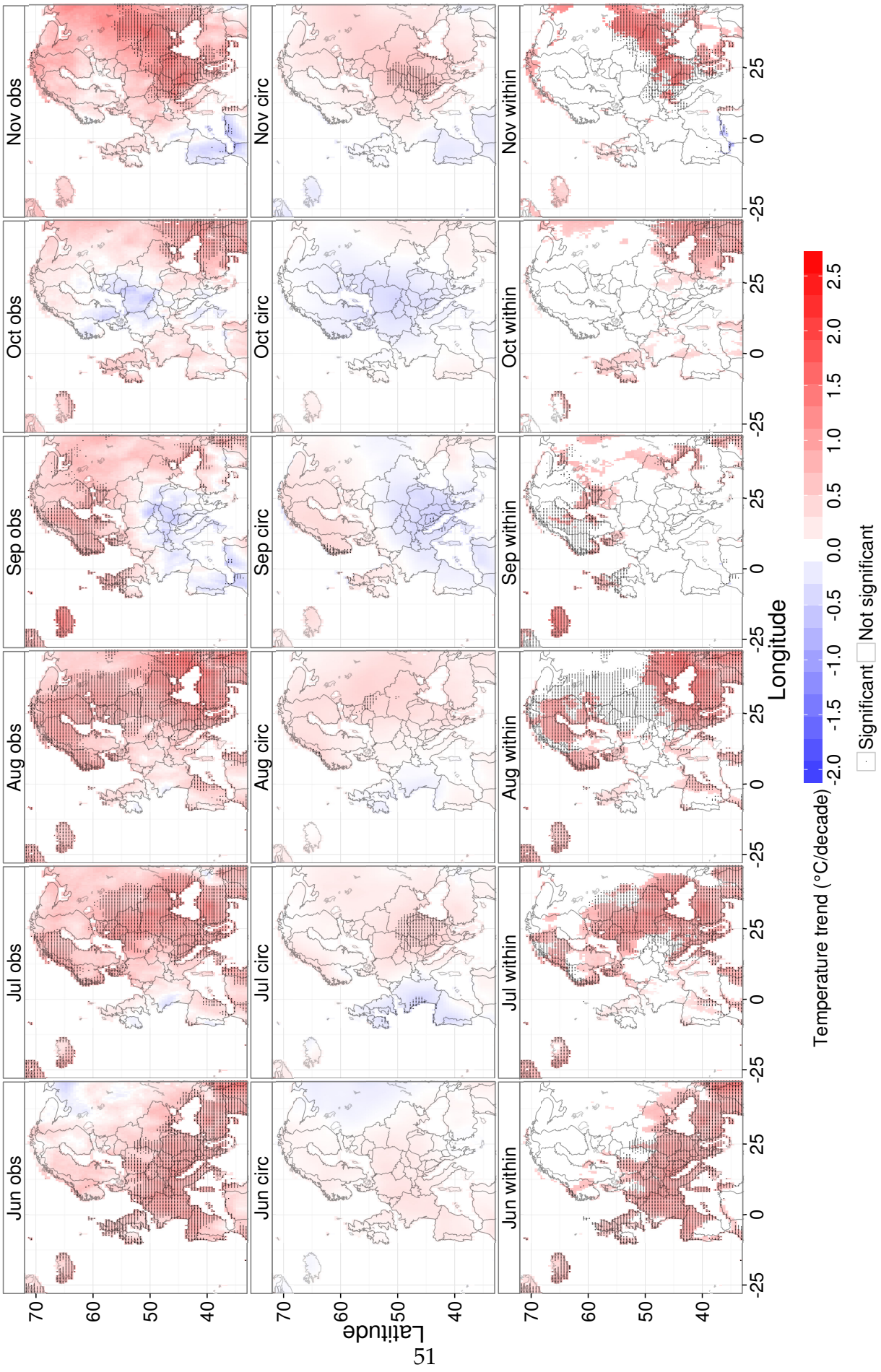

Figure 5.2: Figure 3 from Paper II. Temperature trends for summer and autumn (1981–2010) for a) estimated observed WFDEI trends. b) circulation-induced component of the WFDEI trend. c) Within-type changes (in colour). Regions shaded by dots mark significant trends. From (Nilsen *et al.*, 2017b).

May, September and December. In January and February, Figure 5.2 displays strong cooling (in eastern Europe in January and in Scandinavia in February), whereas Figure 5.1 displays warming or no trend. Circulation-induced trends (middle row) differed in January. This example shows that trends are sensitive to a slight change in time period (1979–2009 vs 1981–2010), but agreed well for months other than January and February. Trends explained by circulation changes (compare the bottom row of Figure 5.1 with dots in the middle row of Figure 5.2) aligned reasonably well, for instance for February (eastern Europe), May (France, Spain), July (eastern Europe) and September (Norway). The two bottom rows of Figure 5.2 and Figure 5.1 deviates to a large extent, however. This deviation reflects the different methods used in Paper I and Paper II (discussed further in Section 6.2). The circulation-induced warming May and to a smaller extent February is captured in both Figures, but Figure 5.1 showed circulation-induced trends in other months and regions as well. Last but not least, regions of within-type change differed greatly.

Regions where temperature changes could partly be attributed to within-type changes may potentially suggest the presence of feedbacks between the land surface and atmosphere. In Paper II, that was the case for South Norway in spring and summer.

5.3 Paper III: Five decades of warming: impacts on snow cover in Norway

Strong decreases in the snow season duration in spring have been linked to accelerated spring warming (Thackeray and Fletcher, 2016). Paper III (led by J. Rizzi) was motivated by the strong winter trends detected in Paper I. Further, in Paper II, April was highlighted as a month with significant warming that could not be attributed to changes in the synoptic-type frequency. The aim of Paper III was to detect changes in snow indices and climate variables in Norway and to assess the snow albedo feedback as a possible driver of these changes. In this study, we performed a detailed analysis of trends and changes in snow climatology using the datset SeNorge (1×1 km, covering mainland Norway) for different 30-year periods within 1961–2010. Trend analyses of monthly temperature were done for 1981–2010, the same period as in Paper II. Relationships between snow water equivalent (SWE), snow cover extent (SCE), temperature (T), and precipitation (P) were presented for Norway as a whole, and for four macro regions (North, South-East, South-West and Mountains) and 19 sub-regions.

Main results The snow cover extent declined in all four macro regions. The strongest reduction occurred in spring, particularly in April for low-lying regions in South Norway and in May, further inland and further north (see Figure 3 in Paper III). Between 1981–2010 and 1961–1990, SCE decreased by nearly 25 000 km^2 in April and more than 25 000 km^2 in May (8% of the total land area of mainland Norway). November and December experienced the second largest loss of SCE (about 15 000 km^2; Figure 5a in Paper III). The regions South-East and South-West experienced the most dramatic reduction in SCE, relative to their areas. The region Mountain experienced a decline in SCE, but an increase in SWE due to increased precipitation rates (Figure 5a and b, in spring).

Snow changes were accompanied by a decrease in the length of the snow season, particularly in spring. Correlation analyses showed that SCE was negatively correlated with temperature (significant in all months except summer), supporting our hypothesis that the snow albedo feedback enhances snowmelt in spring. A stronger difference in spring than in autumn was expected because both snow cover and sunlight is abundant in spring. Further, strong temperature trends were found in April across all of Norway, accompanied by strong SCE reductions in the same month. These findings support the hypothesis of an active snow albedo feedback, particularly in spring.

Further analyses of SeNorge temperature trends showed widespread warming in July, August and September, in addition to April (for the period 1981–2010; Figure 7 in Paper III), confirming trends detected in WFDEI from Paper II. The strongest warming was observed in North Norway in December, close to 3 °C/decade, however, only a part of these trends were significant. In winter, the interannual variability of trends was high (shown as a large inter-quartile range), which explained why the highest trends in North Norway were not significant in all grid cells. Boxplots of temperature trends (Sen slopes) for three 30-year periods revealed that trends were sensitive to the time period chosen (Figure 8 in Paper III). For April, the warming accelerated between 1961–1990, 1971–2000 and 1981–2010. August and September also displayed accelerated warming.

5.4 Paper IV: Diagnosing land–atmosphere coupling in a seasonally snow-covered region (South Norway)

The processes driving within-type changes detected in Paper II, supported by strong snow and temperature changes in Paper III, were further explored in the model dia-

gnostic study in Paper IV. South Norway was chosen as the study area for modelling based on a range of factors:

i) the presence of within-type changes in April and July–September,

ii) availability of a high-resolution dataset for Norway (SeNorge),

iii) because this region allowed testing both the snow albedo feedback and the soil moisture–temperature feedback in one study region,

iv) because previous studies have documented drying summer conditions in South Norway (Wilson *et al.*, 2010; Stahl *et al.*, 2012) and

v) the discriminative capability of the SVG classification was considered sufficiently high to give trust in the main results for South Norway.

Although North Norway displays strong within-type changes in many months (particularly in winter), this region was not considered for the model-diagnostic study, partly because of the low discriminative capability far away from central Europe (as discussed in Section 3.3). Because we are interested in the snow albedo feedback and soil moisture–temperature feedback, the location of within-type changes in April and summer were given more weight than the strong within-type signal in North Norway in winter (when the ground is expected to be fully snow-covered throughout the period and no snow albedo feedback is expected).

To our knowledge, the soil moisture–temperature feedback has not peviously been studied for Norway, where evapotranspiration is generally energy limited rather than soil moisture limited. The experiments for the coupled model WRF–Noah-MP were therefore designed to simulate anomalously dry conditions to trigger soil moisture-limited conditions. The warm summer of 2014 and the warm and dry summer of 2006 were chosen for the purpose.

Main results Changes in the snow cover had direct effects on temperature, soil moisture, and evapotranspiration during the melting period, supporting that the snow albedo feedback enhanced the spring warming in the region influenced by snow changes and, for a large part of South Norway, even after snowmelt. For example, air temperatures over snow-free ground were about 5 °C higher than air temperatures over snow-covered ground (at station Kyrkjestølen).

The soil moisture–temperature feedback was diagnosed by correlating soil moisture and latent heat, $\rho(SM, LE)$; i.e., the terrestrial leg of land–atmosphere coupling,

and by correlating latent heat and air temperature, $\rho(LE, T)$; i.e., the atmospheric leg (Dirmeyer, 2011). The postitive soil moisture–temperature feedback acted in the Oslofjord region (along the southeastern coast of South Norway) during 2014 and 2006. Both the atmospheric leg, Figure 5.3a–f, and the terrestrial leg were present during 15 July–14 August, to a larger degree in 2006 than in 2014. Thus, a positive feedback on temperature was initiated by the warmer than average conditions in 2014 (and for 2006: warmer and drier than average conditions), and further enhanced by a soil moisture limitation on evapotranspiration. A longer snow-free season did not influence this soil moisture–temperature feedback, likely because the changes in the initial ground conditions were not large enough to induce a sufficiently low soil moisture content. Changing the atmospheric boundary forcing to the warm and dry 2006 summer had a larger effect on the strength and extent of the coupling leading to a positive feedback, than changing the initial conditions. Thus, the enhanced warming was caused by a lack of rainfall rather than a longer snow-free season.

To strengthen our confidence in the model results, correlations were calculated for the estimated observed dataset of interpolated temperatures, and modelled evapotranspiration and soil moisture deficits (SeNorge). SeNorge confirmed WRF–Noah-MP results, displaying enhanced warming in the Oslofjord region (Figure 5.3g–h). SeNorge also confirmed the more widespread pattern of the terrestrial leg than the atmospheric leg. However, differences in the extent of positive coupling between WRF–Noah-MP and SeNorge were seen. In particular, coupling was detected for the (north-)western coast in 2006 and the mountains in WRF–Noah-MP, but not in SeNorge. We proposed some improvements to the evapotranspiration estimations in Noah-MP and in SeNorge that could alleviate discrepancies between the two datasets in further studies, namely i) improper representation of soil depth/root depth and ii) improper parameterisations of for instance evapotranspiration.

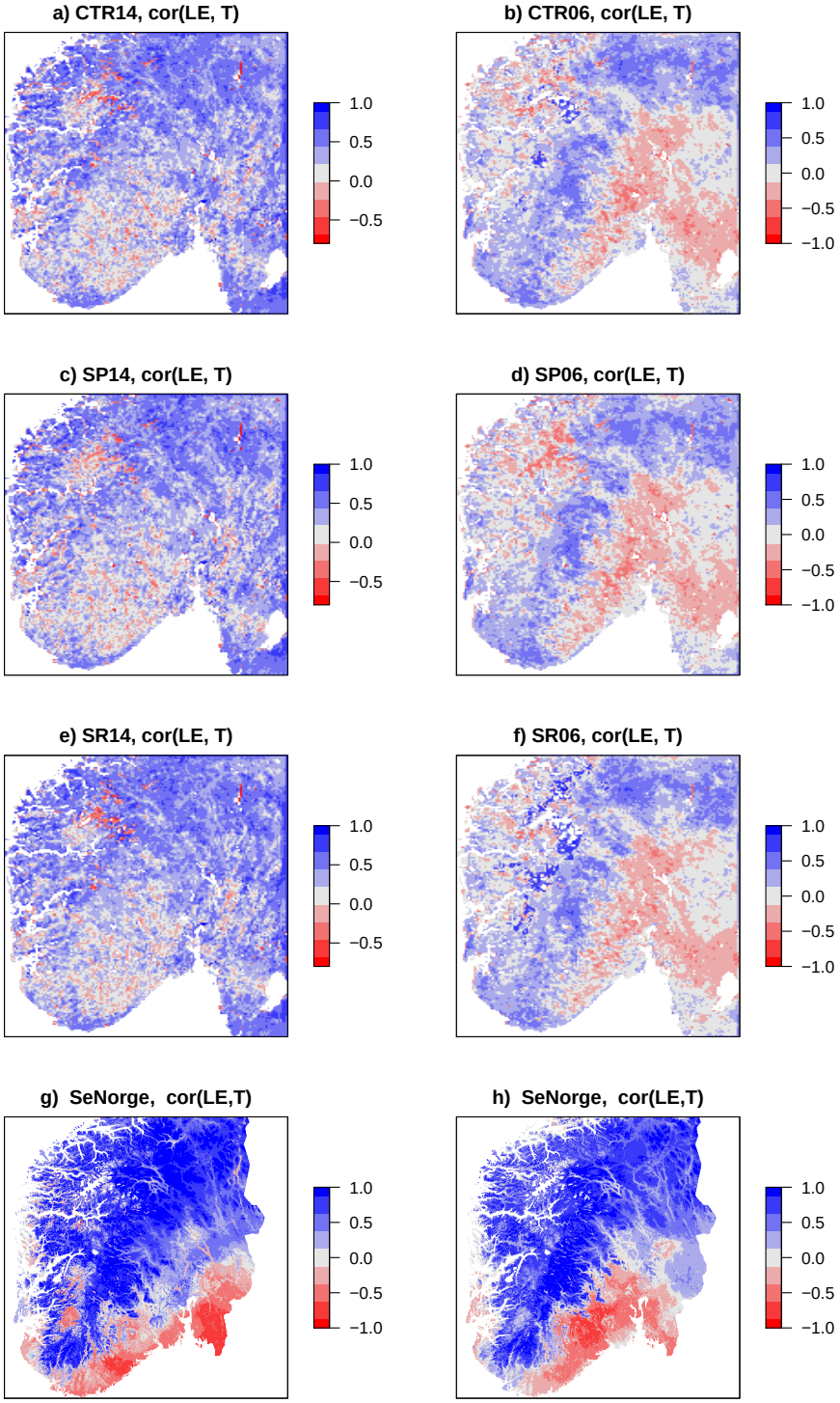

Figure 5.3: Figure 7 from Paper IV. Atmospheric leg of land–atmosphere coupling (negative correlation, $\rho(LE, T)$ indicates coupling) for the period 15 July–14 August 2014 (left) and 2006 (right). Rows 1–3 show CTR, SP and SR, respectively, from the WRF-Noah-MP runs. SeNorge is shown in the last row. A red colour indicate coupling in all plots. From (Nilsen *et al.*, 2017a).

Chapter 6

General discussion

Understanding circulation changes and land–atmosphere interactions are crucial for our understanding of what drives hydroclimatic change. Although the broader picture of climate trends on a global and annual scale is well understood, research efforts are now moving towards understanding the detailed mechanisms leading to temperature change at the regional and seasonal scale. This section discusses the main outcomes of this work, including uncertainties. Suggestions for further studies are integrated in the text.

6.1 Trend detection

6.1.1 Comparing detected trends across time periods and datasets

The trend results depend on choices and assumptions made, specifically, on the chosen dataset, method (e.g. Cahynová and Huth, 2009), time period (Hannaford *et al.*, 2013), and spatial and temporal aggregation. Robust results emerged, however, across different datasets and slightly different periods in Papers I, II and III. SeNorge confirmed the strong winter trends in northern Norway, and significant April, and July–September warming in South Norway (Figure 7 in Paper III). This similarity was expected because temperature datasets are well-constrained by observations and well-tested. SeNorge temperatures are interpolated from stations run by the Norwegian Meteorological Institute, whereas WFDEI is based on a reanalysis datset (ERA-Interim), bias-corrected against CRU stations. Thus, some of the same stations have been used both in SeNorge and WFDEI, giving rise to the same result. However, the station network in SeNorge is finer than the one used by CRU, and has a much finer spatial resolution, which results in a more reliable dataset. Obtaining the same

results with different datsets strenghtens our confidence in the results. Similarly, large patterns of trends in the same direction also strengthens our confidence in the results.

6.1.2 Sensitivity to time period and time scale

Changing the period of WFDEI trends from the period 1979–2009 to 1981–2010 yielded similar results, except for winter trends. Results in Figure 5.1 and Figure 5.2 mainly differed in January and February, when the interannual variability was high. This example shows that a small change at the beginning or end of the period (shifted two years and from 31 years to 30 years) was sufficient to influence the results, at least for certain months. The latest period included the cold winter 2009/2010 (Hurrell and Deser, 2009), which likely caused the cooling trends seen for the 1981–2010 period (in eastern Europe in January and in Scandinavia in February).

In Paper III (Figure 8), the periods were shifted by 10 years, showing a $>$0.5 °C higher trend for the period 1981–2010 than 1961–1990, for December and August. NAO was highlighted as the main cause of winter warming in Paper II, and the importance of NAO has been pointed out in many studies of circulation-induced trends in Europe for the period starting before $\approx$1980 and ending after $\approx$2000 (Cahynová and Huth 2010, (1961–1998), Cahynová and Huth 2016, (1961–2000), Fleig *et al.* 2015, (1963–2001), Kučerová *et al.* 2017, (1957–2002)). Given that NAO explains a large degree of the winter weather in Europe, the temperature trend is strongly related to the chosen time period (see Figure 2.1).

The choice of temporal aggregation also influences the results. Monthly trends, calculated in Papers I, II, and III may mask important sub-monthly signals. One example is the increased evapotranspiration related to leafing in spring, which may occur in the course of a few days or weeks. Still, a monthly time scale is finer than in most published trend studies and reveals strong trends that point towards specific physical processes influencing the warming.

A general recommendation for future studies is to use more than one dataset (STs and climate data), using more than one trend period, and possibly different trend methods and time resolutions. Using gridded data allows for spatially coherent patterns that increases our confidence in the results. Those trends that emerge across datasets, trend periods etc. would be considered (very) robust. This is normally outside of the scope of many studies, but it is possible given the increasing computing power and collaborative efforts in the scientific community today.

6.2 Statistical attribution of recent temperature trends

The role of atmospheric circulation on the local climate has been a topic of research for decades, reviewed by e.g. Huth *et al.* (2008, 2016). In particular, attribution of climatic trends into either circulation changes or within-type changes has received much attention (e.g. Beck *et al.*, 2007; Cahynová, 2010; Küttel *et al.*, 2011; Hertig *et al.*, 2015; Cahynová and Huth, 2016). We developed a probabilstic approach to attribute the relative importance of circulation changes on climate trends (Paper II) to guide us towards regions of possible feedback mechanisms (regions of within-type changes). The following sub-section contains comments on differences between regions detected as circulation changes in Papers I and II. Sub-section 6.2.2, contains comments on differences between regions detected as within-type changes in Papers I and II.

6.2.1 Differences in circulation changes

Circulation changes marked in the bottom rows of Figure 5.1 and Figure 5.2 agreed reasonably well despite the different methods used in Papers I and II. Paper I used the simple trend ratio to compare the estimated observed trend to a circulation-induced trend that would have resulted if changes in the frequency of synoptic types governed the estimated observed trend. Paper II used a probabilistic approach to derive a distribution of circulation-induced trends by resampling. Figure 5.2 marks regions where the median of the distribution was significantly different from zero (dots in the middle row of this figure), that is, for western Europe in May and to a smaller extent central Europe in July and in the Balkans in February (where the estimated observed trend covered limited regions). Thus, the method for determining whether trends are explained by circulation changes is quite similar in the trend ratio method and the probabilistic approach. It is worth noting that circulation changes did not explain the strong warming in Finnmark, northern Norway, in December and January, in either of the methods.

6.2.2 Differences in within-type changes

For within-type changes, however, the two methods differed substantially. In the probabilistic approach, within-type changes are determined by comparing the estimated observed trend to the distribution of circulation-induced trends. The estimated observed trend is attributed to local effects if it is sufficiently far into the tail of the distribution. This is in contrast to the trend ratio, where the trend is either explained by

circulation changes or by within-type changes. Thus, the probabilistic approach has a stricter criterion to assign the within-type change than the trend ratio, and leaves many grid cells blank. There are two reasons for this. The first reason is the requirement for a *significant* estimated observed trend – in Paper I, we did not calculate significance, but discarded trend ratios exceeding 1.5. A less strict significance level on estimated observed trends would render larger regions of significant estimated observed trends. For instance, single dots in Figure 5.2, such as for South Norway in June, would be accompanied by dots covering a larger region with a less strict significance level. The other reason is that the probabilistic approach uses a standard significance level for the difference between m_{circ} and t_{WFDEI} of 0.05. Larger regions of within-type change would appear in case of a less strict significance level on the test that the likelihood that the estimated observed temperature trend belongs to the distribution of circulation-induced trends (H_0 and H_a in Paper II).

Both Cahynová and Huth (2009) and Fleig *et al.* (2015) define within-type changes as changing internal properties of STs (e.g. that STs warm over time). Beck *et al.* (2007), point out that these changes may be caused by uncertainties in the climate data and ST classification, as well as increased radiative forcing from greenhouse gases. If, for instance, a warm ST is consistently mis-classified as a cold ST towards the end of the period, the resulting hypothetical time series would not capture an increased frequency of warm STs, although the estimated observed trend would increase. Further, the trend ratio treats circulation changes and changing properties of STs as mutually exclusive and thus provides a too large region of within-type changes. In reality, there is a gradual transition from circulation changes to within-type changes. The probabilistic approach takes this gradual transition into account, and focuses on regions that are evaluated as within-type changes with high confidence. For the purpose of identifying possible feedback mechanisms, it is important that within-type changes do actually reflect changing properties of STs as a result of a physical change, therefore, trend ratios are not suited as guides towards regions experiencing potential land–atmosphere feedbacks.

Although our probabilistic approach provides more focused regions, and a way of identifying within-type trends that are significantly different from circulation-induced trends, it does not separate the changing properties of STs into influences from land–atmosphere feedbacks, radiative forcing, or uncertainties. Further research is needed to separate out uncertainties from part of the within-type changes that is caused by physical processes. An approach to separate out these causes may be to calculate within-type changes in maximum and minimum temperature and other variables. Given that the soil moisture–temperature feedback is associated with heat waves,

maximum temperatures would provide a better way of distinguishing it from other processes. Further studies could also improve upon our use of fixed months that is not able to detect whether a circulation change in January influences temperatures in February. Detecting changes between months would require using a moving average of e.g. 30 days, or different day lengths. Moreover, Paper II showed many regions and months of strong within-type changes in Europe that would be worth exploring further. The region north of the Black Sea in November, for instance, displayed interesting signals described in Paper II. These signals could be pursued further.

In addition to providing a tool for identifying regions of potential feedbacks, the probabilistic approach may prove useful for statistical downscaling applications. Downscaling approaches that link the local climate to the large-scale atmospheric circulation assume that trends are caused by circulation changes and that they remain stable over time, but this assumption is violated when within-type changes are present (Beck *et al.*, 2007; Vautard and Yiou, 2009; Cahynová and Huth, 2010; Cahynová, 2010). There is thus a need to confirm that circulation changes explain changes in the local climate before applying statistical downscaling methods, a step that is bypassed in many studies. The trend ratio provides a simple means to attributing changes in the local climate to circulation changes, and our method allows the user to define a level of rigidity by assigning a statistical significance to the circulation changes. Our probabilistic approach could be used to highlight regions where the application of the downscaling approach would (not) be considered appropriate.

6.2.3 Using only one classification of synoptic types

Many ST classifications exist, and using more than one classification is recommended by e.g. (Cahynová and Huth, 2016). For Paper II, we think that using only the SVG classification is sufficient to serve as an example of our probabilistic approach and to suggest regions where temperature trends may be explained by circulation changes or within-type changes. However, when using the results from Paper II to select a region for diagnostic modelling studies, results based on several classifications would be more robust.

Most ST classifications are valid for specific regions. For example, Hess Brezowsky Grosswetterlagen (GWL) are developed for central Europe and covers a smaller spatial domain than SVG (P. James, 2014; personal communication); the Lamb catalogue covers the British Isles and Vangenheim-Girs is most useful for estern Europe (Hoy *et al.*, 2013a). Re-running the analyses from Paper II with any of these classifications would likely not improve the quality of the results. Ideally, the analyses should be

re-run with a claddification developed for northern Europe/Scandinavia. Only a few such ST classifications are available that also fullfil the requirement of being updated to 2010. Linderson (2001) applied the Lamb classification to southern Scandinavia, and Tveito (2007) used the Lamb approach to southern Norway. A classification has also been developed for Arctic Norway (Spitsbergen), by Niedzwiedz (2013), used by Isaksen *et al.* (2016). Neither of these classifications were considered in this thesis but it opens up possibilities for new research.

A further option would be to use the cost733class software (Philipp *et al.*, 2010) to develop an updated classification for a given region. This is recommended because low discriminative capability of the classification is one source of within-type change. A poor classification may therefore obscure true signals. A further point to consider if developing a new classification is that the complex topography of Norway will be better resolved by fine-resolution input (for instance by the new ERA5 reanalysis or downscaled products of atmospheric variables.

6.3 Exploring the physical drivers of temperature trends

As a selected case of a region with potential within-type changes, we initally looked into the winter warming in an Arctic station, Karasjok in northern Norway. This station has frequent inversions in winter. The warming at this station may therefore be related to less frequent occurrences of inversions. Although more frequent westerly airflow may cause less frequent inversions, these temperature trends were much stronger than the circulation-induced trends, and could therefore not be explained by circulation changes alone. Other influences on temperature trends in northern Norway include changes in the sea ice extent, sea surface temperature (Hanssen-Bauer and Førland, 1998) and degrading permafrost, which will not be discussed in this thesis. To which degree these processes explain today's changes remains to be tested.

The snow albedo feedback played a role in regions of snowmelt in spring (Papers III and IV). Because of the importance of snow cover on the spring climate at high latitudes, it was expected that the snow albedo feedback would explain the detected spring warming in Norway. Paper IV shows the presence of a positive soil moisture–temperature feedback in parts of South Norway during dry periods in summer, using a coupled land surface–atmosphere model framework. This is likely the first time the soil moisture–temperature feedback has been documented for Norway.

6.3.1 Linkage between statistical analyses and model studies

In this thesis, statistical attribution is employed to separate the temperature trend into a compontent attributed to circulation changes and one component attributed to within-type changes, and were used as a guide towards potentially interesting regions and months. The model-diagnostic studies is employed to delve deeper into causes of within-type changes, but the model study does not give an exhaustive account of all causes of within-type changes. Further, the model study of two summers (2006 and 2014) is not able to explain the full trend over the period 1981–2010.

Although the snow albedo and soil moisture–temperature feedbacks are not the only local factors playing a role in explaining within-type changes, we have showed that these feebacks are relevant causes of temperature anomalies. In particular, the study proves that the soil moisture–temperature feedback could explain enhanced warming, provided sufficiently dry conditions. Combined with observed drying trends (Wilson *et al.*, 2010), this result is a step towards explaining the within-type trends over the full period 1981–2010, despite short model runs. The model-diagnostic approach is the closest we can get to assessing causality without performing controlled physical experiments (which is nearly impossible given the spatial and temporal scales in question).

Further steps are needed to extend the model analyses to the full 30-year period, which would require additional computing power and storage. Moreover, future studies should quantify the influence of improper circulation classification on within-type changes, and should test other feedback mechanisms. Within-type changes may arise from a range of feedback mechanisms, which to a varying degree play a role in different regions and months. Temperature trends at high latitudes may be influenced by a range of local factors, whose influence could be diagnosed for Norway:

i) snow albedo feedback (Dery and Brown, 2007)

ii) changes in wind leading to changes to inversions,

iii) water vapour feedback (Ingram, 2013),

iv) reduced Arctic sea ice cover (Hanssen-Bauer and Førland, 1998; Cohen *et al.*, 2014; Simmons and Poli, 2014),

v) changing sea surface temperatures (Deser *et al.*, 2007),

vi) Planck feedback (Pithan and Mauritsen, 2014),

vii) soil moisture–temperature feedback, which has not received much attention at high latitudes,

viii) low discriminative capatbility of the ST classification, which may also lead to within-type changes.

6.3.2 Potential to improve land surface models

Improving our understanding of the drivers of hydroclimatological change helps the scientific community to improve land surface models (LSMs). Although LSMs are constantly being improved with better model structure and parameterisations, they still lack a number of processes, for instance lateral transport and subgrid scale processes (Niu *et al.*, 2011; Davison *et al.*, 2016). Moreover, LSMs perform poorly in regions of complex terrain and with a seasonal snow cover (Aas *et al.*, 2017), such as in Norway. To improve modelling in these regions, we must determine in which way the LSMs perform poorly. In Paper IV, we mentioned two sources of uncertainty: i) improper representation of soil depth and root depth, and ii) improper parameterisations of e.g. evapotranspiration. Both potentially lead to too much soil moisture. Further studies are planned to explore differences in coupling between SeNorge and WRF–Noah-MP, with the aim to separate the sources i) from ii). Specifically, effects of land cover classes will be eliminated by implementing the same land cover and vegetation maps in WRF–Noah-MP as in SeNorge.

6.3.3 Future changes

Both warming and increased variability in summer dryness are expected to continue with climate change. Seneviratne *et al.* (2006) and Zampieri *et al.* (2009) describe a northward shift of climate regimes with climate change, such that central and eastern Europe become transitional climate regimes during dry periods. Vautard *et al.* (2007) established a link between summer dry conditions in Northern Europe and winter droughts in southern Europe. Trends towards both winter and summer drying are projected for southern Europe (Collins *et al.*, 2013, for the period 2081–2100 relative to 1986–2005). From the model diagnostic study in Paper IV and projections of summer dryness in South Norway (Hanssen-Bauer *et al.*, 2015), it is likely that also South Norway in the future will turn into a transitional evapotranspiration regime during dry periods in summer. This highlights the importance of an increased awareness about enhanced warming trends in Norway and other seasonally snow-covered regions.

Different factors govern evapotranspiration in energy-limited regimes versus soil moisture-limited regimes. Evapotranspiration trends increase with warming in both regimes. In moist climates, evapotranspiration increases with incoming short wave radiation, and in both moist and dry climates, evapotranspiration increases soil moisture, but more strongly in soil moisture–limited climates (van Heerwaarden *et al.*, 2010). When projecting trends in evapotranspiration, it is therefore important to know which regime applies. For regions that exhibit energy-limitation during parts of the year and soil moisture-limitation during other parts of the year, a correct characterisation of the regime is a requirement to correctly estimate the evapotranspiration. A shift from one evapotranspiration regime to another must be taken into account when projecting trends in evapotranspiration. Paper IV provides information about evapotranspiration regime shifts in Norway during two warm summers, which may prove valuable for improved evapotranspiration estimation in Norway.

Chapter 7

Conclusions

The main goal of this thesis was to detect recent monthly hydroclimatic trends and assess the climatological cause of those trends through statistical attribution and a model diagnostic study (the research papers are summarised in Figure 1.1 and Chapter 5). The main outcomes of this thesis is a novel probabilistic approach for statistical attribution of trends (Paper II) and an improved understanding of local factors enhancing temperatures (Paper IV). Paper II improves upon limitations inherent in existing methodologies by evaluating the statistical significance of synoptic circulation changes on observed climate trends. Using a classification of synoptic types, we attributed temperature trends either to changes in the frequency of synoptic types (circulation changes), or to changes within the synoptic types (within-type changes). South Norway was identified as a region with a potential for positive land–atmosphere feedbacks (within-type changes), and was therefore selected as the study region for targeted experiments using the regional climate model WRF coupled to the land surface model Noah-MP. Because recent seasonal temperature trends in Europe have been accompanied by large changes in the snow cover and summer drying, we focused on the snow albedo feedback and the soil moisture–temperature feedback.

The four research questions from the introduction may be answered as follows:

1. Which regions and months have experienced significant trends in hydroclimatology in Europe?

   Temperature trends for the period 1979–2009 showed a general warming, which was most pronounced in winter, spring and summer (Paper I). Annual temperature trends for the period 1981–2010 showed warming for nearly all of Europe. This warming was distributed unequally across months,

displaying significant temperature trends in large parts of Europe for April–August and November (Paper II). For Norway, significant temperature trends were detected in April and July–September. Strong winter warming was detected in northern Norway in Papers I and II.

Strong trends in snow indices (snow cover extent, snow water equivalent and snow duration) were detected for Norway, particularly in spring and at low elevations (Paper III). Between 1981–2010 and 1961–1990, the snow cover extent in mainland Norway decreased by more than 6% (20 000 km^2) in April and May. Temperature trends were detected for the estimated observed dataset for Norway (SeNorge) for April, July–September, as well as in northern Norway in winter, confirming results in 1a).

2. Can the detected trends for Europe be attributed to circulation changes or within-type changes?

   Circulation changes could explain the large-scale warming for Europe in February for the period 1979–2009, as well as localised warming in other months (Paper I). Elsewhere, circulation changes could not account for all the estimated observed warming, which implies that other factors, such as positive land–atmosphere feedbacks, contributed to the warming.

   By applying the probabilistic approach to Europe for the period 1981–2010, we found that warming in large parts of Europe for April, June–August could partly be attributed to within-type changes. For Norway, within-type changes could partly explain the warming in April and July–September (Paper II).

3. How do snow cover changes influence warming in a region with seasonal snow cover?

   Significant negative correlation between temperature and snow cover extent strongly suggested the snow albedo feedback as a main cause for April warming in South Norway (Paper III), confirmed by the model diagnostic experiments (Paper IV).

4. For regions with within-type changes in Norway, can the detected trends be attributed to the snow albedo feedback (in spring) or the soil moisture–temperature feedback (in summer)?

During the anomalously warm summer of 2014 and the warm and dry summer of 2006, the warming could partly be attributed to the positive soil moisture–temperature feedback, at least during parts of the summer (Paper IV). This signal appeared in two independent datasets – the WRF–Noah-MP model results and SeNorge. Further studies are required to determine which processes cause these differences between WRF–Noah-MP and SeNorge, which further contributes to identify needs for improvement in the model parameterisation or input data.

Decreases in the snow cover during spring are projected for Norway, and an increased probability of dry conditions during summer is projected for South Norway. Therefore, the snow albedo feedback and the soil moisture–temperature feedback are expected to continue to enhance warming in the future. The combined methodology of identifying within-type changes with land–atmosphere feedbacks may prove valuable when predicting future temperatures. In particular, a correct characterisation of the evapotranspiration regime (soil moisture-limited versus energy-limited) is key because evapotranspiration estimates are very sensitive to the regime. This thesis shows the added value of bringing together different diciplines, namely synoptic climatology and land surface modelling.

Chapter 8

References

Aas KS, Gisnås K, Westermann S, Berntsen TK. 2017. A tiling approach to represent subgrid snow variability in coupled land surface–atmosphere models. *Journal of Hydrometeorology* **18**(1): 49–63, doi:10.1175/JHM-D-16-0026.1.

Barry RG, Perry AH. 1973. *Synoptic climatology:methods and applications*, vol. Applications of mathematics 33. Springer: London: Methuen, ISBN 0-416-08500-8.

Beck C, Jacobeit J, Jones PD. 2007. Frequency and within-type variations of large-scale circulation types and their effects on low-frequency climate variability in central Europe since 1780. *International Journal of Climatology* **27**(4): 473–491, doi:10.1002/joc.1410.

Becker A, Finger P, Meyer-Christoffer A, Rudolf B, Schamm K, Schneider U, Ziese M. 2013. A description of the global land-surface precipitation data products of the Global Precipitation Climatology Centre with sample applications including centennial (trend) analysis from 1901–present. *Earth System Science Data* **5**: 71–99, doi:10.5194/essd-5-71-2013.

Beldring S, Engeland K, Roald LA, Sælthun NR, Voksø A. 2003. Estimation of parameters in a distributed precipitation-runoff model for Norway. *Hydrology and Earth System Sciences* **7**(3): 304–316, doi:10.5194/hess-7-304-2003.

Berghuijs WR, Woods RA, Hrachowitz M. 2014. A precipitation shift from snow towards rain leads to a decrease in streamflow. *Nature Climate Change* **4**: 583–586, doi:10.1038/nclimate2246.

Bergström S. 1995. The HBV model. In: *Computer models of watershed hydrology*, Singh VP (ed), ch. 13, Water Resources Publications: Highlands Ranch, Colorado, pp. 443–476.

Betts RA. 2000. Offset of the potential carbon sink from boreal forestation by decreases in surface albedo. *Nature* **408**(6809): 187–190, doi:10.1038/35041545.

Bony S, Colman R, Kattsov VM, Allan RP, Bretherton CS, Dufresne JL, Hall A, Hallegatte S, Holland MM, Ingram W, Randall DA, Soden BJ, Tselioudis G, Webb MJ. 2006. How well do we understand and evaluate climate change feedback processes? *Journal of Climate* **19**(15): 3445–3482, doi:10.1175/JCLI3819.1.

Brown RD, Robinson DA. 2011. Northern hemisphere spring snow cover variability and change over 1922–2010 including an assessment of uncertainty. *The Cryosphere* **5**(1): 219–229, doi:10.5194/tc-5-219-2011.

Broxton PD, Zeng X, Sulla-Menashe D, Troch PA. 2014. A global land cover climatology using modis data. *Journal of Applied Meteorology and Climatology* **53**(6): 1593–1605, doi:10.1175/JAMC-D-13-0270.1.

Böhm R, Jones PD, Hiebl J, Frank D, Brunetti M, Maugeri M. 2010. The early instrumental warm-bias: a solution for long central European temperature series 1760–2007. *Climatic Change* **101**(1-2): 41–67, doi:10.1007/s10584-009-9649-4.

Cahynová M. 2010. The influence of long-term changes of atmospheric circulation on observed trends of surface climatic elements in the Czech Republic and Europe. PhD thesis, Charles University in Prague, Faculty of Science, Department of Physical Geography and Geoecology.

Cahynová M, Huth R. 2009. Changes of atmospheric circulation in central Europe and their influence on climatic trends in the Czech Republic. *Theoretical and Applied Climatology* **96**(1): 57–68, doi:10.1007/s00704-008-0097-2.

Cahynová M, Huth R. 2010. Circulation vs. climatic changes over the Czech Republic: A comprehensive study based on the COST733 database of atmospheric circulation classifications. *Physics and Chemistry of the Earth, Parts A/B/C* **35**(9–12): 422 – 428, doi:10.1016/j.pce.2009.11.002.

Cahynová M, Huth R. 2016. Atmospheric circulation influence on climatic trends in Europe: an analysis of circulation type classifications from the COST733 catalogue. *International Journal of Climatology* **36**(7): 2743–2760, doi:10.1002/joc.4003.

Callaghan TV, Johansson M, Brown RD, Groisman PY, Labba N, Radionov V, Barry RG, Bulygina ON, Essery RLH, Frolov DM, Golubev VN, Grenfell TC, Petrushina MN, Razuvaev VN, Robinson DA, Romanov P, Shindell D, Shmakin AB, Sokratov SA, Warren S, Yang D. 2012. The changing face of arctic snow cover: A synthesis of observed and projected changes. *AMBIO* **40**(1): 17–31, doi:10.1007/s13280-011-0212-y.

Chapin FS, Sturm M, Serreze MC, McFadden JP, Key JR, Lloyd AH, McGuire AD, Rupp TS, Lynch AH, Schimel JP, Beringer J, Chapman WL, Epstein HE, Euskirchen ES, Hinzman LD, Jia G, Ping CL, Tape KD, Thompson CDC, Walker DA, Welker JM. 2005. Role of land-surface changes in arctic summer warming. *Science* **310**(5748): 657–660, doi:10.1126/science.1117368.

Cohen J, Screen JA, Furtado JC, Barlow M, Whittleston D, Coumou D, Francis J, Dethloff K, Entekhabi D, Overland J, Jones J. 2014. Recent Arctic amplification and extreme mid-latitude weather. *Nature Geosciences* **7**(9): 627–637, doi:10.1038/ngeo2234. Review.

Colleuille H. 2000. Nasjonalt observasjonsnett for markvann. Årsrapport 1999. Technical report, Norwegian Water Resources and Energy Directorate.

Collins M, Knutti R, Arblaster J, Dufresne JL, Fichefet T, Friedlingstein P, Gao X, Gutowski W, Johns T, Krinner G, Shongwe M, Tebaldi C, Weaver A, Wehner M. 2013. *Long-term climate change: Projections, commitments and irreversibility*, book section 12. Cambridge University Press: Cambridge, United Kingdom and New York, NY, USA, ISBN 978-1-107-66182-0, p. 1029–1136, doi:10.1017/CBO9781107415324.024.

Compo GP, Whitaker JS, Sardeshmukh PD, Matsui N, Allan RJ, Yin X, Gleason BE, Vose RS, Rutledge G, Bessemoulin P, Brönnimann S, Brunet M, Crouthamel RI, Grant AN, Groisman PY, Jones PD, Kruk MC, Kruger AC, Marshall GJ, Maugeri M, Mok HY, Nordli O, Ross TF, Trigo RM, Wang XL, Woodruff SD, Worley SJ. 2011. The Twentieth Century Reanalysis Project. *Quarterly Journal of the Royal Meteorological Society* **137**(654): 1–28, doi:10.1002/qj.776.

Corti S, Molteni F, Palmer TN. 1999. Signature of recent climate change in frequencies of natural atmospheric circulation regimes. *Nature* **398**(6730): 799–802, doi:10.1038/19745.

Davison B, Pietroniro A, Fortin V, Leconte R, Mamo M, Yau MK. 2016. What is Missing

from the Prescription of Hydrology for Land Surface Schemes? *Journal of Hydrometeorology* **17**(7): 2013–2039, doi:10.1175/JHM-D-15-0172.1.

Dee DP, Uppala SM, Simmons AJ, Berrisford P, Poli P, Kobayashi S, Andrae U, Balmaseda MA, Balsamo G, Bauer P, Bechtold P, Beljaars ACM, van de Berg L, Bidlot J, Bormann N, Delsol C, Dragani R, Fuentes M, Geer AJ, Haimberger L, Healy SB, Hersbach H, Hólm EV, Isaksen L, Kållberg P, Köhler M, Matricardi M, McNally AP, Monge-Sanz BM, Morcrette JJ, Park BK, Peubey C, de Rosnay P, Tavolato C, Thépaut JN, Vitart F. 2011. The ERA-Interim reanalysis: configuration and performance of the data assimilation system. *Quarterly Journal of the Royal Meteorological Society* **137**(656): 553–597, doi:10.1002/qj.828.

Derksen C, Brown R. 2012. Spring snow cover extent reductions in the 2008–2012 period exceeding climate model projections. *Geophysical Research Letters* **39**(19): L19 504, doi:10.1029/2012GL053387.

Dery SJ, Brown RD. 2007. Recent Northern Hemisphere snow cover extent trends and implications for the snow-albedo feedback. *Geophysical Research Letters* **34**(22): L22 504, doi:10.1029/2007GL031474.

Dery SJ, Stieglitz M, McKenna EC, Wood EF. 2005. Characteristics and Trends of River Discharge into Hudson, James, and Ungava Bays, 1964–2000. *Journal of Climate* **18**: 2540–2557, doi:10.1175/jcli3440.1.

Deser C, Tomas RA, Peng S. 2007. The Transient Atmospheric Circulation Response to North Atlantic SST and Sea Ice Anomalies. *Journal of Climate* **20**(18): 4751–4767, doi:10.1175/JCLI4278.1.

Dickinson RE. 1983. Land surface processes and climate—surface albedos and energy balance. In: *Theory of ClimateProceedings of a Symposium Commemorating the Two-Hundredth Anniversary of the Academy of Sciences of Lisbon*, *Advances in Geophysics*, vol. 25, Saltzman B (ed), Elsevier, pp. 305 – 353, doi:http://dx.doi.org/10.1016/S0065-2687(08)60176-4.

Dingman SL. 2002. *Physical Hydrology*. New Jersey: Prentice-Hall, 2nd edn. 646 pp.

Dirmeyer PA. 2011. The terrestrial segment of soil moisture–climate coupling. *Geophysical Research Letters* **38**(16): L16 702, doi:10.1029/2011GL048268.

Dirmeyer PA, Jin Y, Singh B, Yan X. 2013. Trends in Land–Atmosphere Interactions from CMIP5 Simulations. *Journal of Hydrometeorology* **14**(3): 829–849, doi:10.1175/jhm-d-12-0107.1.

Dirmeyer PA, Schlosser CA, Brubaker KL. 2006. The hydrologic feedback pathway for land–atmosphere coupling. *Journal of Hydrometeorology* **7**: 857–867.

Dirmeyer PA, Schlosser CA, Brubaker KL. 2009. Precipitation, Recycling, and Land Memory: An Integrated Analysis. *Journal of Hydrometeorology* **10**: 278–288.

Dirmeyer PA, Wang Z, Mbuh MJ, Norton HE. 2014. Intensified land surface control on boundary layer growth in a changing climate. *Geophysical Research Letters* **41**(4): 1290–1294, doi:10.1002/2013GL058826. 2013GL058826.

Dyrrdal AV. 2010. An evaluation of norwegian snow maps: simulation results versus observations. *Hydrology Research* **41**(1): 27–37, doi:10.2166/nh.2010.019.

Dyrrdal AV, Saloranta T, Skaugen T, Stranden HB. 2013. Changes in snow depth in Norway during the period 1961–2010. *Hydrology Research* **44**(1): 169–179, doi:10.2166/nh.2012.064.

Dzerdzeevski BL. 1963. Fluctuations of general circulaton of the atmosphere and climate in the twentieth centrury. In: *Changes of Climate*, vol. Arid Zone Research 20, UNESCO, Paris, pp. 285–295.

EEA. 2008. Impacts of Europe's changing climate - 2008 indicator-based assessment. EEA Report No 4/2008, Copenhagen.

EEA. 2017. Global and European temperature. European Environment Agency, Copenhagen. Retreived from https://www.eea.europa.eu/data-and-maps/indicators/global-and-european-temperature-3/assessment.

Eisner S, Flörke M, Chamorro A, Daggupati P, Donnelly C, Huang J, Hundecha Y, Koch H, Kalugin A, Krylenko I, Mishra V, Piniewski M, Samaniego L, Seidou O, Wallner M, Krysanova V. 2017. An ensemble analysis of climate change impacts on streamflow seasonality across 11 large river basins. *Climatic Change* **141**(3): 401–417, doi:10.1007/s10584-016-1844-5.

Engeland K, Engen Skaugen T, Haugen JE, Beldring S, Førland E. 2004. Comparison of evaporation estimated by the HIRHAM and GWB models for present climate and climate change scenarios. Technical Report Climate-Report 17/2004, Norwegian Meteorological Institute, Oslo, Norway.

Engeset R, Tveito O, Alfnes E, Z Mengistu HCU, Isaksen K, Førland EJ. 2004. Snow map system for Norway. In: *Proceedings of Nordic hydrological conference 2004, Tallin 8.-12.august 2004*, *NHP-report*, vol. 48. pp. 112–121.

Erlandsen HB, Haddeland I, Tallaksen LM, Kristiansen J. 2017. The sensitivity of the terrestrial surface energy and water balance estimates in the wrf model to lower surface boundary representations: A south norway case study. *Journal of Hydrometeorology* **18**(1): 265–284, doi:10.1175/JHM-D-15-0146.1.

Feser F, Barcikowska M, Krueger O, Schenk F, Weisse R, Xia L. 2015. Storminess over the North Atlantic and northwestern Europe—A review. *Quarterly Journal of the Royal Meteorological Society* **141**(687): 350–382, doi:10.1002/qj.2364.

Fischer EM, Rajczak J, Schär C. 2012. Changes in European summer temperature variability revisited. *Geophysical Research Letters* **39**(19): L19 702, doi:10.1029/2012GL052730.

Fleig AK, Tallaksen LM, Hisdal H, Hannah DM. 2011. Regional hydrological drought in north-western Europe: linking a new Regional Drought Area Index with weather types. *Hydrological Processes* **25**(7): 1163–1179, doi:10.1002/hyp.7644.

Fleig AK, Tallaksen LM, James P, Hisdal H, Stahl K. 2015. Attribution of European precipitation and temperature trends to changes in synoptic circulation. *Hydrology and Earth System Sciences* **19**(7): 3093–3107, doi:10.5194/hess-19-3093-2015.

Førland E, Hanssen-Bauer I, Haugen JE, Hygen HO, Haakenstad H, Isaksen K, Dyrrdal AV. 2016. Background information for "Klima i Norge 2100" – on freezing/thawing, minimum/maximum temperature, short-term rainfall, wind and permafrost. Technical Report NCCS Report 1/2016, Norwegian Centre for Climate Services.

Gallego-Elvira B, Taylor CM, Harris PP, Ghent D, Veal KL, Folwell SS. 2016. Global observational diagnosis of soil moisture control on the land surface energy balance. *Geophysical Research Letters* **43**(6): 2623–2631, doi:10.1002/2016GL068178. 2016GL068178.

Gayler S, Wöhling T, Grzeschik M, Ingwersen J, Wizemann HD, Warrach-Sagi K, Högy P, Attinger S, Streck T, Wulfmeyer V. 2014. Incorporating dynamic root growth enhances the performance of noah-mp at two contrasting winter wheat field sites. *Water Resources Research* **50**(2): 1337–1356, doi:10.1002/2013WR014634.

Greve P, Gudmundsson L, Orlowsky B, Seneviratne SI. 2016. A two-parameter Budyko function to represent conditions under which evapotranspiration exceeds precipitation. *Hydrology and Earth System Sciences* **20**: 2195–2205, doi:dx.doi.org/10.1175/JAMC-D-12-0239.1.

Greve P, Orlowsky B, Mueller B, Sheffield J, Reichstein M, Seneviratne SI. 2014. Global assessment of trends in wetting and drying over land. *Nature Geosci* **7**(10): 716–721. Letter.

Greve P, Warrach-Sagi K, Wulfmeyer V. 2013. Evaluating Soil Water Content in a WRF-Noah Downscaling Experiment. *Journal of Applied Meteorology and Climatology* **52**(10): 2312–2327, doi:10.1175/JAMC-D-12-0239.1.

Groisman PY, Karl TR, Knight RW. 1994a. Observed impact of snow cover on the heat balance and the rise of continental spring temperatures. *Science* **263**(5144): 198–200.

Groisman PY, Karl TR, Knight RW, Stenchikov GL. 1994b. Changes of Snow Cover, Temperature, and Radiative Heat Balance over the Northern Hemisphere. *Journal of Climate* **7**(11): 1633–1656, doi:10.1175/1520-0442(1994)007<1633:COSCTA>2.0.CO;2.

Halder S, Dirmeyer PA. 2017. Relation of eurasian snow cover and indian summer monsoon rainfall: Importance of the delayed hydrological effect. *Journal of Climate* **30**(4): 1273–1289, doi:10.1175/JCLI-D-16-0033.1.

Hall A, Qu X. 2006. Using the current seasonal cycle to constrain snow albedo feedback in future climate change. *Geophysical Research Letters* **33**(3): n/a–n/a, doi:10.1029/2005GL025127.

Hannaford J, Buys G, Stahl K, Tallaksen LM. 2013. The influence of decadal-scale variability on trends in long European streamflow records. *Hydrology and Earth System Sciences* **17**(7): 2717–2733, doi:10.5194/hess-17-2717-2013.

Hanssen-Bauer I, Førland EJ. 1998. Long-term trends in precipitation and temperature in the Norwegian Arctic: can they be explained by changes in atmospheric circulation patterns? *Climate Research* **10**(2): 143–153, doi:10.3354/cr010143.

Hanssen-Bauer I, Førland EJ, Haddeland I, Hisdal H, Mayer S, Nesje A, Nilsen JEO, Sandven S, Sandø AB, Sorteberg A, Ådlandsvik B. 2015. Klima i Norge 2100. Kunnskapsgrunnlag for klimatilpasning. NCCS Report 2/2015. Technical report, Norwegian Centre for Climate Services, Oslo, Norway. (In Norwegian), pp 204.

Harris I, Jones PD, Osborn TJ, Lister DH. 2014. Updated high-resolution grids of monthly climatic observations – the CRU TS3.10 Dataset. *International Journal of Climatology* **34**(3): 623–642, doi:10.1002/joc.3711.

Hartmann D, Klein Tank A, Rusticucci M, Alexander L, Brönnimann S, Charabi Y, Dentener F, Dlugokencky E, Easterling D, Kaplan A, Soden B, Thorne P, Wild M, Zhai P. 2013. *Observations: Atmosphere and surface*, book section 2. Cambridge University Press: Cambridge, United Kingdom and New York, NY, USA, ISBN ISBN 978-1-107-66182-0, p. 159–254, doi:10.1017/CBO9781107415324.008.

Held IM, Soden BJ. 2000. Water vapor feedback and global warming. *Annual Review of Energy and the Environment* **25**(1): 441–475, doi:10.1146/annurev.energy.25.1.441.

Hertig E, Beck C, Wanner H, Jacobeit J. 2015. A review of non-stationarities in climate variability of the last century with focus on the North Atlantic–European sector. *Earth-Science Reviews* **147**: 1 – 17, doi:dx.doi.org/10.1016/j.earscirev.2015.04.009.

Hisdal H, Stahl K, Tallaksen LM, Demuth S. 2001. Have streamflow droughts in europe become more severe or frequent? *International Journal of Climatology* **21**(3): 317–333, doi:10.1002/joc.619.

Hong SY, Dudhia J, Chen SH. 2004. A revised approach to ice microphysical processes for the bulk parameterization of clouds and precipitation. *Monthly Weather Review* **132**(1): 103–120, doi:10.1175/1520-0493(2004)132<0103:ARATIM>2.0.CO;2.

Hoy A, Jaagus J, Sepp M, Matschullat J. 2013a. Spatial response of two European atmospheric circulation classifications (data 1901–2010). *Theoretical and Applied Climatology* **112**(1-2): 73–88, doi:10.1007/s00704-012-0707-x.

Hoy A, Sepp M, Matschullat J. 2013b. Large-scale atmospheric circulation forms and their impact on air temperature in Europe and northern Asia. *Theoretical and Applied Climatology* **113**(3-4): 643–658, doi:10.1007/s00704-012-0813-9.

Hurrell J, Staff N. 2017. The climate Data Guide: Hurrell North Atlantic Oscillation (NAO) Index (station-based). Technical report, National Center for Atmospheric Research, Boulder, Colorado. Retreived from https://climatedataguide.ucar.edu/climate-data/hurrell-north-atlantic-oscillation-nao-index-station-based 23 May 2017.

Hurrell JW, Deser C. 2009. North atlantic climate variability: The role of the north atlantic oscillation. *Journal of Marine Systems* **78**(1): 28 – 41, doi:dx.doi.org/10.1016/j.jmarsys.2008.11.026.

Hurrell JW, Kushnir Y, Ottersen G, Visbeck M. 2013. *An Overview of the North Atlantic Oscillation*, ch. 1. American Geophysical Union, ISBN 9781118669037, pp. 1–35, doi:10.1029/134GM01.

Huth R. 2001. Disaggregating climatic trends by classification of circulation patterns. *International Journal of Climatology* **21**(2): 135–153, doi:10.1002/joc.605.

Huth R, Beck C, Kučerová M. 2016. Synoptic-climatological evaluation of the classifications of atmospheric circulation patterns over Europe. *International Journal of Climatology* **36**: 2710–2726, doi:10.1002/joc.4546.

Huth R, Beck C, Philipp A, Demuzere M, Ustrnul Z, Cahynová M, Kyselý J, Tveito OE. 2008. Classifications of Atmospheric Circulation Patterns. *Annals of the New York Academy of Sciences* **1146**(1): 105–152, doi:10.1196/annals.1446.019.

Iacono MJ, Delamere JS, Mlawer EJ, Shephard MW, Clough SA, Collins WD. 2008. Radiative forcing by long-lived greenhouse gases: Calculations with the aer radiative transfer models. *Journal of Geophysical Research: Atmospheres* **113**(D13): D13 103, doi:10.1029/2008JD009944.

Im ES, Coppola E, Giorgi F, Bi X. 2010. Local effects of climate change over the Alpine region: A study with a high resolution regional climate model with a surrogate climate change scenario. *Geophysical Research Letters* **37**(5): L05 704, doi:10.1029/2009GL041801.

Ingram W. 2013. Some implications of a new approach to the water vapour feedback. *Climate Dynamics* **40**(3): 925–933, doi:10.1007/s00382-012-1456-3.

Isaksen K, Nordli O, Førland EJ, Łupikasza E, Eastwood S, Niedźwiedź T. 2016. Recent warming on spitsbergen – influence of atmospheric circulation and sea ice cover. *Journal of Geophysical Research: Atmospheres* : n/a–n/adoi:10.1002/2016JD025606. 2016JD025606.

James PM. 2007. An objective classification method for Hess and Brezowsky Grosswetterlagen over Europe. *Theoretical and Applied Climatology* **88**(1): 17–42, doi:10.1007/s00704-006-0239-3.

Janjić ZI. 1994. The step-mountain eta coordinate model: Further developments of the convection, viscous sublayer, and turbulence closure schemes. *Monthly Weather Review* **122**(5): 927–945, doi:10.1175/1520-0493(1994)122<0927:TSMECM>2.0.CO;2.

Jones PD, Lister DH. 2009. The influence of the circulation on surface temperature and precipitation patterns over Europe. *Climate of the Past* **5**(2): 259–267, doi:10.5194/cp-5-259-2009.

Jones PD, Lister DH, Osborn TJ, Harpham C, Salmon M, Morice CP. 2012. Hemispheric and large-scale land-surface air temperature variations: An extensive revision and an update to 2010. *Journal of Geophysical Research: Atmospheres* **117**(D5): D05 127, doi:10.1029/2011JD017139.

Kain JS. 2004. The kain–fritsch convective parameterization: An update. *Journal of Applied Meteorology* **43**(1): 170–181, doi:10.1175/1520-0450(2004)043<0170:TKCPAU>2.0.CO;2.

Kalnay E, Kanamitsu M, Kistler R, Collins W, Deaven D, Gandin L, Iredell M, Saha S, White G, Woollen J, Zhu Y, Leetmaa A, Reynolds R, Chelliah M, Ebisuzaki W, Higgins W, Janowiak J, Mo KC, Ropelewski C, Wang J, Jenne R, Joseph D. 1996. The NCEP/NCAR 40-Year Reanalysis Project. *Bulletin of the American Meteorological Society* **77**(3): 437–471, doi:10.1175/1520-0477(1996)077<0437:TNYRP>2.0.CO;2.

Klein Tank AMG, Können GP, Selten FM. 2005. Signals of anthropogenic influence on European warming as seen in the trend patterns of daily temperature variance. *International Journal of Climatology* **25**(1): 1–16, doi:10.1002/joc.1087.

Koster RD, Dirmeyer PA, Guo Z, Bonan G, Chan E, Cox P, Gordon CT, Kanae S, Kowalczyk E, Lawrence D, Liu P, Lu CH, Malyshev S, McAvaney B, Mitchell K, Mocko D, Oki T, Oleson K, Pitman A, Sud YC, Taylor CM, Verseghy D, Vasic R, Xue Y, Yamada T. 2004. Regions of Strong Coupling Between Soil Moisture and Precipitation. *Science* **305**(5687): 1138–1140, doi:10.1126/science.1100217.

Koster RD, Mahanama SPP, Yamada TJ, Balsamo G, Berg AA, Boisserie M, Dirmeyer PA, Doblas-Reyes FJ, Drewitt G, Gordon CT, Guo Z, Jeong JH, Lawrence DM, Lee WS, Li Z, Luo L, Malyshev S, Merryfield WJ, Seneviratne SI, Stanelle T, van den Hurk BJJM, Vitart F, Wood EF. 2010. Contribution of land surface initialization to subseasonal forecast skill: First results from a multi-model experiment. *Geophysical Research Letters* **37**: L02 402, doi:10.1029/2009GL041677.

Kučerová M, Beck C, Philipp A, Huth R. 2017. Trends in frequency and persistence of atmospheric circulation types over europe derived from a multitude of classifications. *International Journal of Climatology* **37**(5): 2502–2521, doi:10.1002/joc.4861.

Küttel M, Luterbacher J, Wanner H. 2011. Multidecadal changes in winter circulation-climate relationship in Europe: frequency variations, within-type modifications, and long-term trends. *Climate Dynamics* **36**(5-6): 957–972, doi:10.1007/s00382-009-0737-y.

Lamb HH. 1982. *Climate, History and the Modern World*. Methuen: London.

Leathers DJ, Ellis AW. 1996. Synoptic mechanisms associated with snowfall increases to the lee of lakes Erie and Ontario. *International Journal of Climatology* **16**(10): 1117–1135, doi:10.1002/(SICI)1097-0088(199610)16:10<1117::AID-JOC80>3.0.CO;2-4.

Linderson ML. 2001. Objective classification of atmospheric circulation over southern scandinavia. *International Journal of Climatology* **21**(2): 155–169, doi:10.1002/joc.604.

Lorenz R, Davin EL, Seneviratne SI. 2012. Modeling land-climate coupling in Europe: Impact of land surface representation on climate variability and extremes. *Journal of Geophysical Research* **117**(D20): D20 109, doi:10.1029/2012JD017755.

Massei N, Fournier M. 2012. Assessing the expression of large-scale climatic fluctuations in the hydrological variability of daily seine river flow (france) between 1950 and 2008 using hilbert–huang transform. *Journal of Hydrology* **448–449**: 119 – 128, doi:https://doi.org/10.1016/j.jhydrol.2012.04.052.

Mayer S, Maule C, Sobolowski S, Christensen O, Sørup H, Sunyer M, Arnbjerg-Nielsen K, Barstad I. 2015. Identifying added value in high-resolution climate simulations over Scandinavia. *Tellus A* **67**(0).

Miralles DG, Teuling AJ, van Heerwaarden CC, Vila-Guerau de Arellano J. 2014. Mega-heatwave temperatures due to combined soil desiccation and atmospheric heat accumulation. *Nature Geosci* **7**(5): 345–349. Letter.

Nilsen IB, Erlandsen H, Stordal F, Xu CY, Tallaksen LM. 2017a. Diagnosing land–atmosphere coupling in a seasonally snow-covered regions (South Norway). (in prep.).

Nilsen IB, Fleig AK, Tallaksen LM, Hisdal H. 2014. Recent trends in monthly temperature and precipitation patterns in Europe. In: *Hydrology in a Changing World: Environmental and Human Dimensions*, Daniell T, Perrins P (eds), no. 363 in: IAHS

publication, IAHS Press, pp. 132–137. Proceedings of FRIEND-Water 2014, Montpellier, France, October 2014.

Nilsen IB, Stagge JH, Tallaksen LM. 2017b. A probabilistic approach for attributing temperature changes to synoptic type frequency. *International Journal of Climatology* **37**(6): 2990–3002, doi:10.1002/joc.4894.

Niu GY, Yang ZL, Mitchell KE, Chen F, Ek MB, Barlage M, Kumar A, Manning K, Niyogi D, Rosero E, Tewari M, Xia Y. 2011. The community Noah land surface model with multiparameterization options (Noah-MP): 1. Model description and evaluation with local-scale measurements. *Journal of Geophysical Research: Atmospheres* **116**(D12): D12 109, doi:10.1029/2010JD015139.

Orlowsky B, Seneviratne SI. 2010. Statistical analyses of land–atmosphere feedbacks and their possible pitfalls. *Journal of Climate* **23**(14): 3918–3932, doi:10.1175/2010JCLI3366.1.

Osborn TJ. 2011. Winter 2009/2010 temperatures and a record-breaking north atlantic oscillation index. *Weather* **66**(1): 19–21, doi:10.1002/wea.660.

Otero N, Sillmann J, Schnell JL, Rust HW, Butler T. 2016. Synoptic and meteorological drivers of extreme ozone concentrations over Europe. *Environmental Research Letters* **11**(2): 024 005.

Pall P, Aina T, Stone DA, Stott PA, Nozawa T, Hilberts AGJ, Lohmann D, Allen MR. 2011. Anthropogenic greenhouse gas contribution to flood risk in England and Wales in autumn 2000. *Nature* **470**(7334): 382–385, doi:10.1038/nature09762.

Peng S, Piao S, Ciais P, Friedlingstein P, Zhou L, Wang T. 2013. Change in snow phenology and its potential feedback to temperature in the northern hemisphere over the last three decades. *Environmental Research Letters* **8**(1): 014 008.

Philipp A, Bartholy J, Beck C, Erpicum M, Esteban P, Fettweis X, Huth R, James P, Jourdain S, Kreienkamp F, Krennert T, Lykoudis S, Michalides SC, Pianko-Kluczynska K, Post P, Álvarez DR, Schiemann R, Spekat A, Tymvios FS. 2010. Cost733cat – A database of weather and circulation type classifications . *Physics and Chemistry of the Earth, Parts A/B/C* **35**(9–12): 360 – 373, doi:10.1016/j.pce.2009.12.010.

Pithan F, Mauritsen T. 2014. Arctic amplification dominated by temperature feedbacks in contemporary climate models. *Nature Geoscience* **7**(3): 181–184, doi:10.1038/ngeo2071.

Prudhomme C, Genevier M. 2011. Can atmospheric circulation be linked to flooding in Europe? *Hydrological Processes* **25**(7): 1180–1190, doi:10.1002/hyp.7879.

Quesada B, Vautard R, Yiou P, Hirschi M, Seneviratne SI. 2012. Asymmetric European summer heat predictability from wet and dry southern winters and springs. *Nature Clim. Change* **2**(10): 736–741, doi:10.1038/nclimate1536.

Ree BL, Landrø H, Trondsen E, Møen KM. 2011. Evaluering av NVE sitt snøstasjonsnettverk. Technical Report Rapport 2011:04, Norwegian Water Resources and Energy Directorate, Oslo, Norway. In Norwegian.

Rizzi J, Nilsen IB, Stagge JH, Gisnås K, Tallaksen LM. 2017. Five decades of warming: impacts on snow cover in Norway. (Submitted to Hydrology Research).

Rowell DP. 2009. Projected midlatitude continental summer drying: North america versus europe. *Journal of Climate* **22**(11): 2813–2833, doi:10.1175/2008JCLI2713.1.

Rowell DP, Jones RG. 2006. Causes and uncertainty of future summer drying over europe. *Climate Dynamics* **27**(2): 281–299, doi:10.1007/s00382-006-0125-9.

Rydsaa JH, Stordal F, Bryn A, Tallaksen LM. 2016. Effects of shrub cover increase on the near surface atmosphere in northern fennoscand. *Biogeosciences Discussions* **2016**: 1–32, doi:10.5194/bg-2016-373.

Sælthun NR. 1996. The 'Nordic' HBV model. Description and documentation of the model version developed for the project Climate Change and Energy Production. Technical Report NVE Publication 7-1996, Norwegian Water Resources and Energy Directorate, Oslo, Norway.

Saffioti C, Fischer EM, Knutti R. 2015. Contributions of atmospheric circulation variability and data coverage bias to the warming hiatus. *Geophysical Research Letters* **42**(7): 2385–2391, doi:10.1002/2015GL063091.

Saini R, Wang G, Pal JS. 2016. Role of Soil Moisture Feedback in the Development of Extreme Summer Drought and Flood in the United States. *Journal of Hydrometeorology* **17**(8): 2191–2207, doi:10.1175/JHM-D-15-0168.1.

Saloranta TM. 2012. Simulating snow maps for Norway: description and statistical evaluation of the seNorge snow model. *The Cryosphere* **6**(6): 1323–1337, doi:10.5194/tc-6-1323-2012.

Schar C, Vidale PL, Luthi D, Frei C, Haberli C, Liniger MA, Appenzeller C. 2004. The role of increasing temperature variability in European summer heatwaves. *Nature* **427**(6972): 332–336, doi:10.1038/nature02300.

Schwitalla T, Bauer HS, Wulfmeyer V, Aoshima F. 2011. High-resolution simulation over central europe: assimilation experiments during cops iop 9c. *Quarterly Journal of the Royal Meteorological Society* **137**(S1): 156–175, doi:10.1002/qj.721.

Seneviratne SI, Corti T, Davin EL, Hirschi M, Jaeger EB, Lehner I, Orlowsky B, Teuling AJ. 2010. Investigating soil moisture - climate interactions in a changing climate: A review. *Earth-Science Reviews* **99**(3-4): 125–161, doi:10.1016/j.earscirev.2010.02.004.

Seneviratne SI, Luthi D, Litschi M, Schar C. 2006. Land-atmosphere coupling and climate change in europe. *Nature* **443**(7108): 205–209, doi:10.1038/nature05095.

Sheffield J, Wood EF. 2008. Global trends and variability in soil moisture and drought characteristics, 1950–2000, from observation-driven simulations of the terrestrial hydrologic cycle. *Journal of Climate* **21**(3): 432–458, doi:10.1175/2007JCLI1822.1.

Simmons AJ, Poli P. 2014. Arctic warming in ERA-Interim and other analyses. *Quarterly Journal of the Royal Meteorological Society* **141**(689): 1147–1162, doi:10.1002/qj.2422.

Skamarock WC, Klemp JB. 2008. A time-split nonhydrostatic atmospheric model for weather research and forecasting applications. *Journal of Computational Physics* **227**(7): 3465 – 3485, doi:10.1016/j.jcp.2007.01.037. Predicting weather, climate and extreme events.

Skaugen T, Stranden H, Saloranta T. 2012. Trends in snow water equivalent in Norway (1931–2009). *Hydrology Research* **43**: 489–499.

Sneyers R. 1990. *On the Statistical Analysis of Series of Observations*, *WMO Technical note*, vol. 143. Secretariat of the World Meteorological Organization, ISBN 9789263104151. Www.wmo.int/pages/prog/wcp/agm/publications/technical_notes.php.

Stahl K, Hisdal H, Hannaford J, Tallaksen LM, van Lanen HAJ, Sauquet E, Demuth S, Fendekova M, Jódar J. 2010. Streamflow trends in Europe: evidence from a dataset of near-natural catchments. *Hydrology and Earth System Sciences* **14**(12): 2367–2382, doi:10.5194/hess-14-2367-2010.

Stahl K, Tallaksen LM, Hannaford J, van Lanen HAJ. 2012. Filling the white space on maps of European runoff trends: estimates from a multi-model ensemble. *Hydrology and Earth System Sciences* **16**(7): 2035–2047, doi:10.5194/hess-16-2035-2012.

Stone DA, Allen MR, Stott PA, Pall P, Min SK, Nozawa T, Yukimoto S. 2009. The detection and attribution of human influence on climate. *Annual Review of Environment and Resources* **34**(1): 1–16, doi:10.1146/annurev.environ.040308.101032.

Stott PA, Stone DA, Allen MR. 2004. Human contribution to the european heatwave of 2003. *Nature* **432**(7017): 610–614, doi:10.1038/nature03089.

Tedesco M, Brodzik M, Armstrong R, Savoie M, Ramage J. 2009. Pan arctic terrestrial snowmelt trends (1979–2008) from spaceborne passive microwave data and correlation with the arctic oscillation. *Geophysical Research Letters* **36**(21): L21 402, doi:10.1029/2009GL039672.

Thackeray CW, Fletcher CG. 2016. Snow albedo feedback: Current knowledge, importance, outstanding issues and future directions. *Progress in Physical Geography* **40**(3): 392–408, doi:10.1177/0309133315620999.

Theil H. 1950. A rank-invariant method of linear and polynomial regression analysis. *Indag. Math.* **12**: 85–91.

Tietäväinen H, Tuomenvirta H, Venäläinen A. 2010. Annual and seasonal mean temperatures in Finland during the last 160 years based on gridded temperature data. *International Journal of Climatology* **30**(15): 2247–2256, doi:10.1002/joc.2046.

Tveito OE. 2007. Spatial distribution of winter temperatures in Norway related to topography and large-scale atmospheric circulation. In: *Proceedings of the PUB Kick-off meeting held in Brasilia, 20–22 November 2002. IAHS Publ. 30*, IAHS, pp. 186–194, URL `https://iahs.info/uploads/dms/309021.pdf`. Proceedings in ungauged Basins: PUB Kick-off.

Tveito OE, Roald L. 2005. Relations between long-term variations in seasonal runoff and large scale atmospheric circulation patterns. Technical Report Climate-Report 7/2005, Norwegian Meteorological Institute, Oslo, Norway.

van Heerwaarden CC, Vilà-Guerau de Arellano J, Teuling AJ. 2010. Land-atmosphere coupling explains the link between pan evaporation and actual evapotranspiration trends in a changing climate. *Geophysical Research Letters* **37**(21): L21 401, doi:10.1029/2010GL045374.

Vaughan D, Comiso J, Allison I, Carrasco J, Kaser G, Kwok R, Mote P, Murray T, Paul F, Ren J, Rignot E, Solomina O, Steffen K, Zhang T. 2013. *Observations: Cryosphere*, book section 4. Cambridge University Press: Cambridge, United Kingdom and New York, NY, USA, ISBN ISBN 978-1-107-66182-0, p. 317–382, doi: 10.1017/CBO9781107415324.012.

Vautard R, Gobiet A, Jacob D, Belda M, Colette A, Déqué M, Fernández J, García-Díez M, Goergen K, Güttler I, Halenka T, Karacostas T, Katragkou E, Keuler K, Kotlarski S, Mayer S, van Meijgaard E, Nikulin G, Patarčić M, Scinocca J, Sobolowski S, Suklitsch M, Teichmann C, Warrach-Sagi K, Wulfmeyer V, Yiou P. 2013. The simulation of European heat waves from an ensemble of regional climate models within the EURO-CORDEX project. *Climate Dynamics* **41**(9-10): 2555–2575, doi: 10.1007/s00382-013-1714-z.

Vautard R, Yiou P. 2009. Control of recent European surface climate change by atmospheric flow. *Geophysical Research Letters* **36**(22): L22 702, doi:10.1029/2009GL040480.

Vautard R, Yiou P, D'Andrea F, de Noblet N, Viovy N, Cassou C, Polcher J, Ciais P, Kageyama M, Fan Y. 2007. Summertime European heat and drought waves induced by wintertime Mediterranean rainfall deficit. *Geophysical Research Letters* **34**(7): L07 711, doi:10.1029/2006GL028001.

Walton DB, Hall A, Berg N, Schwartz M, Sun F. 2017. Incorporating snow albedo feedback into downscaled temperature and snow cover projections for california's sierra nevada. *Journal of Climate* **30**(4): 1417–1438, doi:10.1175/JCLI-D-16-0168.1.

Weedon GP, Balsamo G, Bellouin N, Gomes S, Best MJ, Viterbo P. 2014. The WFDEI meteorological forcing data set: WATCH Forcing Data methodology applied to ERA-Interim reanalysis data. *Water Resources Research* **50**(9): 7505–7514, doi: 10.1002/2014WR015638.

Wetherald RT, Manabe S. 1995. The mechanisms of summer dryness induced by greenhouse warming. *Journal of Climate* **8**(12): 3096–3108, doi:10.1175/1520-0442(1995)008<3096:TMOSDI>2.0.CO;2.

Whan K, Zscheischler J, Orth R, Shongwe M, Rahimi M, Asare EO, Seneviratne SI. 2015. Impact of soil moisture on extreme maximum temperatures in europe. *Weather and Climate Extremes* **9**: 57 – 67, doi:dx.doi.org/10.1016/j.wace.2015.05.001.

Wilson D, Hisdal H, Lawrence D. 2010. Has streamflow changed in the Nordic countries? - Recent trends and comparisons to hydrological projections. *Journal of Hydrology* **394**(3-4): 334–346, doi:10.1016/j.jhydrol.2010.09.010.

Xu L, Dirmeyer P. 2011. Snow-atmosphere coupling strength in a global atmospheric model. *Geophysical Research Letters* **38**(13): L13 401, doi:10.1029/2011GL048049.

Xu L, Dirmeyer P. 2013a. Snow–atmosphere coupling strength. part i: Effect of model biases. *Journal of Hydrometeorology* **14**(2): 389–403, doi:10.1175/JHM-D-11-0102.1.

Xu L, Dirmeyer P. 2013b. Snow–Atmosphere Coupling Strength. Part II: Albedo Effect Versus Hydrological Effect. *Journal of Hydrometeorology* **14**(2): 404–418, doi:10.1175/JHM-D-11-0103.1.

Yarnal B. 1993. *Synoptic climatology in environmental analysis: a primer*. Belhaven Press: London.

Zaitchik BF, Macalady AK, Bonneau LR, Smith RB. 2006. Europe's 2003 heat wave: a satellite view of impacts and land–atmosphere feedbacks. *International Journal of Climatology* **26**(6): 743–769, doi:10.1002/joc.1280.

Zampieri M, D'Andrea F, Vautard R, Ciais P, de Noblet-Ducoudré N, Yiou P. 2009. Hot European Summers and the Role of Soil Moisture in the Propagation of Mediterranean Drought. *J. Climate* **22**(18): 4747–4758, doi:10.1175/2009jcli2568.1.

Chapter 9

Papers

Paper I

Nilsen, I.B., Fleig, A.K., Tallaksen, L.M., Hisdal, H. (2014): Recent trends in monthly temperature and precipitation in Europe. *Hydrology in a Changing World: Environmental and Human Dimensions. Proceedings of FRIEND-Water 2014, Montpellier, France, October 2014* IAHS Publ. 363.

Paper II

Nilsen, I.B., Stagge, J.H., Tallaksen, L.M. (2015): A probabilistic approach for attributing temperature changes to synoptic type frequency *International Journal of Climatology* 37(6): 2990–3002, DOI: 10.1002/joc.4894.

Paper III

Rizzi, J. **Nilsen, I.B.**, Stagge, J.H., Gisnås, K., and Tallaksen, L.M. (2017): Five decades of warming: impacts on snow in Norway. *Hydrology research* (in production). DOI: 10.2166/nh.2017.051.

Five decades of warming: impacts on snow cover in Norway

Jonathan Rizzi, Irene Brox Nilsen, James Howard Stagge, Kjersti Gisnås and Lena M. Tallaksen

ABSTRACT

Northern latitudes are experiencing faster warming than other regions in the world, which is partly explained by the snow albedo feedback. In Norway, mean temperatures have been increasing since the 1990s, with 2014 being the warmest year on record, 2.2 °C above normal (1961–1990). At the same time, a concurrent reduction in the land area covered by snow has been reported. In this study, we present a detailed spatial and temporal (monthly and seasonal) analysis of trends and changes in snow indices based on a high resolution (1 km) gridded hydro-meteorological dataset for Norway (seNorge). During the period 1961–2010, snow cover extent (SCE) was found to decrease, notably at end of the snow season, with a corresponding decrease in snow water equivalent except at high elevations. SCE for all Norway decreased by more than 20,000 km^2 (6% of the land area) between the periods 1961–1990 and 1981–2010, mainly north of 63 ° N. Overall, air temperature increased in all seasons, with the highest increase in spring (particularly in April) and winter. Mean monthly air temperatures were significantly correlated with the monthly SCE, suggesting a positive land–atmosphere feedback enhancing warming in winter and spring.

Key words | Norway, snow cover, snow water equivalent, trend, warming

Jonathan Rizzi (corresponding author)
Irene Brox Nilsen
James Howard Stagge
Lena M. Tallaksen
Department of Geosciences,
University of Oslo,
P.O. Box 1047, NO-0316 Oslo,
Norway
E-mail: *jonathan.rizzi@geo.uio.no*

Jonathan Rizzi
Norwegian Institute of Bioeconomy Research,
P.O. Box 115, NO-1431 Aas,
Norway

Irene Brox Nilsen
The Norwegian Water Resources and Energy Directorate,
P.O. Box 5091 Majorstua, NO-0301 Oslo,
Norway

Kjersti Gisnås
Norwegian Geotechnical Institute,
P.O. Box 3930 Ullevaal Stadion, NO-0806 Oslo,
Norway

INTRODUCTION

Seasonal snow cover is a fundamental part of the cold climate water balance by storing water during winter until the snowmelt season (Wilson *et al.* 2010; Irannezhad *et al.* 2015) and of the Earth's energy balance by controlling the amount of reflected solar (shortwave) radiation through the high albedo of snow (Betts 2000; Dery & Brown 2007). Snow has major societal and economical importance in regions with a seasonal snow cover, affecting sectors such as hydropower production, agriculture, forestry, recreation and tourism. In the northern hemisphere, snow covers up to 30% of the global land area in winter (Vaughan *et al.* 2013), and its largest influence on the climate is during spring when the day length and solar radiation increase and snow starts to melt (NSIDC 2016). Recent changes in temperature (general warming) and precipitation (both increases and decreases) have altered snow conditions over the northern hemisphere, reducing both the fraction of precipitation falling as snow and the duration of the snow season (Dery & Brown 2007; Callaghan *et al.* 2011); the exception being some high elevation regions, where larger snow volumes have been observed due to an increase in winter precipitation, as reported by Dyrrdal *et al.* (2013) and Skaugen & Randen (2013) for Norway. A reduction in the snow cover, and thus in surface albedo, may enhance the warming signal because more energy is absorbed at the surface. This positive feedback to global warming in regions with a seasonal snow cover is thought to partially explain the accelerated warming over the Northern Hemisphere

doi: 10.2166/nh.2017.051

(Serreze *et al.* 2009). Observed Arctic warming has been more than twice as large as the global average (Cohen *et al.* 2014). Chapin *et al.* (2005) described and quantified the terrestrial feedback and found a 3.3 Wm^{-2} increase in absorbed energy at the surface because of advancing snowmelt, a much greater effect than that of vegetation changes.

Snow cover extent (SCE) in the northern hemisphere has decreased since the late 1960s, with an accelerated rate from 2003 (Derksen & Brown 2012). This is reflected in a large shift of the start and end of the snow season, with a stronger change in spring than in autumn and with larger decreases in maritime regions north of 60° N (Callaghan *et al.* 2011).

The climate of Norway shows large regional as well as local variations spanning over 13° of latitude and climate zones ranging from maritime mild temperate to arctic. It further has a rugged topography ranging from coasts to high mountains over small distances. This makes Norway an interesting cold climate laboratory that provides a unique opportunity to study changes and trends in snow cover and interactions with climate over a wide range of conditions. Such spatial and temporal differences may help identifying the main processes governing observed changes in Norway and provide relevant insights for similar trends in other regions with comparable conditions.

The climate of Norway is warming. Temperature trends for the period 1900–2014 have been found to be statistically significant for all seasons except winter (with a maximum trend of 0.13°C per decade in spring), with 2014 the warmest year in the record (2.2°C above normal, 1961–1990; Gangstø *et al.* 2016). The strongest temperature trends have been observed in northern Norway (Hanssen-Bauer *et al.* 2017). Førland *et al.* (2016) reported a larger temperature trend for the period 1955–2014 than for the longer 1900–2014 period, at 12 lowland stations located across the country. For this shorter period, they found the greatest warming in winter and spring for most stations, with up to 0.63°C per decade in winter at Gardermoen in southeastern Norway. Mean annual precipitation show an overall increase of 18% in the period 1900–2014 (linear trend), with the largest increase seen during autumn (eastern and southern Norway) and spring (west and north) and a less pronounced increase during summer (Hanssen-Bauer *et al.* 2017).

As climate is warming, impacts are felt on the ground. Previous studies have found decreasing trends in several snow indices such as snow depth, SCE and the length of the snow season across Norway (e.g., Dyrrdal 2009; Dyrrdal & Vikhamar-Schuler 2009; Dyrrdal *et al.* 2013). For the period 1981–2010, Dyrrdal *et al.* (2013) found a decline in snow depth at elevations lower than 1,000 m a.s.l. and in coastal regions (particularly at the southwestern coast). On the other hand, increasing snow depth has been observed for inland mountain stations in the period 1961–2010, due to increasing winter precipitation (Dyrrdal *et al.* 2013). A significant decrease in the number of days when precipitation falls as snow was found in half of the 585 meteorological stations studied by Dyrrdal (2009) over the period 1968–2007, particularly after 1990. Similarly, the highest percentage of significant negative trends was found in southern Norway (mainly along the coast). Furthermore, the findings of Dyrrdal *et al.* (2013) point towards an accelerated decline in snow depth during the last decades (i.e., 1961–2010). The above studies, overall, demonstrate a clear decline in snow cover. At the same time, the results also demonstrate a large sensitivity to the selected time period, the region under investigation and the method. Thus, care should be taken when comparing across studies, regions and periods.

The studies referred to above are based on observations from selected stations across Norway, and vary in the number of stations included, spatial coverage, time period chosen and methodology used to detect and map the changes. Thus, there is a need for a more complete view of all Norway to highlight regional differences and drivers of change. The availability of high-resolution observation-based gridded data makes this possible.

In this study, we perform a detailed analysis of trends and changes in snow climatology based on a gridded (1 × 1 km) hydro-meteorological dataset for Norway (seNorge; Tveito *et al.* 2005) covering the period 1961–2010. It is postulated that higher temperatures lead to less snow accumulation during autumn and winter, which when combined with higher winter and spring temperatures, produces an earlier snowmelt. This, in turn, may lead to accelerated warming (i.e., higher temperatures) in spring due to snow albedo feedbacks (see Groisman *et al.* 1994; Dery & Brown 2007).

The study is designed to assess the validity of this hypothesis by measuring process signals through:

i) a temporal analysis, estimating annual, seasonal and monthly changes in snow indices and related climate variables (i.e., precipitation and temperature) for all Norway (national scale) and two regional scales (i.e., 19 climatological regions and four aggregated macro regions; see next section);
ii) a regional analysis, evaluating spatial patterns of changes and correlation between climate variables and snow indices for different spatial scales, ranging from the grid cell scale to the national level;
iii) a comparative analysis of temperature trends and changes in snow indices.

The study adds to previous work by performing a detailed and comparative analysis of temporal and spatial change patterns in snow climatology based on daily time series from 1961 to 2010. The time series analysed include six snow indices as well as mean daily temperature and daily precipitation totals. Four grid cell (local) indices were derived (all available from seNorge): snow cover area (SCA), snow water equivalent (SWE), duration of the snow season, and precipitation falling as either snow (snowfall) or rain (rainfall). In addition, two indices derived at the regional scale were used: SCE, and regional SWE defined over a region or all Norway (regSWE). Norway was separated into 19 prevailing climatological regions following Dyrrdal *et al.* (2012), successively grouped into four macro regions. We derived changes in ten-year (decadal) running mean (monthly and seasonal) and three overlapping 30-year periods (1961–1990, 1971–2000, 1981–2010) for the selected snow indices for all Norway as well as for the separate climatological regions. When comparing across periods, 1961–1990 was used as a reference period.

STUDY AREA AND DATA

Climate regions and snow climatology

The Norwegian mainland area covers 323,781 km^2 and features a long north–south coastline and a mountain chain stretching across the Scandinavian Peninsula (Figure 1). Western Norway is characterized by a complex terrain due to large elevation gradients over small distances, whereas inland regions in eastern Norway have a more undulating landscape.

Despite Norway's high latitudes, the coastal climate is mild and wet (maritime) due to the influence of the North Atlantic Current and the prevailing southwesterlies, bringing mild, maritime air on shore (Aune *et al.* 1993). Precipitation is dominated by frontal storm events most of the year, with additional convective precipitation in inland regions during warm months (Hanssen-Bauer *et al.* 2017). The highest air temperatures are found close to the coast in southern Norway, whereas the lowest are found in the mountains and the far north (Hanssen-Bauer *et al.* 2017) (Figure 1).

Approximately 30% of the annual precipitation in Norway falls as snow (Dyrrdal *et al.* 2013). The geographic distribution of snow is highly irregular in regions of complex topography because of large variations in precipitation and redistribution by wind. The largest amount of snow during the period 1961–1990 was recorded in southwestern Norway, where the mean annual maximum SWE may exceed 1,000 mm. The lowest SWE values are seen along the coast (<100 mm). The duration of the snow season varies accordingly, from less than a month along the coast in southern Norway to more than nine months at high elevations.

In this study, we considered 19 regions defined by Dyrrdal *et al.* (2012), as shown in Figure 1. This regionalization is based on 13 precipitation (Hanssen-Bauer & Førland 1998) and six temperature regions (Hanssen-Bauer & Nordli 1998), later modified by Dyrrdal *et al.* (2012) to separate highlands (higher than 1,000 m a.s.l.) from lower-lying regions (e.g., region 8 was split into regions 8.1 and 8.2). The 19 regions were further aggregated into four larger groups, referred to as macro regions. The four macro regions are labelled according to their location/characteristics, and in the paper we refer to them using their names with a capital letter. The Mountain macro region (composed of the high-elevation parts of five regions) corresponds to areas above 1,000 m a.s.l. in southern Norway; the South West macro region aggregates four regions along the western coast (from Trondheim to Kristiansand; Figure 1); the South East macro region combines five regions located on the east side of the Mountain macro region; and the North macro region aggregates the five northernmost regions (north of Trondheim).

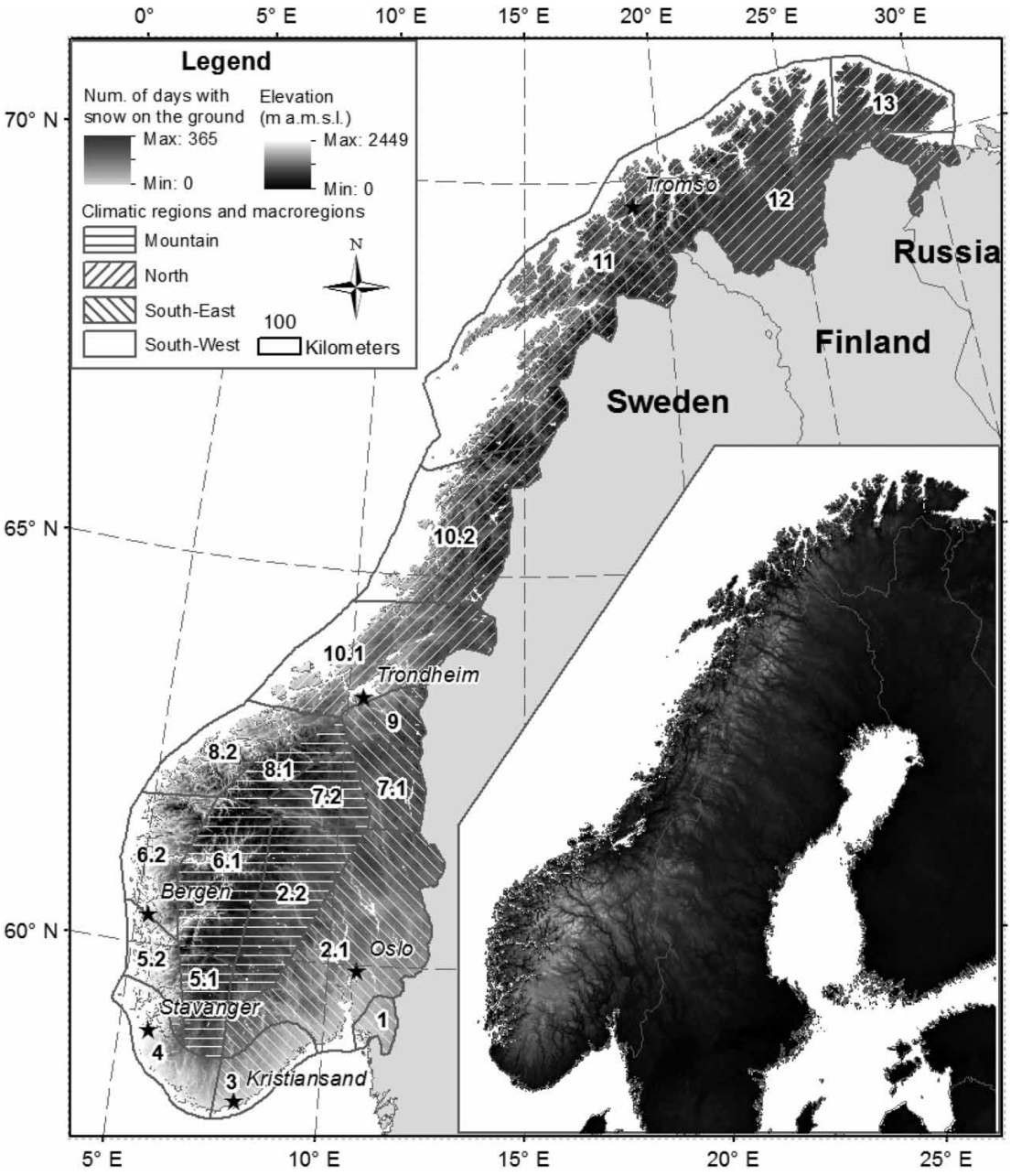

Figure 1 | The study region (Norway). The main map (left) shows mean annual precipitation (1961–1990) along with the 19 regions (numbered from 1 to 13 with subregions) and the four macro regions (shown as hashed areas) used in this study (modified from Dyrrdal *et al.* 2012). The inserted map (right) shows elevation on a 50 × 50 m resolution.

The seNorge dataset

The seNorge dataset is a gridded hydro-meteorological dataset for Norway at 1 km spatial resolution (Tveito *et al.* 2005), tracking SWE, SCA, precipitation and temperature. Regular meteorological observations (from the Norwegian Meteorological Office) are interpolated to the grid cell scale by Optimal Kriging interpolation (Tveito *et al.* 2005; Mohr 2008; Saloranta 2014a). Spatially interpolated values of temperature and precipitation are then used as input to NVE's operational hydrological model (HBV), which includes a snow model (Saloranta 2014b). Within the snow

model, two modules are run in sequence: i) the SWE model for snow pack water balance, based on the original snow routine in the HBV model (Sælthun 1996); and ii) the snow compaction and density module converting SWE into snow depth (Saloranta 2012). A further refinement was later added to the snow compaction module to simulate the spatial variability of SWE and SCA within each grid cell (Saloranta 2014b). Studies evaluating the snow model against observations have shown that the SWE and snow depth agree well (Saloranta 2014a, 2014b). The seNorge dataset covers a total area of about 323,000 grid cells over land. Data are available from the 1st of September 1957 until the present (updated daily).

Snow indices

The snow indices consist of four local grid cell indices and two derived regional indices (Table 1). Local indices for SCA and SWE are taken directly from the seNorge database. The duration of the snow season (D), is derived according to the definition by Dyrrdal & Vikhamar-Schuler (2009), who classified the SCA of each grid cell into five classes (with five different snow cover codes) based on a qualitative description of the amount of snow cover on the ground (Table 2). Following this scheme, we introduced quantitative SCA thresholds (Table 2) for each code based on the SCE in the grid cell following the definition from Dyrrdal *et al.* (2009). Subsequently, the first and last day of the snow season are identified as follows:

- start of snow season: first day in autumn with 10 consecutive days classified with code 4 (i.e., SCA $\geq$ 95%);
- end of snow season: the first day in spring after the last period of five consecutive days classified with a code equal to or less than 2 (i.e., $\leq$50%).

Daily rainfall and snowfall rate were derived by apportioning precipitation into snowfall and rainfall using a temperature threshold of 0.5°C (Saloranta 2012).

The regional indices include SCE and regional average snow water equivalent (regSWE). SCE is the total area covered by snow (in km^2) for a region or all Norway, whereas regSWE is the average SWE (in mm) over all grid cells with snow. SCE is calculated by multiplying the fraction (%) of the SCA with the total area of each grid cell (1 km^2) and then summing the snow covered area over all grid cells in the region or country.

METHODS AND ANALYSIS

Daily time series of snow indices and climate variables were aggregated to the monthly and seasonal time scales before analyses for five decades between 1961 and 2010 and three partially overlapping 30-year periods (1961–1990, 1971–2000, 1981–2010), with 1961–1990 representing the reference period. Four seasons were defined; winter (DJF), spring (MAM), summer (JJA) and autumn (SON). Changes in these time series of snow indices were assessed for each grid cell, regional values, and all Norway by analysing:

- decadal (ten-year) running means for seasonal and monthly snow indices (SCE and SWE) covering the full period (1961–2010; Figure 2);

Table 1 | Snow indices used in the study, separated into local (grid cell) indices and regional indices (derived from grid cell values)

	Symbol	Unit	Description
Grid cell index			
Snow cover area	SCA	% or km^2	Percentage (%) or area (km^2) of grid cell (1 km^2) covered by snow
Snow water equivalent	SWE	mm	Amount of water contained in the snowpack
Snowfall	Snowfall	mm/month	Monthly precipitation falling as snow
Snow season duration	D	days	Length in days from the start to end of snow season
Regional index			
Snow cover extent	SCE	km^2	Total surface covered by snow derived from the grid cell snow covered area (SCA)
Regional SWE	regSWE	mm/month	Spatial average of SWE within each region

Table 2 | Snow cover codes following Dyrrdal & Vikhamar-Schuler (2009)

Snow cover code	Description	Percentage used in this paper
0	No snow	
1	Minor parts of the ground covered with snow	
2	Equal areas with and without snow	SCA = 50%
3	Major parts of the ground covered with snow	
4	Ground fully covered	SCA ≥ 95%

- differences in mean monthly SCE and SWE (grid cell scale) between the last 30-year period (1981–2010) and the first 30-year (1961–1990) reference period, and in the duration of the snow season for each region and macro region (Figures 3 and 4);
- differences in mean monthly SCE, regSWE, temperature and precipitation between the last 30-year period (1981–2010) and the first 30-year (1961–1990) reference period in each macro region (Figure 5);
- correlations between time series of snow indices and climate variables (snowfall, rainfall and temperature) for the complete 50-year period (Figure 6);
- trend magnitude for running mean 30-year periods of temperature (Figure 7);
- variability in monthly temperature trends across Norway (Figure 8).

The trends are calculated using the Theil–Sen estimator (Theil 1950; Sen 1968), which is a nonparametric method for trend detection that is widely applied to hydro-meteorological time series (e.g., Martinez *et al.* 2012). The trend magnitude is defined as the median of the slopes connecting all possible pairs of values of the time series:

$$TS = median\left(\frac{y_j - y_i}{x_j - x_i}\right) \quad (1)$$

where x_i is the time of observation i, y_i is the value of observation i, and $(y_j - y_i)/(x_j - x_i)$ are slopes calculated for all pairs of values.

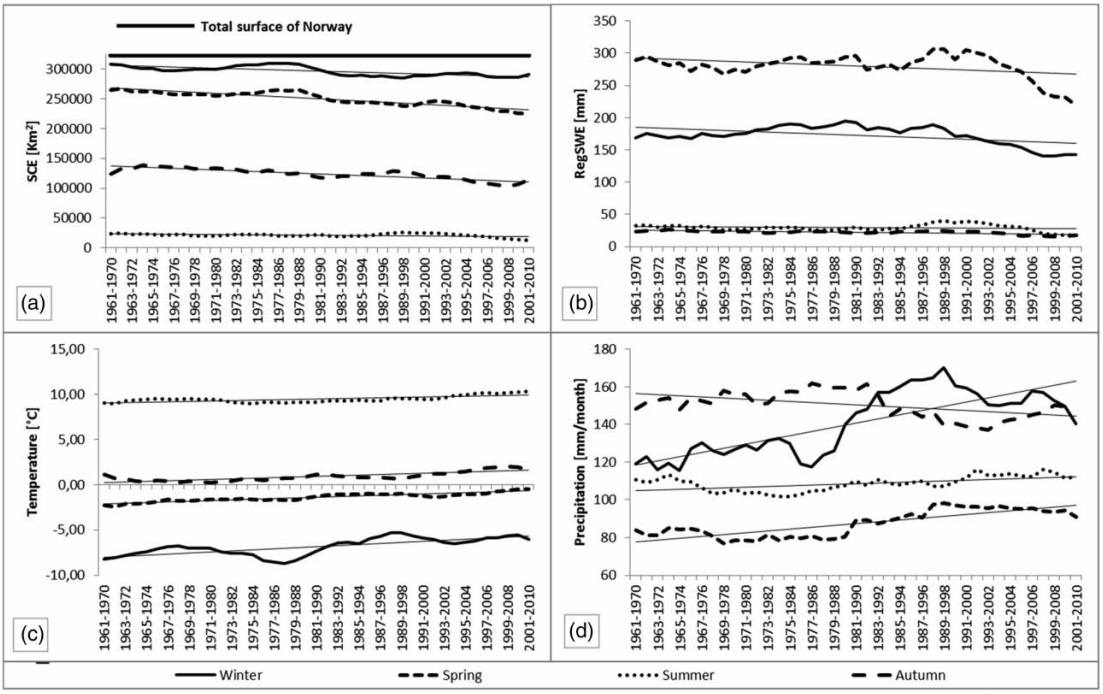

Figure 2 | Seasonal decadal running mean for SCE (a), regSWE (b), temperature (c) and precipitation (d) for all Norway. Black thin continuous lines show linear trends for each season for ease of comparison.

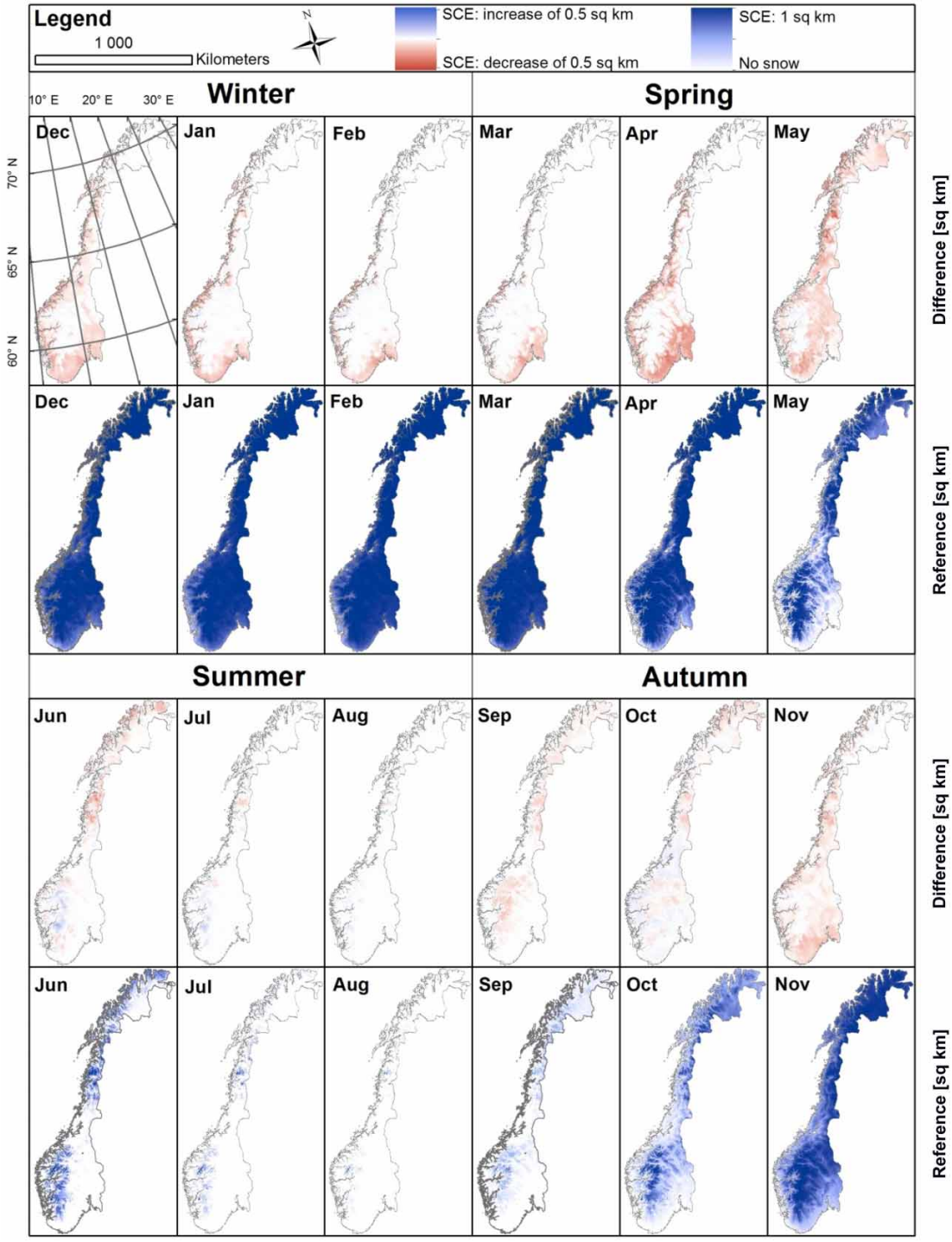

Figure 3 | Difference in mean monthly SCE (km^2) between 1981–2010 and 1961–1990 (first and third row) and mean monthly SCE (km^2) for the reference period 1961–1990 (second and fourth row). Please see the online version of the paper for the coloured figure.

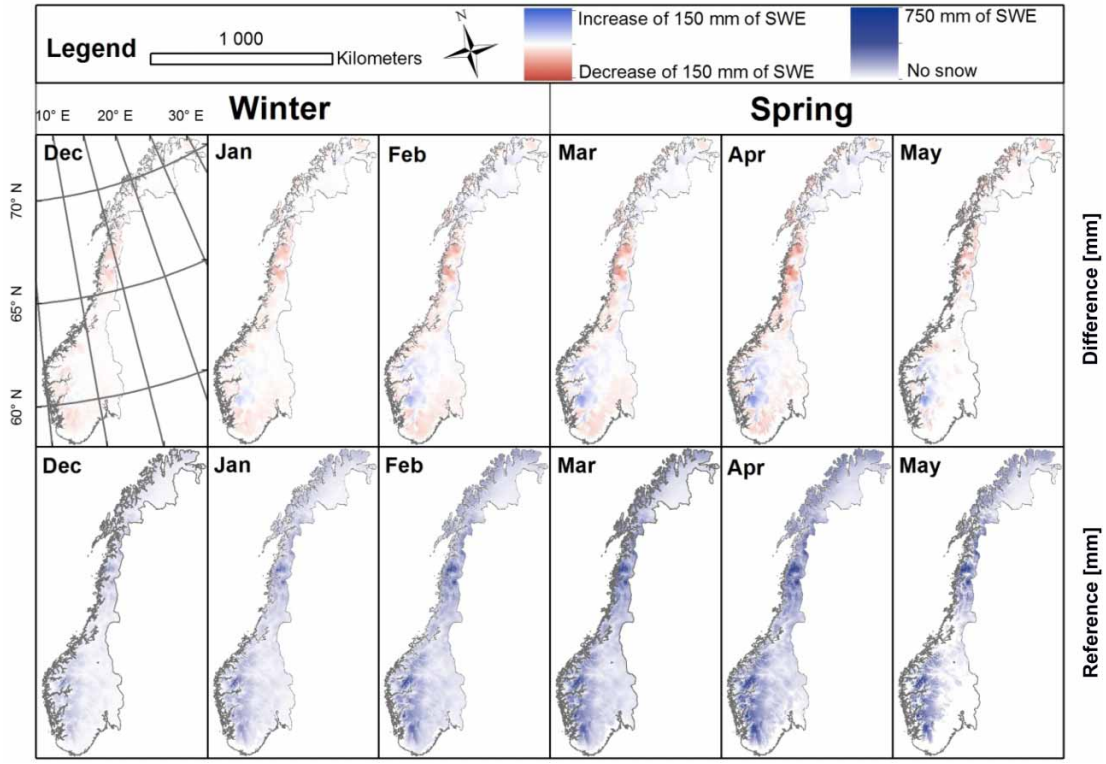

Figure 4 | Differences in mean monthly SWE between 1981–2010 and 1961–1990 (first row) and mean monthly SWE in the reference period 1961–1990 (second row). Please see the online version of the paper for the coloured figure.

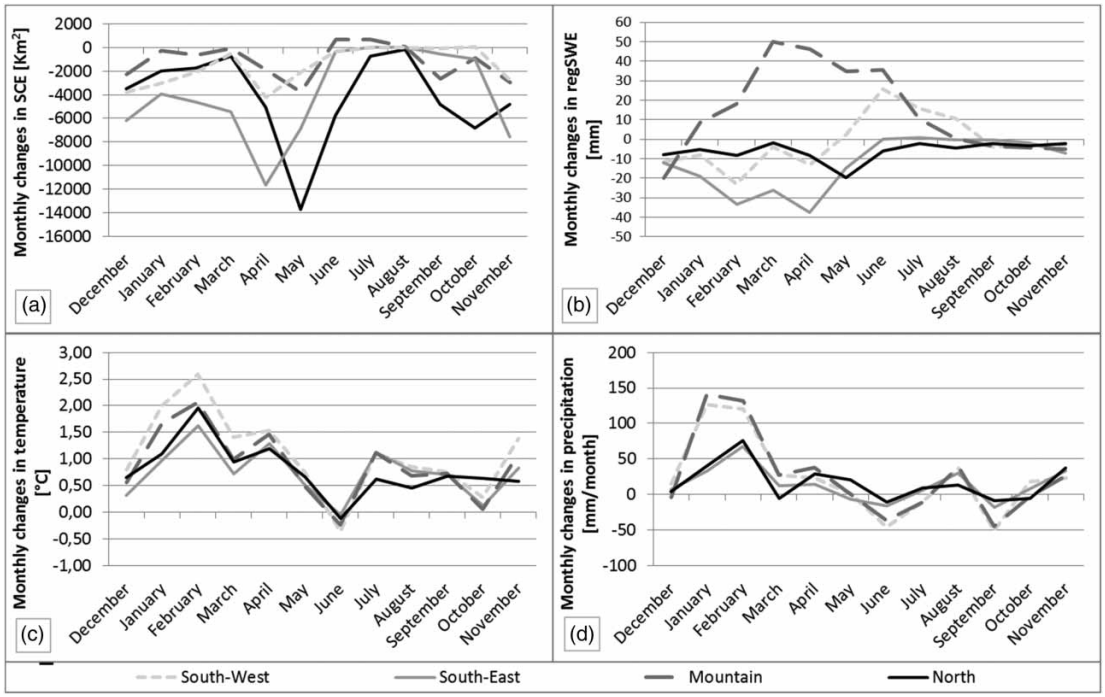

Figure 5 | Difference in mean monthly values between 1981–2010 and the reference period 1961–1990 in each macro region for: SCE (a), regSWE (b), temperature (c) and precipitation (d).

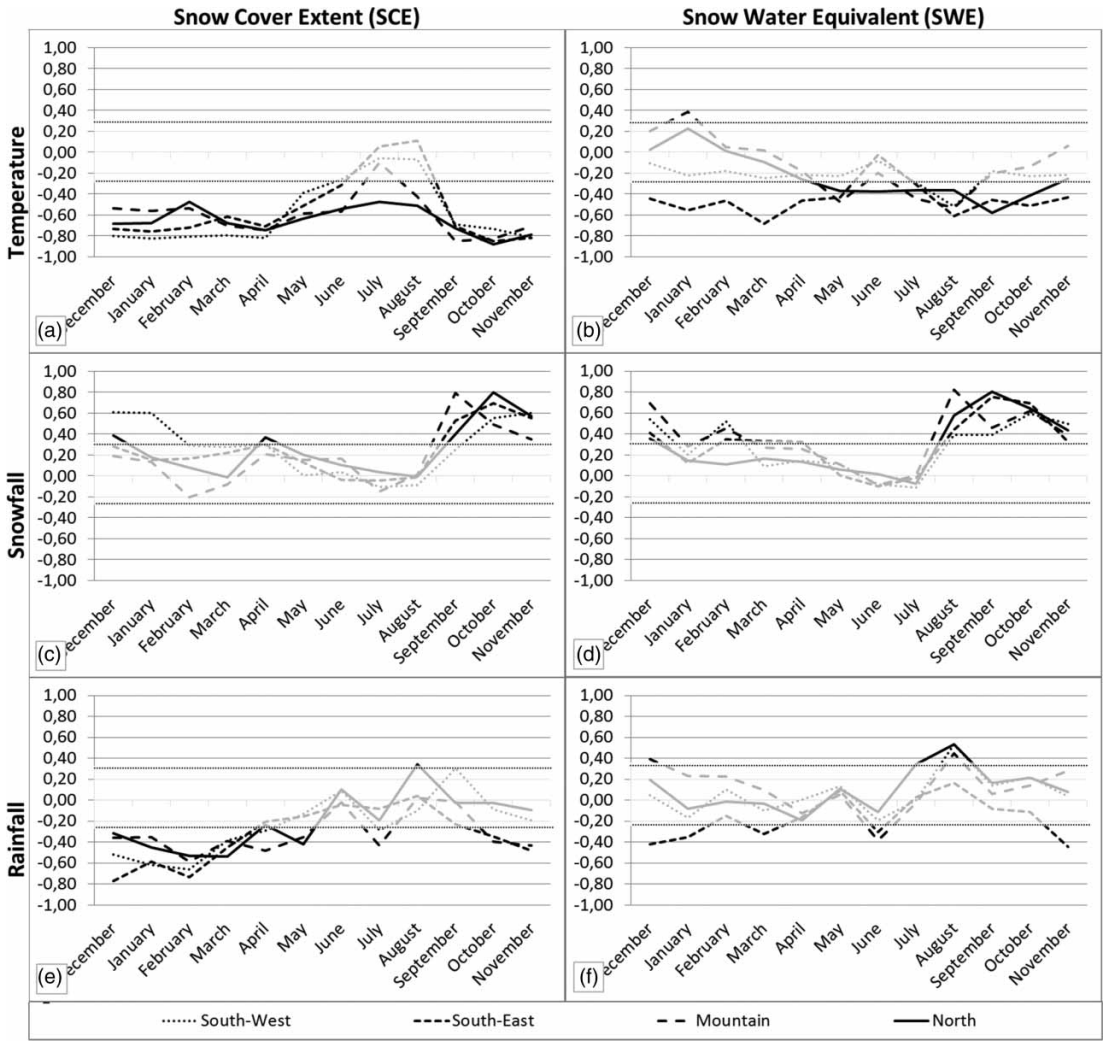

Figure 6 | Monthly correlation coefficient between climate indices and snow indices aggregated for macro regions. The two horizontal lines represent the significance thresholds (5% significance level). Only values higher/lower than these values are significant. Single plots show correlation between (a) temperature and SCE, (b) temperature and regSWE, (c) snowfall and SCE, (d) snowfall and regSWE, (e) rainfall and SCE, (f) Rainfall and regSWE.

Among the advantages of the Theil–Sen estimator are its lower sensitivity to outliers and its higher accuracy, compared to less-robust simple linear regression (El-Shaarawi & Piegorsch 2002). Regional trends were derived by aggregating the grid cell time series across each of the 19 regions and four macro regions prior to deriving the Theil–Sen trend magnitude.

Correlation between climate (temperature, snowfall and rainfall) and snow variables (SCE and SWE) was estimated using the Pearson correlation coefficient (Pearson 1931) at the macro region scale. The significance of the correlation coefficient is calculated as follows (assuming normal distribution):

$$t = \frac{\mathrm{r}}{\sqrt{(1 - r^2)/(\mathrm{N} - 2)}} \tag{2}$$

where t is the critical t-value (we chose a significance level of 0.05), N is the number of observations used in the correlation (here: 50 years, from 1961 to 2010), and r^2 is the explained variance in a linear regression.

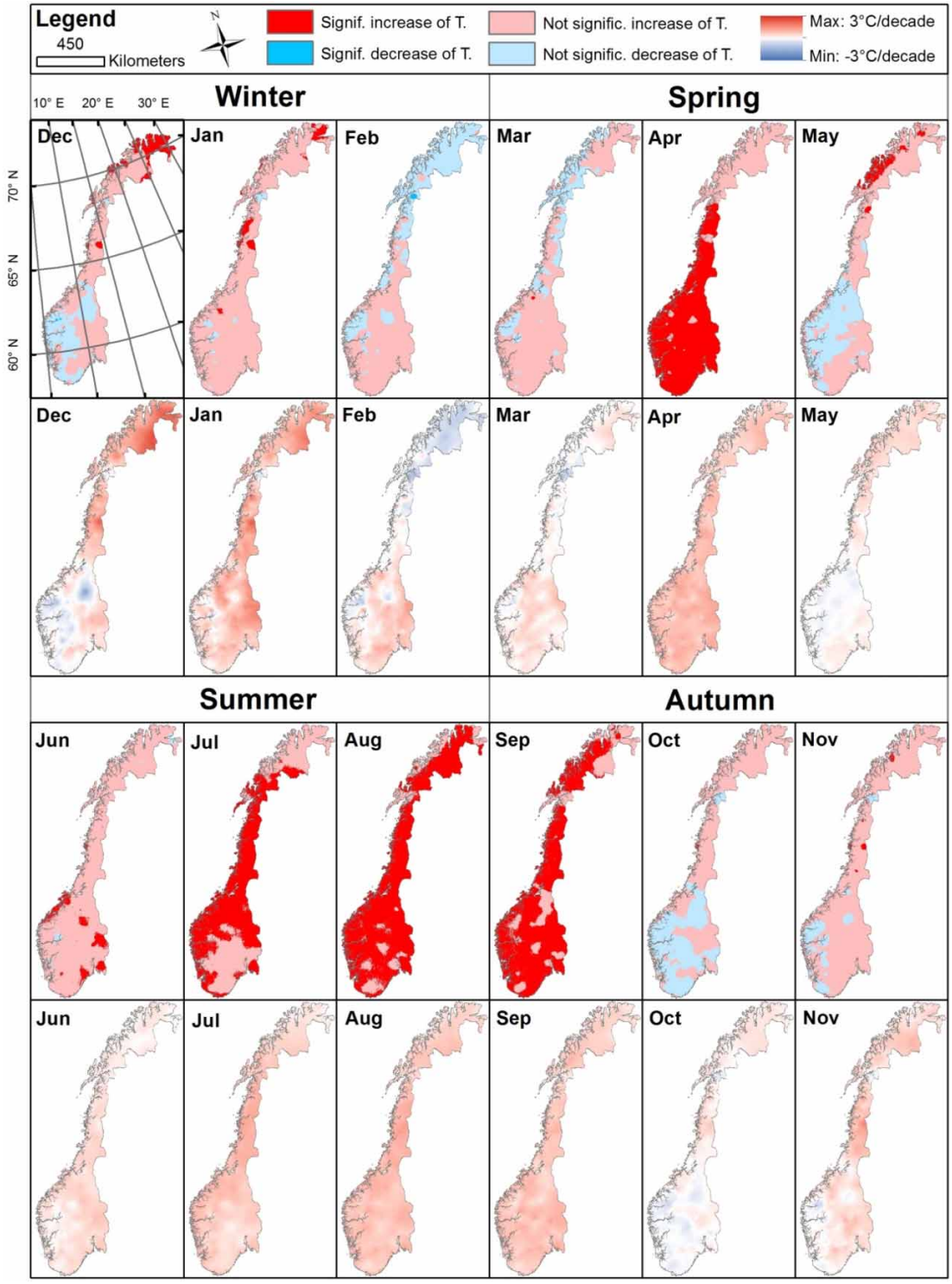

Figure 7 | Spatial distribution of trend in monthly temperature, shown as significance (Mann–Kendall test; first and third rows) and trend magnitude (Theil–Sen trend; second and fourth rows) for the period 1981–2010. Please see the online version of the paper for the coloured figure.

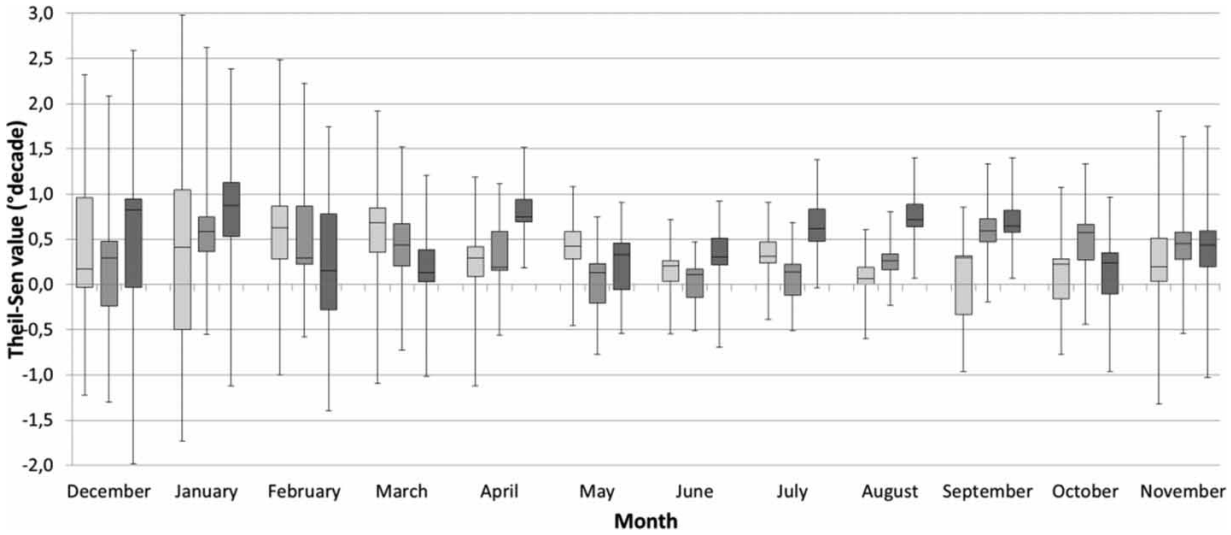

Figure 8 | Boxplots of monthly temperature trend (magnitude) for three periods of 30 years: 1961–1990 (light grey), 1971–2000 (medium grey) and 1981–2010 (dark grey), showing the range of trends across Norway.

RESULTS

We begin by presenting seasonal and monthly changes and trends in local and regional snow indices (SCE and regSWE), including an analysis of their variability in time and space. Further, a comparative analysis of changes and trends in snow indices and climate variables (temperature and precipitation), including their mutual correlation, is presented.

Temporal patterns

Decadal (ten-year) running means of snow cover extent (SCE in km^2) and regional average snow water equivalent (regSWE in mm) for all Norway are shown in Figure 2 along with corresponding values for temperature and precipitation. The whole period (1961–2010) is covered, starting with the decadal mean for 1961–1970 and then shifting the ten-year period forward one year at a time (i.e., 1961–2010, followed by 1962–1971, and so on, until 2001–2010). Each season is plotted separately, together with corresponding linear trends to assist interpretation.

The highest SCEs (Figure 2(a)) are found in winter, with approximately 90% of the country covered by snow, followed by spring. For context, the total Norwegian land area (323,781 km^2) is indicated in the figure by a horizontal line. An overall decrease is seen in SCE, particularly in spring. The macro region average SWE (regSWE; Figure 2(b)) displays a similar decrease in winter and spring. Here the highest values of regSWE are found in spring, despite a lower area coverage (ref. highest SCE in winter). Overall, we see a marked decline in regSWE in more recent decades. In summer and autumn, when there is little snow and glaciers make up much of the SWE area, SWE shows only minor changes.

To help understand these patterns, decadal mean temperature and precipitation for all Norway is also plotted in Figure 2. The decadal mean temperature (Figure 2(c)) increased during all seasons, with the largest increase and highest temporal variability seen in winter (~2–3°C per decade). The data show warmer winters in the early 1970s and early 1990s, and colder winters in the early 1980s. Decadal mean precipitation (Figure 2(d)) shows a much more diverse pattern, particularly in winter and spring. Winter precipitation increased notably from the early 1980s and during the mid 1990s, and a similar, but weaker signal is also found in spring. Summer, on the other hand, shows moderate changes (slightly increasing precipitation) as does autumn (slightly decreasing precipitation). From 1961–1970 to 2001–2010, the annual precipitation (over all Norway) increased by 5%.

To better understand the processes controlling the changes observed in SCA and regSWE for all Norway, we disaggregated the results in space (grid cell scale) as well as in time (monthly averages). The first and third rows of Figure 3 show the difference in mean monthly SCE (in km^2) between 1981–2010 and the reference period 1961–1990, i.e., $SCE_{1981–2010}$ minus $SCE_{1961–1990}$, by month. The mean SCE for the reference period (1961–1990) is shown in the second and fourth row, scaled from no snow to fully covered grid cell. Overall, a decrease in SCE is seen for most months, with the largest reduction in winter and spring. In January and February, the reduction is notable along the coast in southern Norway, extending further inland (mainly in low-lying areas below approximately 300 m a.s.l.), and northwards in spring (April, May) and early winter (November, December). Thus, the largest changes in SCE occurred at the beginning and end of the snow season. Minor, but consistent, changes were seen in summer and early autumn, when the presence of snow is limited to mountain and northern regions. For instance, June shows a reduction in the northern part of Norway where snow is still present, whereas an increase is seen in mountain regions in the south. Increasing SCEs are mainly limited to mountain regions in southwestern Norway in summer (June, July). Minor changes occurred in July and August when snow is mainly present on glaciers.

Using a similar format as Figure 3 (for SCE), Figure 4 shows monthly maps of the differences in mean monthly SWE (in mm/month) between the most recent 30-year period (1981–2010) and the reference period (1961–1990) (first row), along with reference maps of the mean monthly SWE (in mm) over the reference period 1961–1990 (second row). Here, only the winter and spring months are shown because only minor changes are found in summer and autumn. The main features of the SCE maps (Figure 3) are also reflected in SWE (Figure 4), such as a decrease in SWE for winter, becoming more pronounced in spring, particularly along the coast and in the north. However, there are also clear differences to SCE, notably the distinct increase in SWE in mountainous regions in southern Norway, particularly from February to May. These notable increases occur in regions with a high SWE. The exceptions are region 10.2 and the southern part of region 11, which both have high SWE values, but also experience a large decrease in SWE of up to 150 mm between the two periods.

Regional analysis

Differences in mean values of snow indices and climate variables between 1981–2010 and the reference period 1961–1990 are given in Figure 5 for each month and macro region. Changes in the mean seasonal SCE for Norway separated by macro region (Figure 5(a)), show a decrease in SCE for all macro regions in all months (except in Mountain during June and July). This trend is especially strong at the start and end of the snow season. In April and May, SCE decreased by more than 20,000 km^2 over all Norway (around 8% of the total country area), while in November and December, the total reduction over all Norway was around 15,000 km^2. The North had the largest monthly decrease of all macro regions (ca. 15,000 km^2 in May). The South-East experienced a nearly constant decrease of ca. 5,000 km^2 in each month from November to May, except in April, when SCE reduced by ca. 10,000 km^2 in the South-East. In fact, calculating the relative change in per cent, the South-West and South-East had the greatest relative SCE reduction (−4.5% and −5.2%, respectively), followed by North (−2.8%) and Mountain (−1.6%).

During winter and spring, regSWE decreased for all macro regions except for Mountain (Figure 5(b)), where a consistent increase in regSWE was seen from January to July, peaking in March/April. During late spring there was a consistent decrease in regSWE for South-East and North regions, whereas regSWE increased for the South-West in early summer, when snow covers a limited surface area.

Temperature increased for all macro regions and months except June, with the greatest changes occurring in late winter and early spring (Figure 5(c)). South-West registered the highest monthly temperature increase of more than 2.5°C (in February); however, the monthly variability in time overall follows a similar pattern across all macro regions.

Precipitation showed a notable increase in Mountain and South-West in January and February, with an increase of more than 120 mm/month compared to the reference (Figure 5(d)). These two regions overall follow a very

similar seasonal pattern in monthly precipitation changes as do South-East and North although with a dampened amplitude. Here, a maximum precipitation increase is seen in February (more than 50 mm/month) and small changes are observed during the rest of the year. The notable increase in precipitation in winter (January and February) coincides with increasing snow accumulation (SWE; Figure 5(b)) in Mountain, this being the snowfall season.

The reduction in SCE is clearly visible from September onwards, i.e., at the start of the snow season, peaking in November/December and then again towards the end of the snowmelt season in April/May.

To further analyse changes in SCE (Figure 5(a)) in April/May and November/December, we calculated changes in the start and end of the snow season along with mean duration. These variables were calculated based on SCE for each region and macro region over the first and last 30-year periods (1961–1990 and 1981–2010, respectively) and are summarized in Table 3. The snow season duration decreased in all regions except for region 7.1 and four out of the five regions included in Mountain. The largest decrease in snow season duration occurred in the South-West and North macro regions, where the snow season was, on average, 15 and 17 days shorter in 1981–2010 compared to the reference 1961–1990. Conversely, the snow season duration increased in four (of five) regions constituting the Mountain macro region), producing an average snow season increase of 10 days.

The shorter snow season in the other three macro regions was caused by a delay in the start of the snow season of approximately 1 week, and by an earlier end to the snow season in two of the three macro regions (nearly 1 week earlier in the South-West and almost 2 weeks in North; Table 3). All, but two regions, displayed a later start to the snow season (both part of Mountain macro region), whereas the end of the snow season varied more among regions, with a majority showing earlier snow-free dates, but with both positive and negative shifts observed, even within the same macro region. The increase in snow cover duration in Mountain was mainly due to a delayed end of the season, reflecting the larger snow volumes, particularly in the two eastern regions (2.2 and 7.2) with more than 2 weeks.

Table 3 | Changes in the start, end and duration of the snow season between 1981–2010 and the reference period 1961–1990 for each region and macro region

Macro region	South-west					South-east					Mountain					North				
Region	8.2	6.2	5.2	4	*Avg.*	9	7.1	2.1	1	3	*Avg.*	8.1	7.2	6.1	2.2	5.1	*Avg.*	13	11	12	10.2	10.1	*Avg.*
Start	7	9	15	7	***9***	5	4	5	10	3	***5***	5	3	−6	2	−6	***−1***	11	2	10	5	8	***6***
End	2	3	−28	−13	***−6***	−6	8	4	−4	−8	***2***	−2	17	4	16	3	***9***	−14	−16	−4	−11	−9	***−11***
Duration	−5	−6	−43	−20	***−15***	−11	4	−1	−14	−11	***−3***	−7	14	10	14	10	***10***	−25	−18	−14	−15	−17	***−17***

Start/end of the snow season (in days); positive values indicate a later start/end. Duration: negative values indicate a shorter snow season; positive values indicate a longer snow season.

Concurrent changes in snow and climate variables

Monthly correlation coefficients between snow indices (i.e., SCA and SWE) and climate variables (i.e., temperature, rainfall and snowfall) calculated for each macro region are shown in Figure 6. Correlation coefficients greater than 0.28 are statistically significant and marked by a grey shaded area in each plot.

Temperature is significantly negatively correlated with SCE (Figure 6(a)), except in the South-East and South-West during summer, when there is usually no snow, and in Mountain in July, when there is little snow. Temperature shows a significant negative correlation with SWE (Figure 6(b)) in South-East during winter and spring and in South-East and North during autumn. Temperature is positively correlated with SWE in Mountain (significant) in January.

Snowfall is significantly correlated with both SCE and SWE for much of the snow season. Snowfall and SCE (Figure 6(c)) are positively correlated in all macro regions from September (except South-West) to November. The correlation is significant in North and South-West in December and in South-West also in January. Further, the correlation of snowfall with SWE (Figure 6(d)) was positive in all macro regions from August to December and also in February with the exception of South-East. Rainfall has a significant negative correlation with SCE in all seasons except summer and April/May for South-East and South-West (Figure 6(e)). Finally, rainfall and SWE have a negative (significant) correlation during autumn and winter (October through January) for Mountain (Figure 6(f)) and positive correlation during late summer (July through August) for all macro regions, although not statistically significant for the South-West region.

Temperature changes and trends

We analysed temperature trends to assess concurrent spatial and temporal patterns indicating potential feedbacks between snow cover and temperature over the period 1981–2010. The maps in Figure 7 show regions of the trend significance for temperature (first and third row) and the trend magnitude (second and fourth row). The maps reveal a general temperature increase across Norway with notable regional and seasonal patterns. The warming trend is strongest (trend magnitude) in the far north in December and January. In April and again from June to September, the warming trend affects most of Norway. These are also the regions and time of year depicting large-scale significant trends. More localized (significant) warming was found for smaller regions in northern Norway in December, January and May and in southern Norway in June (Figure 7). The strongest trend magnitudes, seen on the Finnmarksvidda plateau (region 12) in December and January, were not significant in all grid cells because of large interannual variability in temperature in this region. Trends towards cooler conditions are found in December, February, May and October; however, these are not significant and thus not commented on further.

Temperature trends were subsequently calculated for the three 30-year periods (1961–1990, 1971–2000 and 1981–2010) to evaluate the rate of change over time, shown as boxplots of all grid cells for each month in Figure 8. The trend is usually stronger in winter and spring (when also the interannual variability is highest), with peak values in January and April for the most recent 30-year period (1981–2010). April, July, August and September also show the strongest trend magnitude in the most recent period), indicating an acceleration of the warming. This is not the case in February, March, May and October; however, all months still show a warming trend. The largest interannual variability in trend magnitude was found in the coldest months of the year, from November to February (Figure 8).

DISCUSSION

The performed analysis allowed us to detect a clear reduction in SCE for all macro regions and a diffused reduction in SWE (with an increase mainly in Mountain). Clear regional and seasonal differences are found – providing insight into what is driving these rapid and diverse spatial and temporal patterns of change. The highest temperature increases are occurring in periods when we also find the largest reduction in SCE and SWE, at a time when the snow cover is still extensive, but melts rapidly (i.e., towards the end of melting period in April and May). The exception is Mountain, where the increase in SWE can be explained by notably higher precipitation during winter. The positive correlation between SWE and rainfall

found for Mountain in December may be caused by refreezing rainfall or precipitation that actually falls as snowfall, but is reported as rain by the model. SCE is less affected by the increase in winter precipitation. The pronounced warming in late summer and early autumn has a minor influence on SWE because the snow cover then is limited.

Comparison to other studies

Our findings are consistent with studies investigating the decline of the Arctic SCE (Tedesco *et al.* 2009; Callaghan *et al.* 2011; Derksen & Brown 2012). Early spring SCE in the Arctic has reduced by 11% in April during the period 1970–2010 (Brown & Robinson 2011), and by 18% in May to June in the period 2008–2012 compared to pre-1970 values (Derksen & Brown 2012), with larger decreases in maritime regions north of 60°N (Callaghan *et al.* 2011). The Arctic spring SCE decline observed over the past decades was found to be largely driven by increasing temperatures (Brown & Robinson 2011; Derksen & Brown 2012), enhanced by snow albedo feedbacks (Groisman *et al.* 1994; Dery & Brown 2007). Warming was, to a lesser extent, influenced by anomalous SST influencing the atmospheric circulation (Bao *et al.* 2011) or energy convergence (Mioduszewski *et al.* 2014).

A decline in snow cover duration is also observed in the Arctic, similar to what we observe for Norway, with up to 5 days per decade in autumn and up to 10 days per decade in the melt season for the periods 1979–2008 (Tedesco *et al.* 2009), 2008–2012 (Derksen & Brown 2012) and 1979–2007 (Callaghan *et al.* 2011). Previous studies of Norway have confirmed a shortening of the snow duration, particularly in southern Norway, with linear trends up to 25 days per decade (Dyrrdal & Vikhamar-Schuler 2009; Dyrrdal 2009, 2010). A significant decrease in the number of snow days was documented at almost half of the 585 meteorological stations studied by Dyrrdal (2009) across all Norway for the period 1960–2007, particularly after 1990 (which is when our first 30-year period ends).

We found the largest reduction in SCE during the snowmelt season. Dyrrdal & Vikhamar-Schuler (2009) similarly found the number of snow days in Norway to decline the most at the end of the melting period. These results are consistent with the explanations of Groisman *et al.* (1994) and Callaghan *et al.* (2011), who highlight that snow albedo feedbacks act more strongly in late spring and summer than at the onset of the snow season. Given the same reduction in SCE, more energy will be available at the surface in spring (end of the snow season) than autumn (start of the snow season), particularly at higher latitudes, when the incoming solar radiation is high. This is especially important north of the Arctic Circle where there is midnight sun in June, whereas the snowfall season usually starts after the autumn equinox. Accordingly, the snow albedo feedbacks are expected to be less important in autumn than in late spring and summer. Our results showed changes in SCE in both spring and autumn. The more mixed results for the snow duration are due to a combination of factors, including regionally varying precipitation trends, which is relevant for regions covering inland and coastal climates (e.g., regions 10.1, 10.2 and 11). Another factor is the high sensitivity to changes in temperature when the temperature is close to zero, which is relevant for regions with mild winters (e.g., regions 3, 4 and 5.2).

SWE changes as reported here for Norway are supported by previous studies, which similarly found increases in SWE at high elevations, particularly in mountain areas in southern Norway. Skaugen *et al.* (2012) found (significantly) increasing SWE for high elevation stations (elevation >850 m a.s.l.) for the period 1961–1990. Dyrrdal *et al.* (2013) analysed trends in snow depth at 926 stations across Norway covering an elevation range of 1–1,700 m a.s.l. and found a significant decline in snow depth across lowland regions for the period 1961–2010. For 1981–2010, the decline was particularly visible at the western coast of Norway, but to a smaller degree in the eastern part – than was the case for the full period 1961–2010. Similarly to Dyrrdal *et al.* (2013), we find an accelerated decline in snow depth across all Norway for lowland regions during the past decades.

Accelerated warming in spring

The trend analyses presented here confirm a general warming in all seasons for Norway; most pronounced in South-West in winter, but with a similar seasonal (monthly) pattern within each macro region. Førland *et al.* (2016) similarly reported warming in all seasons for the period

1955–2014, with the largest temperature increase in winter and spring (12 stations).

As emphasized earlier, the pronounced warming in April coincides with the period of the strongest SCE changes. This suggests that snow albedo feedbacks may play a role, as elaborated above. Further, with less snow on the ground, not only does the ground reflect less incoming radiation, but also, more energy is absorbed and available to heat the ground and lower atmosphere, leading to significant increases of the near surface temperature (Aas *et al.* 2017). The longer snow-free season allows more evapotranspiration and thus, potentially more intense drying of the soil in summer, which again may lead to soil moisture–temperature feedbacks (Seneviratne *et al.* 2010). Chapin *et al.* (2005) concluded that earlier snowmelt explained the increased summer warming in Alaska by snow and vegetation feedbacks during the last decades of the 20th century.

Hydrological impacts

Changes in SWE and snow cover duration significantly influence the flood regime, also affecting sectors like hydropower, water supply and tourism. The hydrological regimes in most inland and northern catchments in Norway are characterized by a snowmelt-generated 'spring flood', which continues into the summer months for glacier and high-alpine catchments (Gottschalk *et al.* 1979; Wilson *et al.* 2010; Vormoor *et al.* 2015). The observed decrease in snow volume during the winter has subsequently led to a shift in the timing and a decrease in snowmelt-generated floods (Wilson *et al.* 2010), which are observed earlier in spring (Dyrrdal *et al.* 2012). This is in agreement with findings from other high-latitude regions, such as Finland (Irannezhad *et al.* 2015), Alaska (Chapin *et al.* 2005) and Canada/US (Brown & Robinson 2011; Mioduszewski *et al.* 2014). This decreasing trend in snow volume is expected to continue into the future as warming trends continue; however, higher precipitation in high elevation regions may counteract this effect to some extent.

Uncertainty

The results of this study, which is based on interpolated climate data and modelled snow data, are affected by uncertainties in the data due to: i) errors in the temperature and precipitation measurements, including reading errors, inhomogeneity, missing data and precipitation undercatch, and ii) errors generated by the models/interpolation methods. Undercatch is particularly a large source of error when measuring snowfall and can reach 80% in areas exposed to high winds (Orskaug *et al.* 2011).

The spatial coverage of temperature and precipitation stations in Norway is denser at low elevations and populated areas, leading to under-representation of mountainous and remote regions. The quality of the seNorge data thus varies in space. seNorge performs well in gauged grid cells, but the performance in grid cells without observations is less reliable. While a grid resolution of 1 km produces an extremely fine grid for national-scale analysis, it does not perfectly reproduce the complex terrain in some extreme areas of Norway. The quality of seNorge also varies in time, because stations have been added and removed from the dataset, depending on data availability.

Trends are highly sensitive to the region and time period considered and care must therefore be taken when comparing across studies, as demonstrated also by our results. In particular, trend studies with annual or seasonally aggregated station values (e.g., Hanssen-Bauer *et al.* 2017) will have more smoothing of extreme values than our monthly data. For example, we found the largest temperature trend of almost 3°C per decade in December in Finnmark (1981–2010) as a grid cell value. In comparison, Hanssen-Bauer *et al.* (2017) found that, for all Norway, the linear temperature trend was highest for spring (0.13°C per decade for 1900–2014). Thus, the seasonal trend magnitudes reported in Hanssen-Bauer *et al.* (2017) are not directly comparable to our monthly trends, which implicitly will result in higher trends. Further, we report temperature trends at the grid cell scale, whereas Hanssen-Bauer *et al.* (2017) reported aggregated seasonal trends for six temperature regions based on station data. However, at individual stations, higher trends were reported (e.g., a linear trend of 0.63°C per decade for one station – Gardermoen).

Not only the trend magnitude, but also the trend significance depends on the time period under study. Natural climate variability adds to a long-term climatic trend, and in a short time series the influence of natural variability will be larger. For instance, we found the strongest trend

magnitudes in December and January (for the period 1981–2010). However, these trends were not significant because of the high temporal variability in temperatures in winter (for all sub-periods). Atmospheric circulation is more variable in winter than in summer (Hurrell & Deser 2009), and winter temperatures are more closely related to the atmospheric circulation in winter than in summer (Vautard & Yiou 2009). The North Atlantic Oscillation (NAO), for example, has a strong influence on winter temperatures in northern Europe (Hurrell & Deser 2009) at an annual to decadal time scale. Between the 1960s and 1990s, NAO was in its positive phase, advecting warm, moist air from the Atlantic towards Norway, but returned to neutral or negative levels after the 1990s (Hurrell & Deser 2009). Our full period, from 1961 to 2010, and sub-periods therein, thus include the increase in NAO in whole or in part.

CONCLUSIONS

In this study, seasonal and temporal changes in snow indices and climate variables have been analysed to answer whether high latitude warming and associated reduction in snow cover and volume, in turn, has led to accelerated warming in spring due to the snow albedo feedback. We have quantified changes in snow indices and climate variables as differences between two partly overlapping 30-year periods and as linear trends over the most recent of these 30-year periods.

First, we looked at the temporal development (decadal running means) for the most recent 50-year period, from 1961 to 2010, and detected a decrease in the SCE, especially at the start and end of the snow season. This implied a shortening of the snow season of 1–3 weeks. The SCE decreased by about 25,000 km^2 for all Norway (8% of the country area) in April and May between the periods 1981–2010 and 1961–1990. A clear temperature increase is seen for most regions and seasons in Norway, with significant warming in spring, and late summer for most of the country.

Our findings suggest that warming, being more pronounced in spring (notably April) caused earlier snowmelt, whereas higher temperatures suppressed snow accumulation in autumn with the exception of high elevation (mountain) regions. Here, higher winter precipitation has led to more snow accumulating and a later end of the snow season. The fact that the largest changes occurred in spring when the days are longer and the solar radiation stronger than in autumn, suggests that snow albedo feedbacks play a role.

This study has identified trends among climate and snow observations that are consistent with snow albedo feedback processes. Further study is needed using coupled land–atmosphere models to explore the coupling mechanism in greater detail.

ACKNOWLEDGEMENTS

This work forms a contribution to LATICE, which is a strategic research area funded by the Faculty of Mathematics and Natural Sciences at the University of Oslo, Norway. The authors would like to acknowledge the Norwegian Water and Energy Directorate (NVE), the Norwegian Meteorological Institute (met.no) and the Norwegian Mapping Authority for providing the seNorge data.

REFERENCES

Aas, K., Gisnås, K., Westermann, S. & Berntsen, T. 2017 A tiling approach to represent subgrid snow variability in coupled land surface–atmosphere models. *Journal of Hydrometeorology* **18**, 49–63. doi: 10.1175/JHM-D-16-0026.1.

Aune, B., Bjørbæk, G. & Førland, E. 1993 *Nasjonalatlas for Norge. Hovedtema 3: Klima (National Atlas for Norway. Main topic 3: Climate)*.

Beisland, C. S., Birkelund, H., Endresen, H., Haddeland, I. & Vik, M. A. 2015 *Et væravhengig kraftsystem - og et klima i endring (A Weather Dependent Power System – and a Changing Climate)*. Report 54:2015. Norwegian Water Resources and Energy Directorate, Oslo, Norway (in Norwegian).

Betts, R. A. 2000 Offset of the potential carbon sink from boreal forestation by decreases in surface albedo. *Nature* **408** (6809), 187–190. doi:10.1038/35041545.

Brown, R. D. & Robinson, D. A. 2011 Northern Hemisphere spring snow cover variability and change over 1922–2010 including an assessment of uncertainty. *Cryosphere* **5** (1), 219–229. doi:10.5194/tc-5-219-2011.

Callaghan, T. V., Johansson, M., Brown, R. D., Groisman, P. Y., Labba, N., Radionov, V., Barry, R. G., Bulygina, O. N., Essery, R. L. H., Frolov, D. M., Golubev, V. N., Grenfell, T. C., Petrushina, M. N., Razuvaev, V. N., Robinson, D. A.,

Romanov, P., Shindell, D., Shmakin, A. B., Sokratov, S. A., Warren, S. & Yang, D. Q. 2011 The changing dace of Arctic snow cover: a synthesis of observed and projected changes. *Ambio* **40**, 17–31. doi:10.1007/s13280-011-0212-y.

Chapin 3rd, F. S., Sturm, M., Serreze, M. C., McFadden, J. P., Key, J. R., Lloyd, A. H., McGuire, A. D., Rupp, T. S., Lynch, A. H., Schimel, J. P., Beringer, J., Chapman, W. L., Epstein, H. E., Euskirchen, E. S., Hinzman, L. D., Jia, G., Ping, C. L., Tape, K. D., Thompson, C. D., Walker, D. A. & Welker, J. M. 2005 Role of land-surface changes in Arctic summer warming. *Science* **310** (5748), 657–660. doi:10.1126/science.1117368.

Cohen, J., Screen, J. A., Furtado, J. C., Barlow, M., Whittleston, D., Coumou, D., Francis, J., Dethloff, K., Entekhabi, D., Overland, J. & Jones, J. 2014 Recent Arctic amplification and extreme mid-latitude weather. *Nature Geoscience* **7** (9), 627–637. doi:10.1038/Ngeo2234.

Derksen, C. & Brown, R. 2012 Spring snow cover extent reductions in the 2008–2012 period exceeding climate model projections. *Geophysical Research Letters* **39**. doi:Artn L19504 10.1029/2012gl053387.

Dery, S. J. & Brown, R. D. 2007 Recent Northern Hemisphere snow cover extent trends and implications for the snow-albedo feedback. *Geophysical Research Letters* **34** (22). doi:Artn L22504 10.1029/2007gl031474.

Dyrrdal, A. V. 2009 *Trend Analysis of Number of Snow Days per Winter Season in Norway*. Met.no Report 07/2009 Climate. The Norwegian Meteorological Institute, Oslo, Norway.

Dyrrdal, A. V. 2010 An evaluation of Norwegian snow maps: simulation results versus observations. *Hydrology Research* **41** (1), 27–37. doi:10.2166/nh.2010.019.

Dyrrdal, A. & Vikhamar-Schuler, D. 2009 *Analysis of Long-Term Snow Series at Selected Stations in Norway*. Met.no Report 05/2009 Climate. The Norwegian Meteorological Institute, Oslo, Norway.

Dyrrdal, A. V., Isaksen, K., Hygen, H. O. & Meyer, N. K. 2012 Changes in meteorological variables that can trigger natural hazards in Norway. *Climate Research* **55** (2), 153–165. doi:10.3354/cr01125.

Dyrrdal, A. V., Saloranta, T., Skaugen, T. & Stranden, H. B. 2013 Changes in snow depth in Norway during the period 1961–2010. *Hydrology Research* **44** (1), 169–179. doi:10.2166/nh.2012.064.

El-Shaarawi, A. H. & Piegorsch, W. W. 2002 *Encyclopedia of Environmetrics*, Vol 2. John Wiley & Sons.

Førland, E., Hanssen-Bauer, I., Haugen, J. E., Hygen, H. O., Haakenstad, H., Isaksen, K. & Dyrrdal, A. V. 2016 *Background Information for 'Klima i Norge 2100'*. NCCS Report 1/2016. Norwegian Centre for Climate Services, Oslo, Norway, pp. 50.

Gangstø, R., Heiberg, H., Kristiansen, S., Mamen, J., Szewczyk-Bartnicka, H. & Tillet Tajet, H. T. 2016 *Været i Norge Klimatologisk månedsoversikt. Året 2015 (The Weather in Norway, Monthly Climatology Summary. The Year 2015)*. Met Info Report 13/2015. The Norwegian Meteorological Institute, Oslo, Norway, pp. 23.

Gottschalk, L., Jensen, J. L., Lundquist, D., Solantie, R. & Tollan, A. 1979 Hydrologic regions in the Nordic countries. *Nordic Hydrology* **10** (5), 273–286.

Groisman, P. Y., Karl, T. R. & Knight, R. W. 1994 Observed impact of snow cover on the heat balance and the rise of continental spring temperatures. *Science* **263** (5144), 198–200. doi:10.1126/science.263.5144.198.

Hanssen-Bauer, I. & Nordli, P. Ø. 1998 *Annual and Seasonal Temperature Variations in Norway 1896–1997*. Met.no Report 25/98 Climate. The Norwegian Meteorological Institute, Oslo, Norway.

Hanssen-Bauer, I., Førland, E. J., Haddeland, I., Hisdal, H., Mayer, S., Nesje, A., Nilsen, J. E. O., Sandven, S., Sandø, A. B., Sorteberg, A. & Ådlandsvik, B. 2017 *Climate in Norway 2100 - A Knowledge Base for Climate Adaption*. NCCS Report 1/2017. Norwegian Centre for Climate Services, Oslo, Norway, pp. 48.

Hurrell, J. W. & Deser, C. 2009 North Atlantic climate variability: the role of the North Atlantic Oscillation. *Journal of Marine Systems* **78** (1), 28–41. doi:10.1016/j.jmarsys.2008.11.026.

Irannezhad, M., Ronkanen, A. K. & Klove, B. 2015 Effects of climate variability and change on snowpack hydrological processes in Finland. *Cold Regions Science and Technology* **118**, 14–29. doi:10.1016/j.coldregions.2015.06.009.

Martinez, C. J., Maleski, J. J. & Miller, M. F. 2012 Trends in precipitation and temperature in Florida, USA. *Journal of Hydrology* **452**, 259–281. doi:10.1016/j.jhydrol.2012.05.066.

Mioduszewski, J. R., Rennermalm, A. K., Robinson, D. A. & Mote, T. L. 2014 Attribution of snowmelt onset in Northern Canada. *Journal of Geophysical Research – Atmospheres* **119** (16), 9638–9653. doi:10.1002/2013jd021024.

Mohr, M. 2008 *New Routines for Gridding of Temperature and Precipitation Observations for 'seNorge.no'*. Met.no Note 08/2008. The Norwegian Meteorological Institute, Oslo, Norway.

NSIDC 2016 *National Snow and Ice Data Center*. https://nsidc.org/cryosphere/snow/ (accessed 27 June 2016).

Orskaug, E., Scheel, I., Frigessi, A., Guttorp, P., Haugen, J. E., Tveito, O. E. & Haug, O. 2011 Evaluation of a dynamic downscaling of precipitation over the Norwegian mainland. *Tellus Series A – Dynamic Meteorology and Oceanography* **63** (4), 746–756. doi:10.1111/j.1600-0870.2011.00525.x.

Pearson, E. S. 1931 The test of significance for the correlation coefficient. *Journal of the American Statistical Association* **26** (174), 128–134.

Peng, S., Piao, S., Ciais, P., Friedlingstein, P., Zhou, L. & Wang, T. 2013 Change in snow phenology and its potential feedback to temperature in the Northern Hemisphere over the last three decades. *Environmental Research Letters* **8** (1), 014008.

Sælthun, N. R. 1996 *The 'Nordic' HBV Model*. Publication 07:1996. The Norwegian Water Resources and Energy Directorate, Oslo, Norway.

Saloranta, T. M. 2012 Simulating snow maps for Norway: description and statistical evaluation of the SeNorge snow

model. *Cryosphere* **6** (6), 1323–1337. doi:10.5194/tc-6-1323-2012.

Saloranta, T. 2014a *New Version (v.1.1.1) of the seNorge Snow Model and Snow Maps for Norway*. Report 6:2014. The Norwegian Water Resources and Energy Directorate, Oslo, Norway.

Saloranta, T. M. 2014b Simulating more accurate snow maps for Norway with MCMC parameter estimation method. *Cryosphere Discussions* **8**, 1973–2003.

Sen, P. K. 1968 Estimates of the regression coefficient based on Kendall's tau. *Journal of the American Statistical Association* **63**, 1379–1389.

Seneviratne, S. I., Davin, L., Hirschi, M., Jaeger, E. B., Lehner, I. & Teuling, A. J. 2010 Investigating soil moisture–climate interactions in a changing climate: a review. *Earth-Science Reviews* **99** (3–4), 125–161.

Serreze, M. C., Barrett, A. P., Stroeve, J. C., Kindig, D. N. & Holland, M. M. 2009 The emergence of surface-based Arctic amplification. *Cryosphere* **3** (1), 11–19.

Skaugen, T. & Randen, F. 2013 Modeling the spatial distribution of snow water equivalent, taking into account changes in snow-covered area. *Annals of Glaciology* **54** (62), 305–313. doi:10.3189/2013AoG62A162.

Skaugen, T., Stranden, H. B. & Saloranta, T. 2012 Trends in snow water equivalent in Norway (1931–2009). *Hydrology Research* **43** (4), 489–499. doi:10.2166/nh.2012.109.

Spilde, D., Langseth, B. & Magnussen, I. H. 2014 *Energibruksrapporten 2013*. Report 11:2014. The Norwegian Water Resources and Energy Directorate, Oslo, Norway, pp. 54 (in Norwegian).

Tedesco, M., Brodzik, M., Armstrong, R., Savoie, M. & Ramage, J. 2009 Pan Arctic terrestrial snowmelt trends (1979–2008) from spaceborne passive microwave data and correlation with the Arctic Oscillation. *Geophysical Research Letters* **36**, L21402. doi:10.1029/2009gl039672.

Theil, H. 1950 A rank-invariant method of linear and polynomial regression analysis. *Indagationes Mathematicae* **12**, 85–91.

Tveito, O. E., Bjørdal, I., Skjelvåg, A. O. & Aune, B. 2005 A GIS-based agro-ecological decision system based on gridded climatology. *Meteorological Applications* **12**, 57–68.

Vaughan, D. G., Comiso, J. C., Allison, I., Carrasco, J., Kaser, G., Kwok, R., Mote, P., Murray, T., Paul, F., Ren, J., Rignot, E., Solomina, O., Steffen, K. & Zhang, T. 2013 *Observations: Cryosphere*. In: IPCC, 2013: Climate Change 2013: The Physical Science Basis Contribution of Working Group I to the Fifth Assessment Report of the Intergovernmental Panel on Climate Change. Cambridge University Press, Cambridge, UK and New York, NY, USA, pp. 317–382.

Vormoor, K., Lawrence, D., Heistermann, M. & Bronstert, A. 2015 Climate change impacts on the seasonality and generation processes of floods – projections and uncertainties for catchments with mixed snowmelt/rainfall regimes. *Hydrology and Earth System Sciences* **19** (2), 913–931. doi:10.5194/hess-19-913-2015.

Wilson, D., Hisdal, H. & Lawrence, D. 2010 Has streamflow changed in the Nordic countries? - Recent trends and comparisons to hydrological projections. *Journal of Hydrology* **394** (3–4), 334–346. doi:DOI 10.1016/j.jhydrol.2010.09.010.

First received 21 March 2017; accepted in revised form 2 August 2017. Available online 18 September 2017

Paper IV

Nilsen, I.B., Erlandsen, H.B., Stordal, F. Xu, C-Y. and Tallaksen, L.M. (2017): Diagnosing land–atmosphere coupling in a seasonally snow-covered region (South Norway). *Manuscript prepared for submission to Journal of Hydroclimatology*.

Diagnosing land–atmosphere coupling in a seasonally snow-covered region (South Norway)

Irene B. Nilsen[1,2], Helene B. Erlandsen[1,2], Frode Stordal[1], Chong-Yu Xu[1] and Lena M. Tallaksen[1]

1 University of Oslo, Oslo, Norway

2 The Norwegian Water Resources and Energy Directorate, Oslo, Norway

Corresponding author address: Department of Hydrology, Norwegian Water Resources and Energy Directorate, P.O. Box 5091, NO-0301, Oslo, Norway i.b.nilsen@geo.uio.no

South Norway has been identified as a region where warming in spring and summer could potentially be enhanced by land–atmosphere coupling. It is hypothesized that warming in South Norway is enhanced by the snow albedo feedback in spring and by the soil moisture–temperature feedback in summer. To examine this, the Weather Research and Forecasting (WRF) model coupled to Noah-MP was used for simulations from mid-May through September 2014. Because the soil moisture–temperature feedback requires dry soil moisture conditions, dry conditions were simulated by i) increasing the length of the snow-free season, and ii) introducing boundary forcing from a warm and dry summer (2006). Six model runs were performed: the first three runs differed only in their initial ground conditions (snow-poor, control and snow-rich) and used boundary forcing from the warm 2014 summer. The next three runs kept the same initial conditions as before and used boundary forcing from the warm and dry 2006 summer. Results show that the snow albedo feedback is an important driver of warming in regions with snow changes during spring. The soil moisture–temperature feedback was detected in the Oslofjord region, at least during parts of the summers 2014 and 2006. Here, the warming was enhanced through reduced evaporative cooling, due to dry soil. The effect of changing the boundary forcing to a warm and dry summer was stronger than increasing the length of the snow-free season. This study contributes to a better understanding of what causes the observed warming in cold climates.

1. Introduction

In Europe, 2014 was ranked as the warmest year on record (Uhe *et al.*, 2016). Recent increases in air temperature has led to, e.g., changed precipitation patterns, altered evapotranspiration, a shorter snow season and less snow cover in the Northern Hemisphere (Hartmann *et al.*, 2013; Vaughan *et al.*, 2013), and may in turn enhance the warming locally and regionally. Specifically, the water stored on the land surface influences the atmosphere by storing energy and moisture, by partitioning moisture and energy fluxes, and by accomodating feedback loops. We focus on feedback mechanisms involving changes in the hydrologic cycle that can alter an initial warming.

The snow albedo feedback plays an important role in the climate system at high latitudes, by controlling the amount of reflected shortwave radiation (Groisman *et al.*, 1994; Thackeray and Fletcher, 2016); see Figure 1a. The snow albedo feedback (Figure 1a) is initiated by warming that reduces the albedo and increases the amount of net radiation available on the ground, which enhances temperatures (e.g. Dickinson, 1983; Groisman *et al.*, 1994; Chapin *et al.*, 2005; Hall and Qu, 2006). The fingerprint of the snow albedo feedback thus lies in the changed shortwave radiation (Letcher and Minder, 2015). This feedback mechanism is most important in spring, when both snow and sunlight is abundant (Callaghan *et al.*, 2012). The latent heat spent on melting snow and ice (latent heat of fusion; 3.3 $\times 10^5$ J/kg) is a considerable heat sink, although it is smaller than the latent heat spent on evaporating water (latent heat of vaporization; 25.0 $\times 10^5$ J/kg at 273 K) (Dingman, 2002). With less snow and so less demand for melt energy, the energy is instead spent on sensible heat and latent heat of vaporization. Chapin *et al.* (2005) documented that a retreating snow cover over Alaska was correlated with warmer summers locally, through a 3 Wm^{-2} per decade higher energy absorbed by snow-free ground. Peng *et al.* (2013) quantified the feedback between spring temperatures and snowmelt over the Northern Hemisphere during the period 1980–2006. For Norway, they found a decrease in the snow season of more than five days per decade, partly due to the snow albedo feedback. Near-surface warming immediately after snowmelt was also documented for Norway in a high-resolution WRF model, in a study by Aas *et al.* (2017).

Another example of a feedback mechanism is the soil moisture–temperature feedback, which has been observed for southern and central Europe, especially during hot summers and heat waves (Zampieri *et al.*, 2009; Fischer *et al.*, 2012; Stéfanon *et al.*, 2014). In the soil moisture–temperature feedback loop (Figure 1b), a spell of warm and dry weather causes an anomalously low soil moisture storage that limits evapotranspiration (evaporative cooling) and thus enhances the initial warming (Seneviratne *et al.*, 2010; Miralles *et al.*, 2014)). Zampieri *et al.* (2009) found land surface–atmosphere feedbacks acting during the ten hottest summers since 1948 in southern and central Europe.

The positive soil moisture–temperature coupling is most pronounced in transitional zones between dry and wet evapotranspiration regimes where soil moisture controls evapotranspiration (Koster *et al.*, 2004; Seneviratne *et al.*, 2006), for instance in southern and central Europe (Zampieri *et al.*, 2009; Stéfanon *et al.*, 2014). Dry and transitional regimes are termed soil moisture-limited, as opposed to wet regimes which are termed energy-limited (Figure 1c) (Seneviratne *et al.*, 2010). During warm and dry conditions, an energy-limited regime may become transitional (Zampieri *et al.*, 2009; Dirmeyer *et al.*, 2009; Seneviratne *et al.*, 2010) and evapotranspiration becomes restricted by the available soil moisture. There are at least two ways South Norway could shift from an energy-limited regime to a transitional regime: drying through rainfall deficit and drying through a longer snow-free season. A rainfall deficit may occur as a result of an anomalous atmospheric condition, leading to soil desiccation (e.g. Rowell and Jones, 2006; Dirmeyer *et al.*, 2009; Stéfanon *et al.*, 2014).

The groundwater and soil moisture levels in South Norway are saturated right after snowmelt, slowly depleting throughout the summer, and reaching their lowest levels during winter (Gottschalk *et al.*, 1979; Colleuille *et al.*, 2007) (Figure 2c, green band). Earlier snowmelt, and thus a longer snow-free season, would allow the soil moisture to deplete further and it may trigger a soil moisture–temperature feedback (Xu and Dirmeyer, 2013). Quiring and Kluver (2009) found that a low maximum snow depth in winter was correlated with lower than normal summer soil moisture in the U.S. Great Plains, although the signals were weak. Increased evapotranspiration due to a shorter snow season (Wetherald and Manabe, 1995) and lower snow volumes have been observed to increase the probability of summer dryness in mid-latitude Europe (Rowell and Jones, 2006) and in Norway (Colleuille *et al.*, 2008; Wilson *et al.*, 2010; Wang, 2016). Wilson *et al.* (2010) found decreasing summer streamflow and increasing drought deficits in southern and eastern Norway for three historic periods (1920–2005, 1941–2005 and 1961–2000) and noted that they may be linked to earlier snowmelt. A similar decrease in streamflow in South Norway for May–September was found by Stahl *et al.* (2012), who studied runoff trends for Europe (1963–2000). In Norway, the soil moisture is generally dominated by rainfall during summers of sufficient rainfall, however, an anomalous snow storage is expected to have an effect during dry summers.

Methods of diagnosing land–atmosphere coupling range from correlations between the land state and atmospheric state (e.g. Dirmeyer *et al.*, 2009; Halder and Dirmeyer, 2017) to running complex ensemble simulations with models comparing one fully coupled soil moisture ensemble with a prescribed soil moisture ensemble (Koster *et al.*, 2004; Seneviratne *et al.*, 2006, 2010). An advantage of the correlation metrics is that they do not require an ensemble and may be applied on both observed and gridded datasets (Seneviratne *et al.*, 2010). The correlation between soil moisture (SM) and latent heat (LE), ρ(SM,LE), reveals whether the soil moisture controls the latent heat flux, or the other way around (Guo *et al.*, 2006). Coupling occurs only if the soil moisture is low enough to control the latent heat i.e., a positive correlation between the soil moisture and latent heat. This is referred to as the terrestrial leg of land–atmosphere coupling (Guo *et al.*, 2006; Dirmeyer, 2011). Given that the terrestrial leg is present, less evaporative cooling may further lead to decreased evaporative cooling and increased sensible heat flux (Seneviratne *et al.*, 2006; Lorenz *et al.*, 2012). If the reduced evaporative cooling is sufficient to enhance warming, there is a negative correlation between latent heat and air temperature, $\rho(LE, T)$, denoted the atmospheric leg. For land–atmosphere coupling to be present, both the terrestrial and atmospheric legs must be in place (Dirmeyer, 2011; Dirmeyer *et al.*, 2014; Halder and Dirmeyer, 2017). In energy-limited regimes, soil moisture and latent heat are negatively correlated; when latent heat increases, it depletes the soil moisture storage (Dirmeyer, 2011; Halder and Dirmeyer, 2017). If, however, the regime shifts to a transitional or soil moisture-limited regime, the soil moisture controls latent heat. When soil moisture decreases, latent heat is reduced because of a lack of moisture. Such positive correlations indicate a necessary, but not sufficient, part of the coupling.

In a previous study, we used statistical attribution of temperature changes for the period 1981–2010 to identify regions where air temperature trends could not be attributed to changes in atmospheric circulation (Nilsen *et al.*, 2017). For those regions, local feedback mechanisms explain at least a part of the detected warming trend. Europe has experienced dramatic snow changes in spring and drying in summer, and the same is true for Norway (Dyrrdal, 2009; Wilson *et al.*, 2010). In the current paper, we focus on South Norway, in April and July–September

("spring" and "summer").

A likely explanation for the April warming is the snow albedo feedback. In a study of the interrelationships between snow indices and climate variables, we found that the greatest declines in snow cover extent in South Norway occurred in spring (Rizzi *et al.*, 2017). A decrease in the snow cover extent corresponding to 6% of the Norwegian land area was detected for April and May between the periods 1961–1990 and 1981–2010. On the other hand, the warming in July to September found in Nilsen *et al.* (2017) may be caused by a soil moisture–temperature feedback, provided that the soil becomes sufficiently dry. To our knowledge, no modelling studies have tested to what degree the soil moisture–temperature feedback is relevant in South Norway. Provided that trends towards earlier melting and summer dryness continue, such a coupling would become more common with climate change.

In this study, we hypothesize that the warming detected for April was enhanced by the snow albedo feedback, and that the warming detected for July–September was enhanced by the soil moisture–temperature feedback (provided sufficiently dry conditions). The warm summer of 2014 is a plausible candidate for dry conditions and is chosen for simulations with a coupled WRF–Noah-MP model. To simulate drier conditions, we i) perturbed the length of the snow-free season, and ii) introduced boundary forcing from a warmer and drier summer than 2014 (2006). In a similar fashion, Saini *et al.* (2016) changed the initial soil moisture conditions to study the response of precipitation differences in one wet and two dry years. However, Saini *et al.* (2016) tested whether extreme events would become less extreme with changed initial soil moisture, whereas we try to trigger extremely dry conditions. In total, six model runs were performed: the first three runs differed only in their initial ground conditions (snow-poor, control and snow-rich, as characteristic of the lenght of the snow-free season) and used boundary forcing from the warm 2014 summer. The next three runs kept the same initial conditions as before and used boundary forcing from the warm and dry 2006 summer. Last, the results were compared with a gridded, high-resolution (1×1 km) estimated observed dataset for Norway (SeNorge) (Beldring *et al.*, 2003; Tveito *et al.*, 2005).

Specific objectives are:

a) Comparing air temperature in model runs with and without snow present (snow albedo feedback) for a warm summer (2014).

b) Assessing the effect of the length of the snow-free season on the soil moisture–temperature feedback.

c) Assessing the effect of lower soil moisture content on the soil moisture–temperature feedback.

d) Comparing the soil moisture–temperature feedback in WRF–Noah-MP with a dataset for Norway, SeNorge.

2. Materials and methods

2.1. Study area and years

South Norway spans a wide range of climate zones over a small spatial scale, ranging from a maritime moist and temperate climate in the western part, to a drier inland climate in the eastern part. The landscape of South Norway encompasses coasts and high mountains. Above the tree line and along the coast, bare bedrock or bedrock covered by shallow till is common, whereas thicker soils are found in valley bottoms (Jørgensen *et al.*, 2013). Regions with small subsurface storage lead to quicker drying of the soil moisture (Beldring *et al.*, 2003).

Two anomalously warm years were chosen to simulate dry conditions: 2014 and 2006. The spring of 2014 was the warmest spring on record, spanning the period from 1900 to 2016, for March–May (MAM) in South Norway (Table 1). The spring precipitation was approximately 20% higher than the 1961–1990 climatology, resulting in a snow cover close to normal conditions. The summer of 2014 (June–August, JJA) was approximately 2°C warmer than climatology, and the precipitation was close to the climatology. The groundwater levels peaked in May during snowmelt but, due to a warm spell in June, the soil moisture content was low in late June, July and late September, as shown at the station Groset (Wang, 2016).

The winter and spring of 2006 started out colder than the climatology and with less snow than normal, but warm and dry conditions developed in May–July, leading to early snowmelt (Colleuille *et al.*, 2008). Some groundwater stations in the mountains experienced their lowest levels in 30 years (Colleuille *et al.*, 2008). At the time, the summer of 2006 was the fourth warmest on record, and South Norway was 2.3°C warmer than the 1961–1990 climatology. Drought conditions developed during June 2006, intensifying in mid-August due to

Table 1: *Temperature (T) and precipitation (P) from the years 2014 and 2006 compared with climatology. Data provided by the Norwegian Meteorological Institute.*

		Spring	Summer
Climatology 1961–1990	T	0.5°C	9.9°C
2014 anomaly	T	+2.6°C	+1.7°C
2006 anomaly	T	–0.9°C	+2.3°C
Climatology 1961–1990	P	209.3 mm	288.2 mm
2014 anomaly	P	+17.6%	–0.7%
2006 anomaly	P	+5.5%	–11.6%

lower than average rainfall. In late-August, heavy rainfall alleviated the drought, but dry and warm conditions continued into September 2006.

In addition, data from 1995 were used to mimic initial conditions for a snow-rich year, but were not used for boundary forcing. The spring of 1995 was anomalously snow-rich, although the average spring temperature and precipitation were close to climatology. Southeastern Norway experienced an extreme flood in June 1995, because of the quick melting of the large snow volumes in conjunction with intense rainfall (Lundquist and Repp, 1997).

2.2. Data

Atmospheric fields and surface data required for the WRF–Noah-MP model runs were taken from the global reanalysis dataset ERA-Interim (Dee *et al.*, 2011) for the periods July 1994–May 1995, May 2006–September 2006, and July 2013–September 2014 (inclusive). These data are available at a 6-hourly time step and at a 0.75° spatial resolution, interpolated to 0.5°. Data from 2006 and 2014 were used as boundary conditions (i.e. boundary forcing), whereas initial conditions from 1995 and 2014 were used in various combinations with the 2006 and 2014 boundary forcings (see Section 2.4).

Observations of snow, soil moisture and soil temperature were provided for validation by the Norwegian Water Resources and Energy Directorate (NVE); Figure 2. In total, 12 stations measuring snow water equivalent were chosen, based on data availability for 2014 (blue circles in Figure 2a), in addition to four stations measuring soil moisture and soil temperature (brown crosses in Figure 2a). Note that station Groset is both a SWE station and a soil moisture station. Air temperature was also provided for the stations measuring soil temperature and soil moisture (Abrahamsvoll, Kise, Groset and Ås), but due to a bias in the temperature at Groset and Ås, we used data from the Norwegian Meteorological Institute at Møsstrond (close to Groset) and Ås. Soil temperature is measured in nine segments in the vertical, 15 cm apart. Soil moisture is measured with Time Domain Reflectometry in six segments in the vertical for all stations, at -10 cm, -20 cm, -30 cm, -40 cm, -60 cm and -100 cm. Because the soil moisture sensors lack calibration, the relative variation is considered more accurate than the absolute values (pers. comm. Thea Wang, NVE).

A gridded dataset of daily meteorological and hydrological variables is available for Norway at 1×1 km horizontal resolution, namely the SeNorge dataset (Beldring *et al.*, 2003; Tveito *et al.*, 2005). Gridded air temperature and precipitation in SeNorge are interpolated from observations, produced by the Norwegian Meteorological Institute (Tveito *et al.*, 2005), whereas hydrological variables are modelled using the Gridded Water Balance model (GWB) by NVE (Bergström, 1995; Beldring *et al.*, 2003). GWB is a conceptual hydrological model calibrated against runoff data. We used air temperature, evapotranspiration (in mm) and soil moisture deficit (in mm) from this dataset, in addition to WRF–Noah-MP, to assess the coupling strength. Note that SeNorge provides soil moisture *deficit*, in contrast to soil moisture stations and WRF–Noah-MP that use volumetric water content. Soil moisture deficit is a measure of how much water might be retained in the soil before runoff takes place, defined as the "amount of depleted water between the field capacity and the actual water content" (Colleuille *et al.*, 2007).

2.3. WRF–Noah-MP model description

Model runs were conducted using the Weather Research and Forecasting (WRF) (Skamarock and Klemp, 2008) model version 3.7.1. (Table 2). The WRF model was set up for two nested domains, with a horizontal resolution of 15 and 3 km respectively, using two-way nesting (Figure 3). They were run using 42 vertical levels up to 10 hPa,

Table 2: *WRF–Noah-MP model configuration.*

		Reference
Atmospheric model	WRF v 3.7.1	(Skamarock and Klemp, 2008)
Land surface	Noah-MP with default options	(Niu *et al.*, 2011)
Microphysics	WRF Single-Moment 3-class (WSM3)	(Hong *et al.*, 2004)
Boundary layer physics	Mellor-Yamada-Janjic (MYJ)	(Janjić, 1994)
Surface layer	Eta surface layer scheme	(Janjic, 2002)
Radiation (LW & SW)	Rapid Radiative Transfer (RRTMG)	(Iacono *et al.*, 2008)
Cumulus	Kain-Fritsch in d01, resolved in d02	(Kain, 2004)
Simulation period	Experiments: 12 May–30 September	
Spin-up period	10.5–12.5 months (depending on run)	
Forcing data (boundary condition)	ERA-Interim; 2014, 2006, 1995	(Dee *et al.*, 2011)
Land cover	20-class MODIS 15 arc seconds	(Broxton *et al.*, 2014)
Timestep	45 s	
Nesting	Two-way nesting	
Resolution in d01	15 km (100×100 cells)	
Resolution in d02	3 km (155×185 cells)	

with a time step of 45 s. The lateral boundary conditions were derived from the ERA-Interim reanalysis (Dee *et al.*, 2011) and included varying sea surface temperature. Smoothing was activated at the boundaries.

The choice of parameterizations was partly based on sensitivity tests and partly on Aas *et al.* (2017), who proposed a new subgrid tiling approach to improve the representation of snow processes at high altitudes in South Norway. The main difference from Aas' setup is our choice of the simpler WRF Single-Moment 3-class (WSM3) microphysics scheme, motivated by Mooney *et al.* (2013). Sensitivity tests were conducted for the period July 2013–July 2014, for the outer domain. The model output was compared with observed air temperature, soil temperature, soil moisture, and snow water equivalent (SWE) at all available stations. The combinations of parameterizations best resembling the ground observations were chosen, based on having the lowest bias and using visual inspection (not shown). The following parameterizations were selected: the 20-class MODIS land cover classification (Broxton *et al.*, 2014) and the Mellor-Yamada-Janjic (MYJ) planetary boundary layer with Eta surface layer (Janjić, 1994). The MODIS land cover has the highest spatial resolution of the available land cover classes in the WRF model (15 arc seconds). Further, the multioption version Noah-MP (Niu *et al.*, 2011) was used with default options (Yang *et al.*, 2011).

Noah-MP contains four soil layers with a fixed soil depth of 2 m, with vertical water transport between the layers, and horizontal transport of overland flow and groundwater flow, but no routing or interflow (Niu *et al.*, 2011; Davison *et al.*, 2016). Root depths in Noah-MP are static, and depend only on the vegetation type. In MODIS, South Norway is covered by evergreen needleleaf and mixed forest in the eastern part (Østlandet), where roots have access to all soil layers. Three of the four soil layers (down to 1 m depth) are available to plants at high elevations, above approximately 1000 m a.s.l. (open shrubland, grasslands and mixed tundra). Noah-MP further computes SWE, snow depth and snow cover fraction in up to three snow layers; new layers are added when the thickness increases. Noah-MP allows water transfer between those layers. Snowfall and snowmelt are activated based on temperature thresholds. The snowmelt is radiation-based and accounts for refreezing. Potential evapotranspiration is modelled using the Penman-Monteith equation with aerodynamic resistances calculated using the Monin-Obukhov similarity theory (Cai *et al.*, 2014). Transpiration rate, canopy water content, stomatal resistance, and other canopy processes are calculated for a separate vegetation layer, using a two-stream radiation scheme and Ball-Perry stomatal resistance.

2.4. Experimental design

As shown in Table 3 and Figure 3, boundary forcing data were taken from the warm summer of 2014 and the warm and dry summer of 2006, and initial conditions were produced by spin-up runs for 2013/2014 and 1994/1995. 2014 was initially chosen as a candidate for dry conditions (to increase the likelihood of soil moisture–temperature coupling) and observations from 2013/2014 were used for validation when setting up the model.

Table 3: *Experimental design, swapping initial ground conditions between the perturbations and control, with boundary forcing from two different summers – either the warm summer 2014 or the warm and dry summer 2006. All experiments were run with boundary forcing from 12 May–30 September. Swapping implies replacing initial ground conditions in the inner domain (d02) with regridded results of the spin-up for the outer domain (d01). Spin-up started 1 July in all runs, and ended either 12 May (CTR and SR) or 11 July (SP). CTR used spin-up from 2013/2014, whereas SR used spin-up from 1994/1995. See also Figure 3.*

	Experiment	Forcing	Initial ground conditions from spin-up
CTR_{14}	Control, warm summer	2014 May–September	12 May 2014 (10.5 months spin-up)
SP_{14}	Snow-poor, warm summer	″	swapped 11 July 2014 (12.5 months spin-up)
SR_{14}	Snow-rich, warm summer	″	swapped 12 May 1995 (10.5 months spin-up)
CTR_{06}	Control, warm and dry summer	2006 May–September	swapped 12 May 2014 (10.5 months spin-up)
SR_{06}	Snow-poor, warm and dry summer	″	swapped 11 July 2014 (12.5 months spin-up)
SP_{06}	Snow-rich, warm and dry summer	″	swapped 12 May 1995 (10.5 months spin-up)

A spin-up period was required to allow the ground conditions to adjust before the model runs started, and to define initial conditions for the model runs (Figure 3). ”Ground conditions” comprise SWE, snow depth, snow albedo, soil moisture, skin temperature, initial temperature, soil category fraction at the bottom and top, and an indicator function for snow (1 = snow, 0 = no snow). The spin-up was performed for the outer domain only, and the result from the last timestep of spin-up was used as initial ground conditions. Substituting results from the last timestep of the spin-up into the beginning of simulations starting 12 May is hereafter called *swapping* (after Saini *et al.*, 2016). Before swapping outer-domain results into the inner domain, the coarse results were regridded to 3 km resolution, matching the inner domain (inspired by Aas *et al.*, 2017). Two years underwent spin-up: 1 July 2013–11 July 2014 and 1 July 1994–12 May 1995. Three different initial ground conditions were produced from the spin-ups: The control run (CTR_{14}) used initial conditions from 12 May 2014 (no swapping). The snow-poor run (SP_{14}) swapped ground conditions on 12 May 2014 with those from mid-July, representing two months earlier snowmelt. The snow-rich run (SR_{14}) swapped ground conditions on 12 May 2014 with those from mid-May in the snow-rich year 1995. In all cases, the spin-up started 1 July the previous year to let the ground temperature and moisture adjust before the snow started accumulating. The second way to deplete the soil moisture is to repeat the runs with atmospheric forcing from a warm and dry summer (2006). To be comparable with the first three model runs, the initial ground conditions with 2006 forcing were identical to those run with 2014 forcing. In total, six model runs were performed with the inner domain activated.

2.5. Analyses

The snow-rich and snow-poor runs were compared to the control through time series and maps of differences. Because the variables cannot be assumed to be normally distributed, the non-parametric Wilcoxon signed rank test (Wilcoxon, 1945) was used to test the significance of the differences (two-tailed, 5% level). This paired test compares the medians between the model run and the control, and decides whether the median difference between pairs is zero. All model results were averaged from a 6-hourly resolution to daily data before analyses. Cumulative variables, such as rainfall, surface runoff and subsurface flow were converted from cumulative values to unaccummulated values.

Soil moisture–temperature coupling was diagnosed as the correlation between the land surface and a surface flux (here: $\rho(SM, LE)$, the terrestrial leg), and between the surface flux and the atmosphere (here: $\rho(LE, T)$, the atmospheric leg). Positive correlations indicate a coupling for the terrestrial leg and negative correlations indicate a coupling for the atmospheric leg that leads to a positive feedback. A red colour is used consistently in figures to indicate coupling. Correlations were also calculated for SeNorge data for comparison. Because SeNorge provides soil moisture deficit (in mm), and not the volumetric soil moisture content (%), SeNorge provides a proxy for the terrestrial leg, $\rho(SMdeficit, LE)$. Thus, a negative correlation between soil moisture deficit and latent heat implies a contribution to positive feedback. The atmospheric leg for SeNorge is comparable to WRF–Noah-MP, however. Note: in the WRF context, ”latent heat” is used for latent heat of vaporization, not latent heat of fusion.

3. Results

Initial sensitivity analyses were used to determine the best land cover class, land surface model and planetary boundary layer scheme (not shown). MODIS 15s land cover, Noah-MP land surface model, and MYJ planetary boundary layer scheme were chosen for further analyses. Results from this preliminary sensitivity analysis were validated against air temperature, snow, soil temperature and soil moisture at the stations shown in Figure 2. Air temperature and soil temperature were well reproduced at the four temperature stations. For SWE, the median of all stations agreed well with observations, but SeNorge had a larger spread than the observations. Soil moisture was not well reproduced at the four stations measuring soil moisture, partly because of poor data quality.

In the following, Section 3.1 presents effects of initial ground conditions on the feedbacks and coupling strength. WRF–Noah-MP results with 2014 boundary forcing and different initial ground conditions are used for this purpose. CTR_{14} used the default ground conditions from 12 May 2014, whereas initial conditions from the snow-poor run, SP_{14}, were swapped with conditions from mid-July 2014 and initial conditions from the snow-rich run, SR_{14}, were swapped with conditions from mid-May 1995. Section 3.2 presents the effect of an alternative boundary forcing (a warm and dry summer, 2006). WRF–Noah-MP results are compared to SeNorge results in Section 3.3.

3.1. Effects of initial ground conditions on the snow albedo feedback and the soil moisture–temperature coupling strength

Time series and boxplots of the three runs with 2014 boundary forcing are shown for the station Kyrkjestølane in Figure 4. Daily values of soil moisture, evapotranspiration and temperature are plotted throughout the summer, 15 May–30 September, leaving out three days from the start of the run during which the atmosphere span up. The boxplots show the temporal distribution of each of the variables for the snow-rich run minus the control, and for the snow-poor run minus the control. Kyrkjestølane station had snow well into the summer and is therefore displayed to show the effect of snowmelt timing on soil moisture, evapotranspiration and air temperature. Time series of soil moisture show values close to saturation when snow was present (SM$\approx$0.35) and drier conditions when snow was absent (SM$\approx$0.25) (Figure 4b). Thus, soil moisture was clearly influenced by the presence of snow. Air temperatures differed by about 5 °C between the runs with snow and the runs without snow (Figure 4c). Shortwave radiation was lower for the snow-covered model runs than the snow-free runs (not shown). After all model runs had become snow-free, only minor differences were seen between runs.

Spatially, the largest differences between model runs (SP and SR compared with CTR) were seen where the snow cover was present in the model runs (Figure 5). SWE in the snow-poor run, SP_{14}, showed the largest difference from the control at the highest elevations (compare with Figure 3), and for 15 May–14 June. The snow-rich run, SR_{14}, and CTR_{14} differed most in a fringe between high and lower elevations, with no difference at the highest elevations where both the snow-rich run and the control had snow. In the second month, 15 June–14 July, differences in SWE were found only at high elevations, whereas almost no differences were seen in the third and fourth months (not shown). Differences in SWE between model runs were as much as 1500 mm (Figure 5a). A similar spatial pattern to SWE was visible for soil moisture, latent heat and temperature (Figures 5b–d). Significantly less moisture was available in SP_{14} than in CTR_{14}, especially in the mountains, but also at the southeastern coast. The opposite was true for SR_{14}. SP_{14} experienced significant negative evapotranspiration differences along the southeastern coast, in line with the lower soil moisture there. Most of South Norway experienced significant differences in air temperature between the model runs and control, influencing regions beyond the snow-covered area. The differences between runs were small in regions outside the snow-covered areas and for the third and fourth months (15 July–14 August and 15 August–14 September) for all variables considered in Figure 5 (Supplementary Figure S1). The exception was at the southeastern coast for soil moisture, evapotranspiration and air temperature in the first month after snowmelt, and for temperature (SP_{14}) at high elevation areas several months after snowmelt.

To investigate the land–atmosphere coupling further, correlations were mapped for the period 15 July–14 August in Figure 6 for the terrestrial leg of coupling, $\rho(SM, LE)$, and Figure 7 for the atmospheric leg of coupling, $\rho(LE, T)$. A red color indicates land–atmosphere coupling, highlighting negative correlations for the terrestrial leg and positive correlations for the atmospheric leg, in both cases contributing to an overall positive feedback loop. The terrestrial leg was present across South Norway, although quite scattered, indicating a soil moisture limitation on evapotranspiration. Comparing CTR_{14} in Figure 6 with SR_{14} and SP_{14} showed almost no difference, except within

the snow-covered regions. A weak atmospheric leg (Figures 7a, c, and e) could be detected, mainly scattered across the southeastern coast and further inland than the terrestrial leg. A soil moisture limitation on evapotranspiration was thus detected for the summer of 2014 in parts of our model domain.

3.2. Effects of alternative boundary forcing on the soil moisture–temperature coupling strength

To increase the likelihood of dry ground conditions, and thus positive land–atmosphere coupling, we introduced atmospheric boundary forcing from a summer with little rainfall and high temperatures (2006), shown in Figures 6b, d, and f and Figures 7b, d, and f. The terrestrial leg contributing to a positive feedback loop was found in most of South Norway. The atmospheric leg was apparent in the lowlands of eastern and western Norway, omitting a band approximately following the Scandinavian mountains (Figures 7b, d, and f). The drier conditions in 2006 thus led to stronger and more wide-spread coupling than in 2014 but, again, small differences between runs with different initial conditions were seen.

Other variables and metrics such as the evaporative fraction and Bowen ratio are shown in Supplementary Figures S2–S3. In 2006, a higher evaporative fraction, higher Bowen ratio, and a stronger coupling were visible than in 2014. The southern part of the domain was drier, and slightly warmer, in 2006 than in 2014, averaged over the period 15 July–14 August (Supplementary Figure S4).

3.3. Soil moisture–temperature coupling in SeNorge

Next, we compare the WRF–Noah-MP results with the gridded 1×1 km dataset SeNorge (in Figures 6g–h and Figures 7g–h). A proxy for the terrestrial leg, the correlation of soil moisture *deficits* with temperature, is shown in red to indicate a coupling yielding an overall positive feedback. Because SeNorge contains soil moisture deficits, these correlations are the inverse of the correlations shown previously for WRF–Noah-MP results. The proxy for the terrestrial leg in SeNorge showed coupling in the lowland regions across South Norway, for 2014 as well as 2006 (Figures 6g–h). The terrestrial leg proxy in SeNorge, $\rho(SMdeficit, LE)$, differed from WRF–Noah-MP correlations, $\rho(SM, LE)$, by being less scattered, and with a much stronger signal in the lowlands (red, indicating coupling) which was separated from the mountain signal (blue, indicating no coupling contributing to a positive feedback). Further, correlations in 2006 showed more wide-spread coupling in WRF–Noah-MP – where almost the whole domain showed coupling – than in SeNorge, where the mountains showed no coupling.

For the atmospheric leg, the SeNorge data cover a slightly smaller region than the terrestrial leg proxy (Figure 7g–h). The red region in these figures, covering the coasts southeast and southwest of Oslo is hereafter called "the Oslofjord region". The atmospheric leg in SeNorge in 2014 was stronger and more spatially coherent than WRF–Noah-MP. For 2006, SeNorge captured the signal along the southeastern part well, but SeNorge did not show any sign of coupling in western Norway, as seen in WRF–Noah-MP. The positive soil moisture–temperature feedback (both the terrestrial and atmospheric leg of coupling) occurred during the summer of other years as well, but was not as pronounced as in 2006 (not shown).

Last, time series for a grid cell experiencing coupling (marked as grid cell "A" in Figure 2) are shown in Figure 8. The four soil moisture measurement stations did not experience strong coupling, therefore, grid cell "A" was chosen based on maps of coupling for 2014. A markedly lower soil moisture content was seen in SP_{14} than in the two other runs. This was especially true from approximately early July to mid-August. Almost no difference between runs was seen in September. Lower latent heat was seen for SP_{14}, again with the largest differences in July and August, of up to 5 Wm^{-2}. A similar, but opposite, pattern was seen for sensible heat, also about 5 Wm^{-2} (not shown). Similarly, hardly any difference was seen in temperature between the runs except for a few days within the first month after the start. Temperatures in SR_{14} were a little lower than CTR_{14}, and coincided with lower soil moisture and latent heat in SR_{14} during the first few days.

4. Discussion

4.1. Effects of initial ground conditions on the snow albedo feedback and soil moisture recharge

In our previous attribution study of temperatures, Nilsen *et al.* (2017) found significant temperature trends in Norway during spring and summer for the period 1981–2010 that could be attributed to local feedback mechanisms. In this study, we conclude that the snow albedo feedback enhances spring warming. The fingerprint of the snow albedo feedback – increased available energy when snow is absent – was detected as up to 5 °C higher temperatures in model runs with snow present than in model runs without snow present (Figure 4c). This magnitude of warming is in agreement with, for example, Walsh and Ross (1988) and Letcher and Minder (2015). Temperature differences in Figure 5 reached far outside the snow-covered regions, consistent with Letcher and Minder (2015) who studied the snow albedo feedback in a mountain region in Colorado. They noted that the increased shortwave radiation associated with a lower albedo was balanced by atmospheric circulation, such that advected energy allowed for warming outside regions with snow present.

4.2. Effects of alternative initial ground conditions on the soil moisture–temperature coupling strength

A minimal effect of snowmelt timing on soil moisture, evapotranspiration and air temperature was visible at Kyrkjestølane (Figure 4), Groset, Kise, and Ås (not shown). A larger difference was found in model grid cells along the southeastern coast. For instance, grid cell "A", showed less soil moisture and evapotranspiration for the snow-poor model run. Similarly, studies by Quiring and Kluver (2009), Xu and Dirmeyer (2013), and Halder and Dirmeyer (2017) linked earlier snowmelt with lower soil moisture for two regions with a sesonal snow cover, in the Great Plains, the Northern Hemisphere and Tibet, respectively. The maps in Xu and Dirmeyer (2013) show that an indirect effect of snowmelt on soil moisture played a role in southeastern Norway.

A soil moisture limitation on evapotranspiration is consistent with the terrestrial leg that happens when the soil moisture drops below a critical soil moisture content (SM_{crit} on the Budyko curve in Figure 1c). Temperatures at grid cell "A" were only marginally affected by the lower soil moisture, even during periods when evapotranspiration was limited by soil moisture (the atmospheric leg was not discernible). According to Guo *et al.* (2006), the atmospheric leg not only requires a soil moisture limitation on evapotranspiration, but also requires that the variability of evapotranspiration is sufficiently high to affect temperatures. This is one reason for the small temperature reponse to lower soil moisture. For grid cells experiencing both the terrestrial and atmospheric leg of coupling (in the Oslofjord region, especially during 2006), the drying led to increased sensible heat at the expense of evaporative cooling and enhanced the initial warming. Here, summer warming was enhanced by the soil moisture–temperature feedback, at least during parts of the summer.

From our model results, we cannot conclude that the soil moisture–temperature coupling was caused by a longer snow-free season. This is in line with Erlandsen *et al.* (2017), who studied the response of the water cycle to changed snow cover in a WRF–Noah-UA model study for Norway. They did not either detect any influence of changed snow cover on soil moisture and, in turn, on evapotranspiration rates in summer.

The small differences between SP_{14}, CTR_{14}, and SR_{14} may trace back to the soil classification used for initialization in Noah-MP. Several schemes in Noah-MP depend on soil and vegetation parameters given in lookup tables, for instance, the water storage capacity. The MODIS land cover types used in this study classify all parts of South Norway as various loams and do not capture the shallow tills, or exposed bedrock along the coast and in the mountains of South Norway. Instead, Noah-MP assumes a constant soil depth of 2 m throughout the domain, whereas the soil depth in reality varies from tens of metres to zero (on bare bedrock) (Jørgensen *et al.*, 2013; Geological Survey of Norway, 2017). Large parts of Norway lie at high elevations with shallow soils. With a too thick soil depth, the maximum soil moisture storage capacity is overestimated.

Evapotranspiration is also sensitive to the vegetation type – for instance the root depth. In MODIS, South Norway is covered by evergreen needleleaf and mixed forest in the southeastern part, where roots have access to all soil layers. Three of the four soil layers (down to 1 m depth) are available to plants at high elevations (open shrubland, grasslands and mixed tundra). In reality, roots would not reach 1 m where the soils are shallow. Most roots are found in the top 0.5 m of soil, even though pine and birch may reach depths of 3 m (Wielgolaski, 1978). In the model, the vegetation has access to water even if the top soil is drier than SM_{crit}, so that transpiration does

not become soil moisture-limited during dry periods. This was also found by Gayler *et al.* (2014), who tested a new root growth option by limiting the maximum rooting depth to 1 m in a deep-rooted site, and 0.3 m in shallower soils, and assumed an exponential decrease of the active root length. Further, root depths vary throughout the year and grow to a maximum depth in late summer, instead of having a static depth as in Noah-MP. For station Abrahamsvoll, having subalpine birch forest with grass, heather and moss covering the ground, the root depth has been measured to 0.4 m at its deepest in August (Øverlie, 2007). In Noah-MP, this grid cell is represented by the open shrublands vegetation class, reaching 1 m fixed root depth. By having a fixed root depth – and representing the soil as one bulk layer – Noah-MP underestimates the variability of, for instance, soil moisture and evapotranspiration in the upper layer and overestimates it in deeper layers (Gayler *et al.*, 2014). Thus, Abrahamsvoll and other grid cells would likely reach the critical soil moisture more quickly in reality than in the model. For the snow-poor run, as well as CTR_{14} and SR_{14}, the soil moisture content stayed in the energy-limited part of the Budyko curve. Whether this model behaviour is realistic, or reflects that evapotranspiration was not sufficiently reduced due to thick soil and too long roots, remains to be investigated.

4.3. Effects of alternative boundary forcing on the coupling strength

Stronger coupling that leads to a positive feedback was detected when applying boundary forcing from a warm and dry summer (2006) than in the warm summer with normal rainfall (2014). Further, larger areas of coupling were seen for 2006 than 2014, implying that the effect of changing the boundary forcing to a warm and dry summer was stronger than the effect of increasing the snow-free season. During the summer of 2006, the low soil moisture was initiated by anomalously dry atmospheric conditions caused by blocking high pressure systems located over the Baltics. A similar atmospheric situation, that is, a persistent blocking situation with high pressure systems centered over France and Iberia, initiated the European heat waves in 2003 and 2010 (Miralles *et al.*, 2014). These dry conditions turned out to be necessary to drive larger regions into soil moisture-limitation.

Our results show the strongest soil moisture–temperature feedback along the southeastern coast (atmospheric leg). When comparing the feedback strength in the lowlands, mountains and coastal regions of France, Stéfanon *et al.* (2014) found the strongest soil moisture–temperature feedback in the lowlands, where the low soil moisture content led to increased sensible heat at the expense of latent heat. The feedback was dampened by atmospheric circulation, namely wind convergence, in the mountains and by moist air advection at the coasts (Stéfanon *et al.*, 2014). No such effects were seen in Nilsen *et al.* (2017), likely due to a too coarse spatial resolution, which was approximately four times coarser than in Stéfanon *et al.* (2014).

4.4. Differences between the coupling strength in SeNorge and WRF–Noah-MP

Correlations for SeNorge confirmed a more wide-spread coupling in 2006 than in 2014, especially for the terrestrial leg, confirming our results. Unlike in Noah-MP, the soil depth or root depth is not explicitly represented in the GWB model producing SeNorge evapotranspiration and soil moisture deficits. The GWB model is calibrated against observed runoff and is therefore more representative for boreal conditions than Noah-MP, which assumes 4 m soil depth in all grid cells. However, some limitations exist. A very simple estimation of evapotranspiration is employed. Potential evapotranspiration is represented by a linear relationship with temperature, with monthly correction factors, and the actual evapotranspiration is calculated as potential evapotranspiration with a soil moisture limitation, similar to the Budyko curve (Beldring *et al.*, 2003; Engeland *et al.*, 2004). Evapotranspiration in SeNorge has been validated against observations in Norway and Sweden by Engeland *et al.* (2004), who found that the GWB model overestimates evapotranspiration in early summer, because of its seasonal parameterization. The observations showed the highest evapotranspiration in August, not in June. Soil moisture in SeNorge has been validated against station observations and a physically-based column soil model (Colleuille *et al.*, 2007). Soil moisture deficits were overestimated in summer because of too high evapotranspiration, and were underestimated in winter. The groundwater simulations agreed well with observations at two stations: Abrahamsvoll, depicted in Figure 1a, and Fana at the western coast (Colleuille *et al.*, 2007). The SeNorge data are considered more reliable than WRF–Noah-MP results with respect to the more realistic soil and root depths, and because GWB is calibrated against runoff. Still, there are considerable uncertainties in the evapotranspiration and soil moisture data from SeNorge due to a lack of validation and sparse observations. Despite these differences between WRF–Noah-MP and SeNorge, we found a robust signal along the southeastern coast in both datasets, supporting the WRF–Noah-MP results.

When comparing the land–atmosphere coupling in WRF–Noah-MP with results from SeNorge, different spatial extents and magnitudes appeared, which suggests uncertainties. The strongest coupling was detected in the eastern part of South Norway, both in WRF–Noah-MP and SeNorge. A soil moisture–temperature feedback in this region was expected because it is characterized as a more dry inland climate, and previous studies have detected reduced streamflow here during summer (Stahl *et al.*, 2012). However, coupling was also detected for the (north-)western coast in 2006 and the mountains in WRF–Noah-MP but not in SeNorge. The western part lies in a maritime moist and temperate climate where temperatures are primarily governed by advection rather than local feedback processes. Further studies are required to determine which processes cause these differences between WRF–Noah-MP and SeNorge, which contributes to identify needs for improvement in the parameterizations or input data.

5. Conclusions

In this study, we have tested whether the warming trends (1979–2010) detected in April and July–September in Nilsen *et al.* (2017) was amplified by the snow albedo feedback in spring, and by the soil moisture–temperature feedback in summer (under sufficiently dry conditions). Six model runs of the WRF model coupled to Noah-MP were performed for South Norway for a warm summer with normal rainfall (2014) and a warm and dry summer (2006). The first three runs differed only in their initial ground conditions (snow-poor, control and snow-rich) and used boundary forcing from 2014. The next three runs kept the same initial conditions as before, and used forcing from 2006.

The main conclusions are:

- The snow albedo feedback enhanced the warming during snowmelt in the region influenced by snow changes, and also slightly beyond the snow-covered area.
- The positive soil moisture–temperature feedback acted during summer in the Oslofjord region (along the southeastern coast), at least during parts of the summer. A stronger and more widespread coupling leading to a positive feedback was seen in the driest year (2006). Thus, anomalous atmospheric conditions led to dry soils which in turn limited the evapotranspiration and enhanced the initial warming.
- A longer snow-free season did not strengthen this soil moisture–temperature feedback, likely because the changed initial ground conditions were not large enough to induce a positive feedback.
- Changing the atmospheric boundary forcing to dry summer conditions (2006) had a larger effect on the strength and extent of the coupling leading to a positive soil moisture–temperature feedback, than changing the initial conditions. Thus, the enhanced warming was caused by a lack of rainfall rather than a longer snow-free season.
- A 1x1 km gridded estimated observed dataset for Norway (SeNorge) confirmed to some extent WRF–Noah-MP results, displaying enhanced warming along a positive soil moisture–temperature feedback in the Oslofjord region.

The snow albedo feedback will continue to be relevant, since dramatic changes in snow season duration are projected for Norway (Hanssen-Bauer *et al.*, 2015). Further, dry conditions have become more frequent in South Norway during the past decades (Wilson *et al.*, 2010), and summer dryness is expected for South Norway in the future (Hanssen-Bauer *et al.*, 2015). The positive soil moisture–temperature feedback in summer is thus likely to become more frequent with climate change, for Southern Norway.

Land surface model estimates of evapotranspiration depend on the parameterization of processes as well as input data, such as soil types and vegetation types. To improve the estimation of evapotranspiration, more realistic land cover and vegetation information is needed when setting up WRF models for regions with complex topography, shallow soils and short roots, such as our study region. Follow-up studies using detailed maps for Norway in Noah-MP are planned.

Acknowledgements

This work forms a contribution to LATICE, which is a strategic research area funded by the Faculty of Mathematics and Natural Sciences at the University of Oslo. The authors wish to thank the Norwegian Water Resources and

Energy Directorate for providing observed and gridded data and the Norwegian Meteorological Institute for providing temperature and precipitation data. We would further like to thank NCAR for providing a versions of WRF and Noah-MP open for all users. Thanks to M. Mesquita (Uni Research, Bergen, Norway), for ideas on the experimental design, and Pardeep Pall for comments on the manuscript.

References

Aas KS, Gisnås K, Westermann S, Berntsen TK. 2017. A tiling approach to represent subgrid snow variability in coupled land surface–atmosphere models. *Journal of Hydrometeorology* **18**(1): 49–63, doi:10.1175/JHM-D-16-0026.1.

Beldring S, Engeland K, Roald LA, Sælthun NR, Voksø A. 2003. Estimation of parameters in a distributed precipitation-runoff model for Norway. *Hydrology and Earth System Sciences* **7**(3): 304–316, doi:10.5194/hess-7-304-2003.

Bergström S. 1995. The HBV model. In: *Computer models of watershed hydrology*, Singh VP (ed), ch. 13, Water Resources Publications: Highlands Ranch, Colorado, pp. 443–476.

Broxton PD, Zeng X, Sulla-Menashe D, Troch PA. 2014. A global land cover climatology using modis data. *Journal of Applied Meteorology and Climatology* **53**(6): 1593–1605, doi:10.1175/JAMC-D-13-0270.1.

Cai X, Yang ZL, David CH, Niu GY, Rodell M. 2014. Hydrological evaluation of the Noah-MP land surface model for the Mississippi River Basin. *Journal of Geophysical Research: Atmospheres* **119**(1): 23–38, doi:10.1002/2013JD020792. 2013JD020792.

Callaghan TV, Johansson M, Brown RD, Groisman PY, Labba N, Radionov V, Barry RG, Bulygina ON, Essery RLH, Frolov DM, Golubev VN, Grenfell TC, Petrushina MN, Razuvaev VN, Robinson DA, Romanov P, Shindell D, Shmakin AB, Sokratov SA, Warren S, Yang D. 2012. The changing face of arctic snow cover: A synthesis of observed and projected changes. *AMBIO* **40**(1): 17–31, doi:10.1007/s13280-011-0212-y.

Chapin FS, Sturm M, Serreze MC, McFadden JP, Key JR, Lloyd AH, McGuire AD, Rupp TS, Lynch AH, Schimel JP, Beringer J, Chapman WL, Epstein HE, Euskirchen ES, Hinzman LD, Jia G, Ping CL, Tape KD, Thompson CDC, Walker DA, Welker JM. 2005. Role of land-surface changes in arctic summer warming. *Science* **310**(5748): 657–660, doi:10.1126/science.1117368.

Colleuille H, Beldring S, Mengistu Z, Wong WK, Haugen LE. 2007. Groundwater and soil water system for norway based on daily simulations and real-time observations. In: *Aquifer Systems Management: Darcy's Legacy in a World of Impending Water Shortage: Selected Papers on Hydrogeology 10*, Chery L, de Marsily G (eds), ch. 43, IAH - Selected Papers on Hydrogeology, CRC Press, Taylor and Francis group, pp. 567–579.

Colleuille H, Holmqvist E, Beldring S, Haugen LE. 2008. Betydning av grunnvanns- og markvannsforhold for tilsig og kraftsituasjon. Technical Report Rapport 2008:12, Norwegian Water Resources and Energy Directorate, Oslo, Norway. In Norwegian.

Davison B, Pietroniro A, Fortin V, Leconte R, Mamo M, Yau MK. 2016. What is Missing from the Prescription of Hydrology for Land Surface Schemes? *Journal of Hydrometeorology* **17**(7): 2013–2039, doi:10.1175/JHM-D-15-0172.1.

Dee DP, Uppala SM, Simmons AJ, Berrisford P, Poli P, Kobayashi S, Andrae U, Balmaseda MA, Balsamo G, Bauer P, Bechtold P, Beljaars ACM, van de Berg L, Bidlot J, Bormann N, Delsol C, Dragani R, Fuentes M, Geer AJ, Haimberger L, Healy SB, Hersbach H, Hólm EV, Isaksen L, Kållberg P, Köhler M, Matricardi M, McNally AP, Monge-Sanz BM, Morcrette JJ, Park BK, Peubey C, de Rosnay P, Tavolato C, Thépaut JN, Vitart F. 2011. The ERA-Interim reanalysis: configuration and performance of the data assimilation system. *Quarterly Journal of the Royal Meteorological Society* **137**(656): 553–597, doi:10.1002/qj.828.

Dickinson RE. 1983. Land surface processes and climate—surface albedos and energy balance. In: *Theory of ClimateProceedings of a Symposium Commemorating the Two-Hundredth Anniversary of the Academy of Sciences of Lisbon*, *Advances in Geophysics*, vol. 25, Saltzman B (ed), Elsevier, pp. 305 – 353, doi:http://dx.doi.org/10.1016/S0065-2687(08)60176-4.

Dingman SL. 2002. *Physical Hydrology*. New Jersey: Prentice-Hall, 2nd edn. 646 pp.

Dirmeyer PA. 2011. The terrestrial segment of soil moisture–climate coupling. *Geophysical Research Letters* **38**(16): L16 702, doi:10.1029/2011GL048268.

Dirmeyer PA, Schlosser CA, Brubaker KL. 2009. Precipitation, Recycling, and Land Memory: An Integrated Analysis. *Journal of Hydrometeorology* **10**: 278–288.

Dirmeyer PA, Wang Z, Mbuh MJ, Norton HE. 2014. Intensified land surface control on boundary layer growth in a changing climate. *Geophysical Research Letters* **41**(4): 1290–1294, doi:10.1002/2013GL058826. 2013GL058826.

Dyrrdal AV. 2009. Trend analysis of number of snow days per winter season in Norway. Technical Report met.no Report 07/2009 Climate, Norwegian Meteorological Institute, Oslo, Norway.

Engeland K, Engen Skaugen T, Haugen JE, Beldring S, Førland E. 2004. Comparison of evaporation estimated by the HIRHAM and GWB models for present climate and climate change scenarios. Technical Report Climate-Report 17/2004, Norwegian Meteorological Institute, Oslo, Norway.

Erlandsen HB, Haddeland I, Tallaksen LM, Kristiansen J. 2017. The sensitivity of the terrestrial surface energy and water balance estimates in the wrf model to lower surface boundary representations: A south norway case study. *Journal of Hydrometeorology* **18**(1): 265–284, doi:10.1175/JHM-D-15-0146.1.

Fischer EM, Rajczak J, Schär C. 2012. Changes in European summer temperature variability revisited. *Geophysical Research Letters* **39**(19): L19 702, doi:10.1029/2012GL052730.

Gayler S, Wöhling T, Grzeschik M, Ingwersen J, Wizemann HD, Warrach-Sagi K, Högy P, Attinger S, Streck T, Wulfmeyer V. 2014. Incorporating dynamic root growth enhances the performance of noah-mp at two contrasting winter wheat field sites. *Water Resources Research* **50**(2): 1337–1356, doi:10.1002/2013WR014634.

Geological Survey of Norway. 2017. Maps and data. URL `http://www.ngu.no/emne/kartinnsyn`. Retreived on 18 May 2017 from http://www.ngu.no/emne/kartinnsyn.

Gottschalk L, Jensen J, Lundquist D, Solantie R, Tollan A. 1979. Hydrologic Regions in the Nordic Countries. *Nordic Hydrology* **10**: 273–286.

Groisman PY, Karl TR, Knight RW, Stenchikov GL. 1994. Changes of Snow Cover, Temperature, and Radiative Heat Balance over the Northern Hemisphere. *Journal of Climate* **7**(11): 1633–1656, doi:10.1175/1520-0442(1994)007<1633:COSCTA>2.0.CO;2.

Guo Z, Dirmeyer PA, Koster RD, Sud YC, Bonan G, Oleson KW, Chan E, Verseghy D, Cox P, Gordon CT, McGregor JL, Kanae S, Kowalczyk E, Lawrence D, Liu P, Mocko D, Lu CH, Mitchell K, Malyshev S, McAvaney B, Oki T, Yamada T, Pitman A, Taylor CM, Vasic R, Xue Y. 2006. GLACE: The Global Land–Atmosphere Coupling Experiment. Part II: Analysis. *Journal of Hydrometeorology* **7**(4): 611–625, doi:10.1175/JHM511.1.

Halder S, Dirmeyer PA. 2017. Relation of eurasian snow cover and indian summer monsoon rainfall: Importance of the delayed hydrological effect. *Journal of Climate* **30**(4): 1273–1289, doi:10.1175/JCLI-D-16-0033.1.

Hall A, Qu X. 2006. Using the current seasonal cycle to constrain snow albedo feedback in future climate change. *Geophysical Research Letters* **33**(3): n/a–n/a, doi:10.1029/2005GL025127.

Hanssen-Bauer I, Førland EJ, Haddeland I, Hisdal H, Mayer S, Nesje A, Nilsen JEO, Sandven S, Sandø AB, Sorteberg A, Ådlandsvik B. 2015. Klima i Norge 2100. Kunnskapsgrunnlag for klimatilpasning. NCCS Report 2/2015. Technical report, Norwegian Centre for Climate Services, Oslo, Norway. (In Norwegian), pp 204.

Hartmann D, Klein Tank A, Rusticucci M, Alexander L, Brönnimann S, Charabi Y, Dentener F, Dlugokencky E, Easterling D, Kaplan A, Soden B, Thorne P, Wild M, Zhai P. 2013. *Observations: Atmosphere and surface*, book section 2. Cambridge University Press: Cambridge, United Kingdom and New York, NY, USA, ISBN ISBN 978-1-107-66182-0, p. 159–254, doi:10.1017/CBO9781107415324.008.

572 Hong SY, Dudhia J, Chen SH. 2004. A revised approach to ice microphysical processes for the bulk parameterization
573 of clouds and precipitation. *Monthly Weather Review* **132**(1): 103–120, doi:10.1175/1520-0493(2004)132<0103:
574 ARATIM>2.0.CO;2.

575 Iacono MJ, Delamere JS, Mlawer EJ, Shephard MW, Clough SA, Collins WD. 2008. Radiative forcing by long-lived
576 greenhouse gases: Calculations with the aer radiative transfer models. *Journal of Geophysical Research: Atmospheres*
577 **113**(D13): D13 103, doi:10.1029/2008JD009944.

578 Janjić ZI. 1994. The step-mountain eta coordinate model: Further developments of the convection, viscous sublayer,
579 and turbulence closure schemes. *Monthly Weather Review* **122**(5): 927–945, doi:10.1175/1520-0493(1994)122<0927:
580 TSMECM>2.0.CO;2.

581 Jørgensen P, Sørensen R, Prestvik O. 2013. *Norske jordarter*. Norsk jordforening. 104 pp. Retrieved on 27 March
582 2017 from `http://www.bioforsk.no/ikbViewer/Content/114780/Norske_jordarter.pdf`.

583 Kain JS. 2004. The kain–fritsch convective parameterization: An update. *Journal of Applied Meteorology* **43**(1):
584 170–181, doi:10.1175/1520-0450(2004)043<0170:TKCPAU>2.0.CO;2.

585 Koster RD, Dirmeyer PA, Guo Z, Bonan G, Chan E, Cox P, Gordon CT, Kanae S, Kowalczyk E, Lawrence D,
586 Liu P, Lu CH, Malyshev S, McAvaney B, Mitchell K, Mocko D, Oki T, Oleson K, Pitman A, Sud YC, Taylor
587 CM, Verseghy D, Vasic R, Xue Y, Yamada T. 2004. Regions of Strong Coupling Between Soil Moisture and
588 Precipitation. *Science* **305**(5687): 1138–1140, doi:10.1126/science.1100217.

589 Letcher TW, Minder JR. 2015. Characterization of the Simulated Regional Snow Albedo Feedback Using a Regional
590 Climate Model over Complex Terrain. *Journal of Climate* **28**: 7576–7595, doi:10.1175/JCLI-D-15-0166.1.

591 Lorenz R, Davin EL, Seneviratne SI. 2012. Modeling land-climate coupling in Europe: Impact of land surface
592 representation on climate variability and extremes. *Journal of Geophysical Research* **117**(D20): D20 109, doi:
593 10.1029/2012JD017755.

594 Lundquist D, Repp K. 1997. The1995 flood in southeastern Norway. Operational forecasting, warning and
595 monitoring of a 200-year flood. In: *Destructive Water: Water-Caused Natural Disasters, their Abatement and Control*,
596 Leavsley GH, Lins HF, Nobilis F, Parker RS, Schneider VS, Van de Ven FHM (eds), no. 239 in: IAHS publication,
597 IAHS Press, pp. 245–252. Proceedings of the Conference held at Anaheim, California, USA, June 1996.

598 Miralles DG, Teuling AJ, van Heerwaarden CC, Vila-Guerau de Arellano J. 2014. Mega-heatwave temperatures
599 due to combined soil desiccation and atmospheric heat accumulation. *Nature Geosci* **7**(5): 345–349. Letter.

600 Mooney PA, Mulligan FJ, Fealy R. 2013. Evaluation of the sensitivity of the weather research and forecasting model
601 to parameterization schemes for regional climates of europe over the period 1990–95. *Journal of Climate* **26**(3):
602 1002–1017, doi:10.1175/JCLI-D-11-00676.1.

603 Nilsen IB, Stagge JH, Tallaksen LM. 2017. A probabilistic approach for attributing temperature changes to synoptic
604 type frequency. *International Journal of Climatology* **37**(6): 2990–3002, doi:10.1002/joc.4894.

605 Niu GY, Yang ZL, Mitchell KE, Chen F, Ek MB, Barlage M, Kumar A, Manning K, Niyogi D, Rosero E, Tewari M,
606 Xia Y. 2011. The community Noah land surface model with multiparameterization options (Noah-MP): 1. Model
607 description and evaluation with local-scale measurements. *Journal of Geophysical Research: Atmospheres* **116**(D12):
608 D12 109, doi:10.1029/2010JD015139.

609 Øverlie T. 2007. Vann i Jord. Technical Report Rapport 2007:22, Norwegian Water Resources and Energy Directorate,
610 Oslo, Norway. In Norwegian.

611 Peng S, Piao S, Ciais P, Friedlingstein P, Zhou L, Wang T. 2013. Change in snow phenology and its potential
612 feedback to temperature in the northern hemisphere over the last three decades. *Environmental Research Letters*
613 **8**(1): 014 008.

614 Quiring SM, Kluver DB. 2009. Relationship between winter/spring snowfall and summer precipitation in the
615 northern great plains of north america. *Journal of Hydrometeorology* **10**(5): 1203–1217, doi:10.1175/2009JHM1089.1.

Rizzi J, Nilsen IB, Stagge JH, Gisnås K, Tallaksen LM. 2017. Five decades of warming: impacts on snow cover in Norway. (Submitted to Hydrology Research).

Rowell DP, Jones RG. 2006. Causes and uncertainty of future summer drying over europe. *Climate Dynamics* **27**(2): 281–299, doi:10.1007/s00382-006-0125-9.

Saini R, Wang G, Pal JS. 2016. Role of Soil Moisture Feedback in the Development of Extreme Summer Drought and Flood in the United States. *Journal of Hydrometeorology* **17**(8): 2191–2207, doi:10.1175/JHM-D-15-0168.1.

Seneviratne SI, Corti T, Davin EL, Hirschi M, Jaeger EB, Lehner I, Orlowsky B, Teuling AJ. 2010. Investigating soil moisture - climate interactions in a changing climate: A review. *Earth-Science Reviews* **99**(3-4): 125–161, doi:10.1016/j.earscirev.2010.02.004.

Seneviratne SI, Luthi D, Litschi M, Schar C. 2006. Land-atmosphere coupling and climate change in europe. *Nature* **443**(7108): 205–209, doi:10.1038/nature05095.

Skamarock WC, Klemp JB. 2008. A time-split nonhydrostatic atmospheric model for weather research and forecasting applications. *Journal of Computational Physics* **227**(7): 3465 – 3485, doi:10.1016/j.jcp.2007.01.037. Predicting weather, climate and extreme events.

Stahl K, Tallaksen LM, Hannaford J, van Lanen HAJ. 2012. Filling the white space on maps of European runoff trends: estimates from a multi-model ensemble. *Hydrology and Earth System Sciences* **16**(7): 2035–2047, doi:10.5194/hess-16-2035-2012.

Stéfanon M, Drobinski P, D'Andrea F, Lebeaupin-Brossier C, Bastin S. 2014. Soil moisture-temperature feedbacks at meso-scale during summer heat waves over western europe. *Climate Dynamics* **42**(5): 1309–1324, doi:10.1007/s00382-013-1794-9.

Thackeray CW, Fletcher CG. 2016. Snow albedo feedback: Current knowledge, importance, outstanding issues and future directions. *Progress in Physical Geography* **40**(3): 392–408, doi:10.1177/0309133315620999.

Tveito OE, Bjørdal I, Skjelvåg AO, Aune B. 2005. A GIS-based agro-ecological decision system based on gridded climatology. *Meteorological Applications* **12**(1): 57–68, doi:10.1017/S1350482705001490.

Uhe P, Otto FEL, Haustein K, van Oldenborgh GJ, King AD, Wallom DCH, Allen MR, Cullen H. 2016. Comparison of methods: Attributing the 2014 record european temperatures to human influences. *Geophysical Research Letters* **43**(16): 8685–8693, doi:10.1002/2016GL069568. 2016GL069568.

Vaughan D, Comiso J, Allison I, Carrasco J, Kaser G, Kwok R, Mote P, Murray T, Paul F, Ren J, Rignot E, Solomina O, Steffen K, Zhang T. 2013. *Observations: Cryosphere*, book section 4. Cambridge University Press: Cambridge, United Kingdom and New York, NY, USA, ISBN ISBN 978-1-107-66182-0, p. 317–382, doi:10.1017/CBO9781107415324.012.

Walsh JE, Ross B. 1988. Sensitivity of 30-day dynamical forecasts to continental snow cover. *Journal of Climate* **1**(7): 739–754, doi:10.1175/1520-0442(1988)001<0739:SODDFT>2.0.CO;2.

Wang T. 2016. Groset forsøksfelt (016.H5) Grunnvanns- og markvannsundersøkelser – Tilstandsoversikt 2014–2015. Technical Report Oppdragsrapport 2016:2, Norwegian Water Resources and Energy Directorate, Oslo, Norway. In Norwegian.

Wetherald RT, Manabe S. 1995. The mechanisms of summer dryness induced by greenhouse warming. *Journal of Climate* **8**(12): 3096–3108, doi:10.1175/1520-0442(1995)008<3096:TMOSDI>2.0.CO;2.

Wielgolaski FE. 1978. *Planter og omgivelser*. Universitetsforlaget: Tromsø, Norway. In Norwegian, available online from `http://www.nb.no/nbsok/nb/ada4f5fb0896a22b1043f230a44f3973?lang=no#0`.

Wilcoxon F. 1945. Individual comparisons by ranking methods. *Biometrics Bulletin* **1**(6): 80–83, doi:10.2307/3001968.

Wilson D, Hisdal H, Lawrence D. 2010. Has streamflow changed in the Nordic countries? - Recent trends and comparisons to hydrological projections. *Journal of Hydrology* **394**(3-4): 334–346, doi:10.1016/j.jhydrol.2010.09.010.

Xu L, Dirmeyer P. 2013. Snow–Atmosphere Coupling Strength. Part II: Albedo Effect Versus Hydrological Effect. *Journal of Hydrometeorology* **14**(2): 404–418, doi:10.1175/JHM-D-11-0103.1.

Yang ZL, Niu GY, Mitchell KE, Chen F, Ek MB, Barlage M, Longuevergne L, Manning K, Niyogi D, Tewari M, Xia Y. 2011. The community noah land surface model with multiparameterization options (noah-mp): 2. evaluation over global river basins. *Journal of Geophysical Research: Atmospheres* **116**(D12): D12 110, doi:10.1029/2010JD015140.

Zampieri M, D'Andrea F, Vautard R, Ciais P, de Noblet-Ducoudré N, Yiou P. 2009. Hot European Summers and the Role of Soil Moisture in the Propagation of Mediterranean Drought. *J. Climate* **22**(18): 4747–4758, doi:10.1175/2009jcli2568.1.

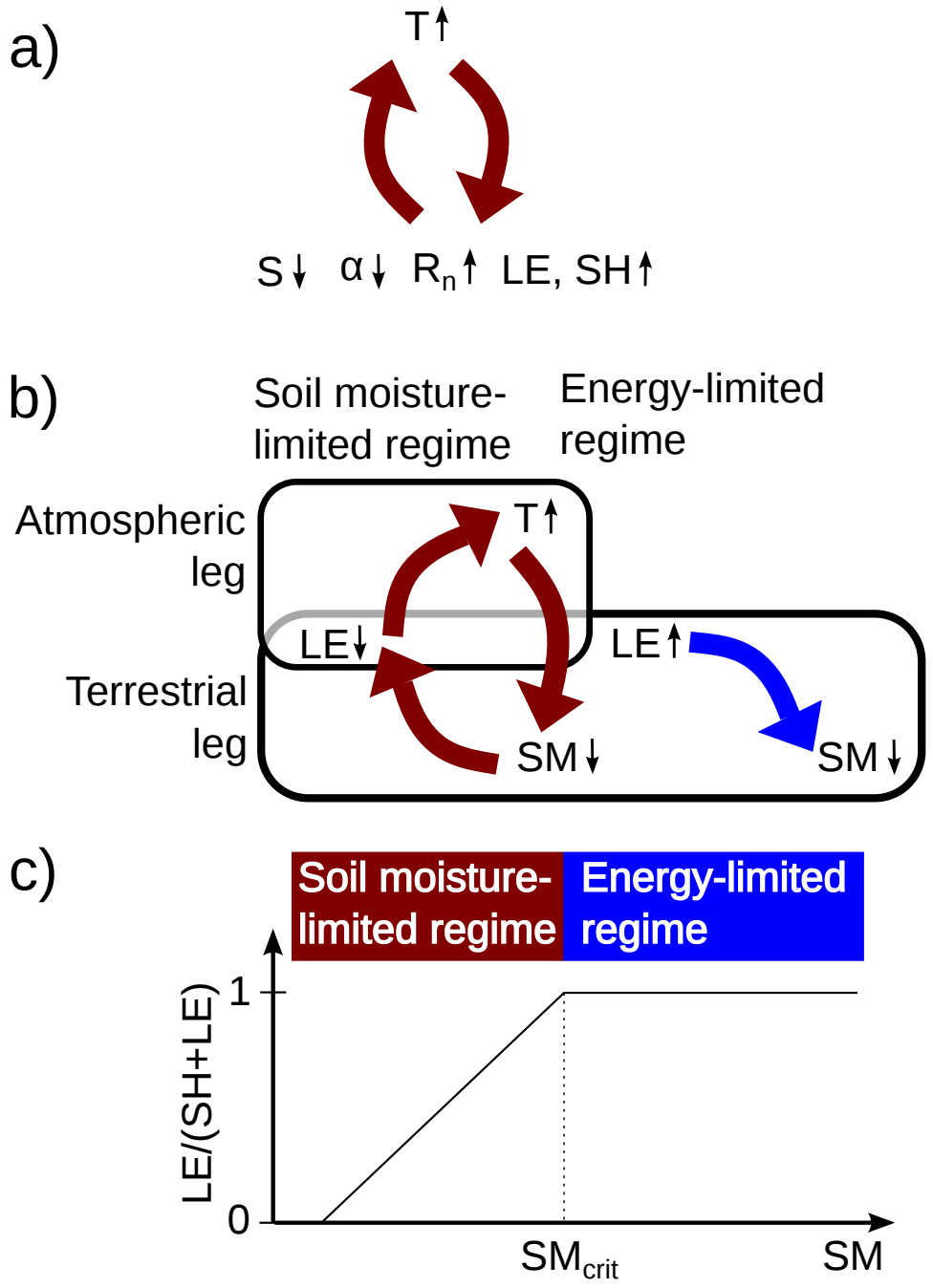

Figure 1: *a) The snow albedo feedback. An initial warming leads to reduced snow cover, S, and reduced albedo, α, that allows more shortwave radiation to be absorbed in the ground. The result is an increase in the net radiation, R_n, that leaves more energy available for latent heat, LE and sensible heat, SH, ultimately increasing the air temperature, T. b) Soil moisture–temperature coupling. In energy-limited regimes, the soil moisture, SM, does not control the latent heat, rather, when the latent heat increases, it depletes the soil moisture storage. An initial warming that reduces the soil moisture below a critical value, SM_{crit}, shifts the regime into a soil moisture-limited regime. Here, the soil moisture limits latent heat (positive correlation; the terrestrial leg), and the warming is enhanced by the reduced evaporative cooling (negative correlation; the atmospheric leg). c) Schematic illustration of the Budyko framework. Above SM_{crit}, latent heat is not limited by the soil moisture. Below SM_{crit}, latent heat becomes limited by soil moisture, protentially triggering a soil moisture–temperature feedback.*

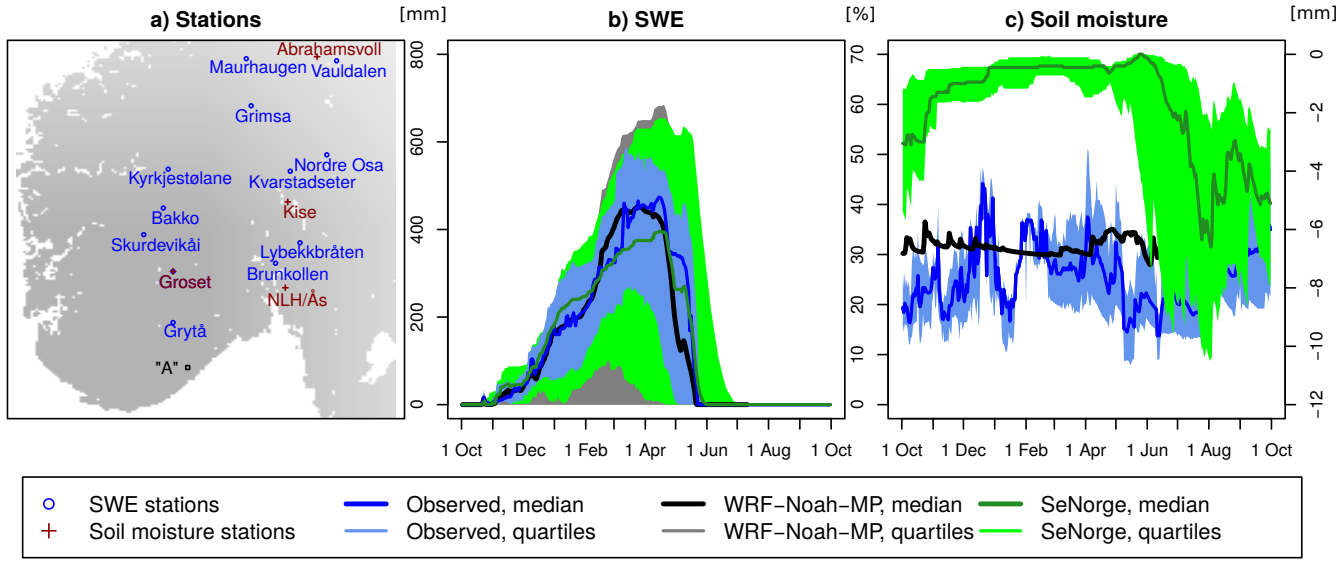

Figure 2: *a) SWE stations in blue, soil moisture stations in brown, and grid cell "A" in black. b) Variability across SWE stations for observations (blue), WRF model runs (black), and SeNorge (green). The bold lines show the median, and the shading shows the 25th to 75th percentile range. The variability of SWE is calculated for observations at the 12 SWE stations (note that Groset is both a SWE and soil moisture station), and for SeNorge and WRF–Noah-MP, grid cells closest to the observations stations. c) Variability of soil moisture content (in %; left axis) for observations and WRF–Noah-MP, and soil moisture deficit (in mm; right axis) for SeNorge. The variability is calculated for four soil moisture stations and grid cells closest to the observations stations (for SeNorge and WRF–Noah-MP).*

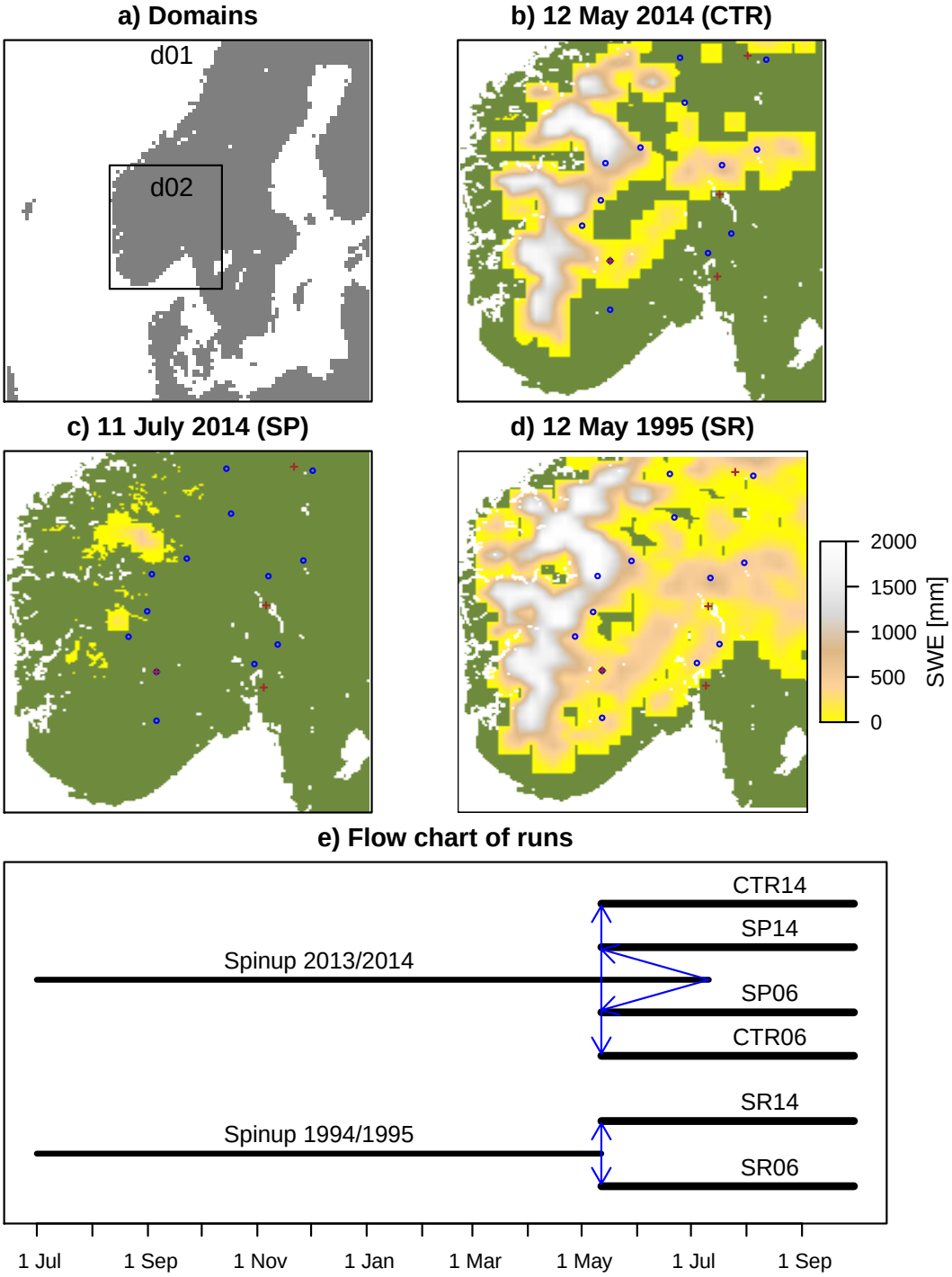

Figure 3: *a) Model domains, b–d) initial SWE at the start of the model run at b) 12 May 2014 (CTR), c) 11 July 2014 (snow-poor; SP, two months earlier melting), and d) 12 May 1995 (snow-rich; SR). e) Schematic of the different model runs. Note that in addition to SWE, we swapped snow depth, snow albedo, soil moisture, skin temperature, initial temperature, soil category fraction at the bottom and top, and an indicator function for snow.*

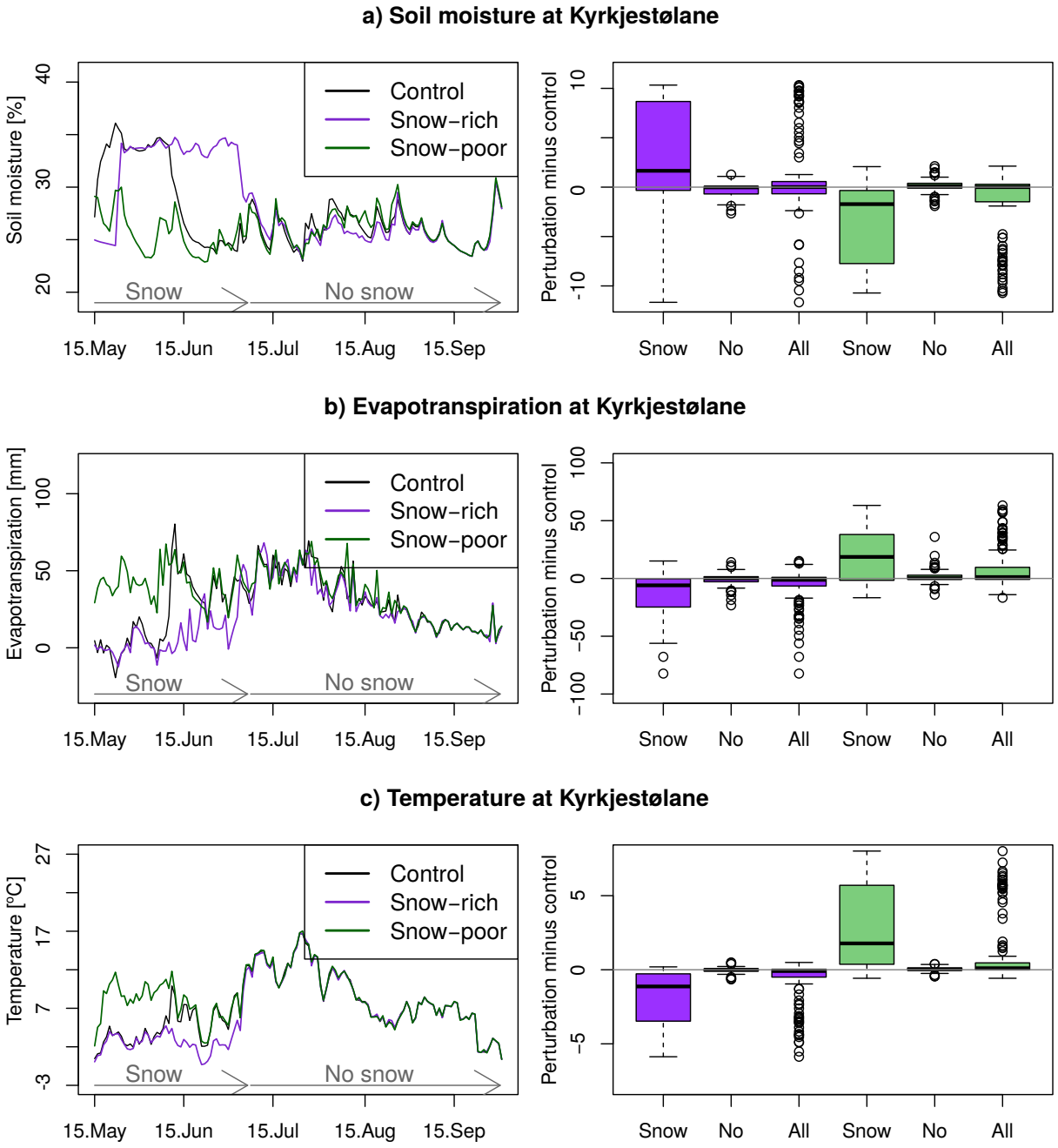

Figure 4: *Model results for the grid cell containing Kyrkjestølane, as time series (left) and boxplots (right), for a) soil moisture, b) evapotranspiration, and c) air temperature. Daily values are plotted throughout the summer (15 May–30 September, leaving out three days from the start of the run to let the atmosphere spin up). Boxplots show the temporal distribution of the variable for the snow-rich run minus the control (purple boxes), and for the snow-poor run minus the control (green boxes). Boxplots marked "Snow" (boxes 1 and 4) show the distribution of differences before SR_{14} became snow-free (4 July; see arrows in the time series), boxes marked "No" (boxes 2 and 5) show the distribution after SR_{14} became snow-free, and boxes marked "All" (boxes 3 and 6) show the distribution for the whole period.*

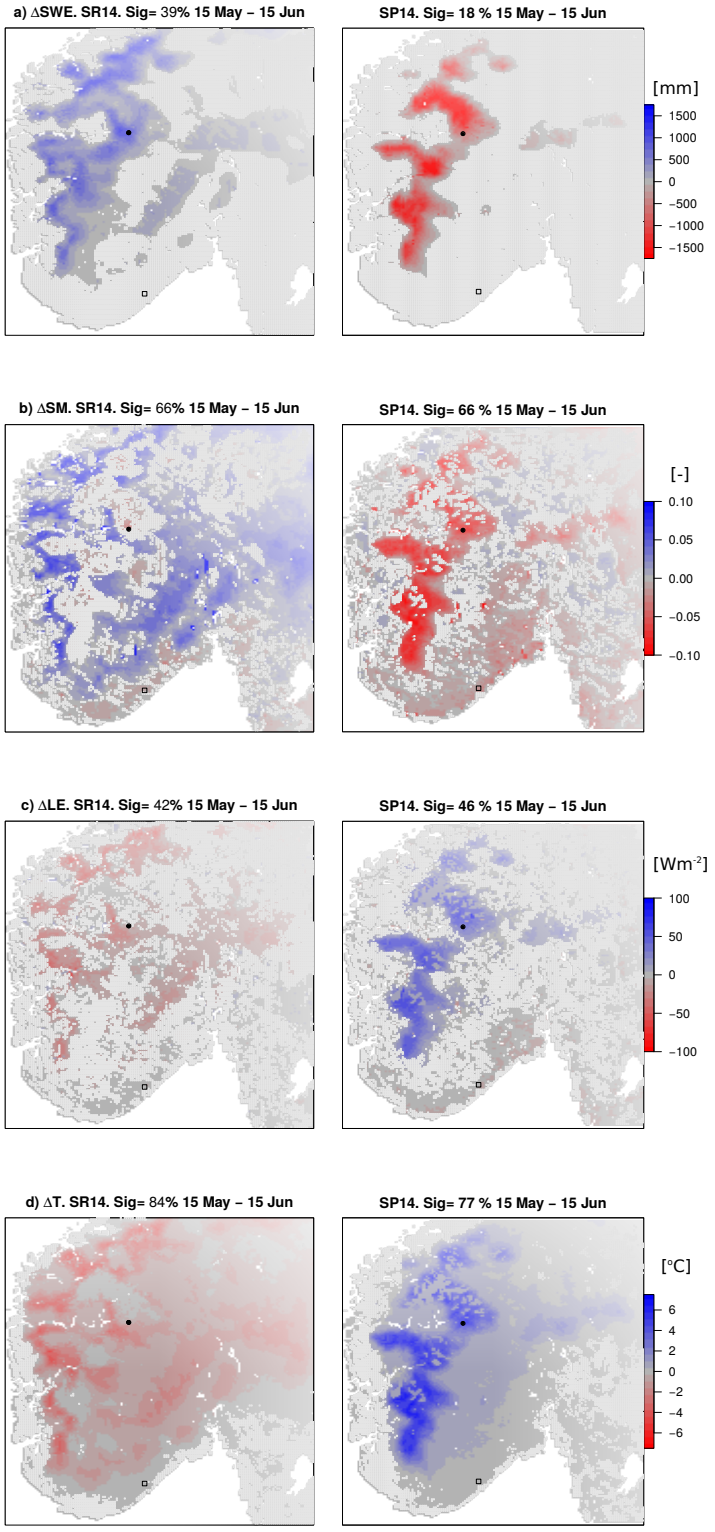

Figure 5: *Map of differences between model runs and control for a) SWE, b) soil moisture, c) latent heat, and d) air temperature for the first month of simulation. Column 1 shows the difference between the snow-rich run and control, $SR_{14} - CTR_{14}$; column 2 shows the difference between the snow-poor run and control, $SP_{14} - CTR_{14}$. A red (blue) color denotes a smaller (larger) value of the variable in the run than in the control. Significant differences between the run and the control, using the Wilcoxon signed rank test, are shown in color, whereas light gray grid cells are not significant. Two grid cells are marked on the plot, Kyrkjestølane (black dot), and grid cell "A" (open black square), for which grid cells the time series are shown in Figures 4 and 8, respectively. The number of significant grid cells is listed as a percentage for each panel.*

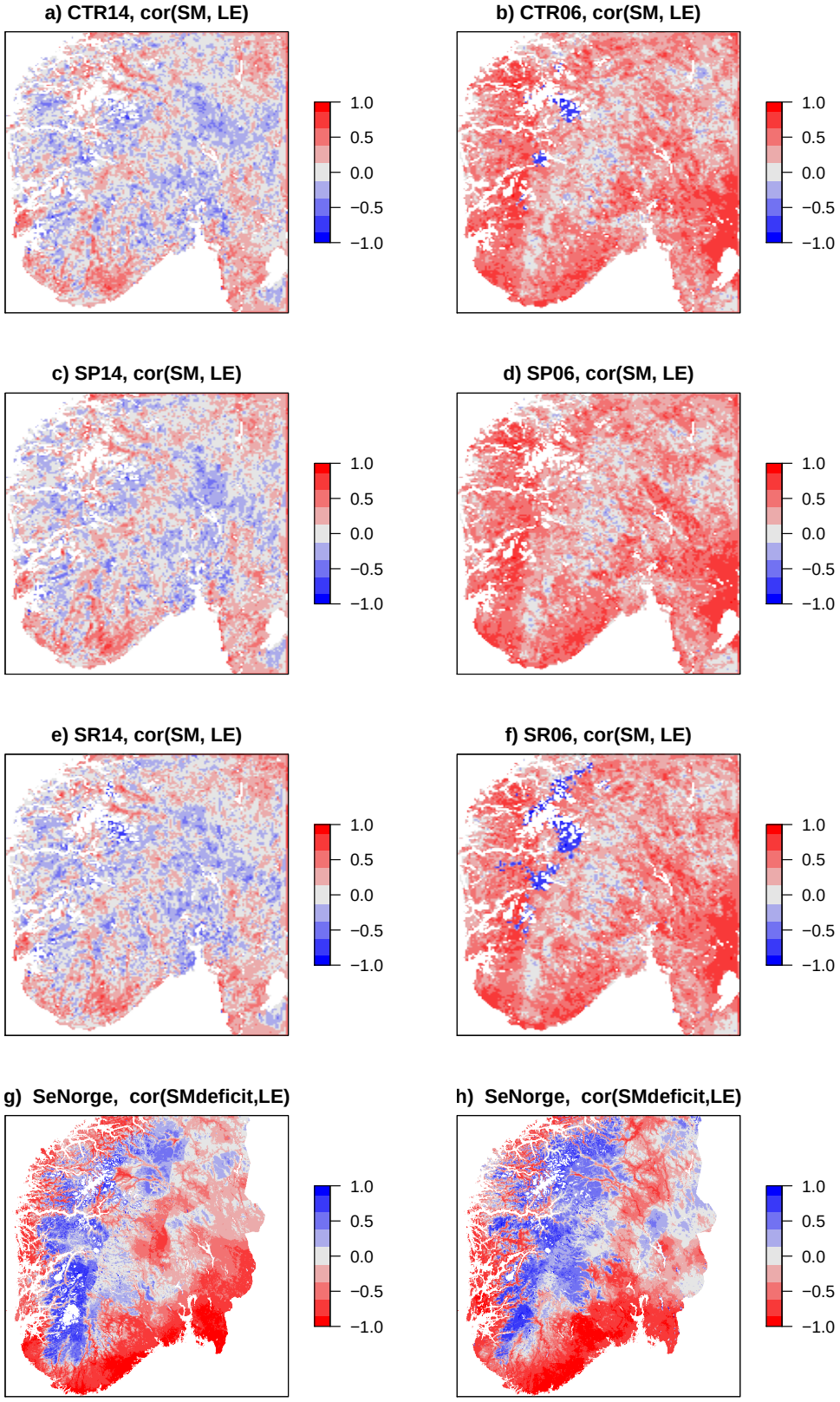

Figure 6: *Terrestrial leg of land–atmosphere coupling (positive correlation, ρ(SM,LE), indicates coupling) for the period 15 July–14 August 2014 (a, c, e, and g) and 2006 (b, d, f, and h). Rows 1–3 show CTR, SP and SR, respectively, from the WRF-Noah-MP runs. SeNorge is shown in the last row. Because SeNorge contains soil moisture deficits, and not volumetric water content, SeNorge correlations are the inverse of the correlations shown for WRF–Noah-MP results. A red color indicates coupling in all plots.*

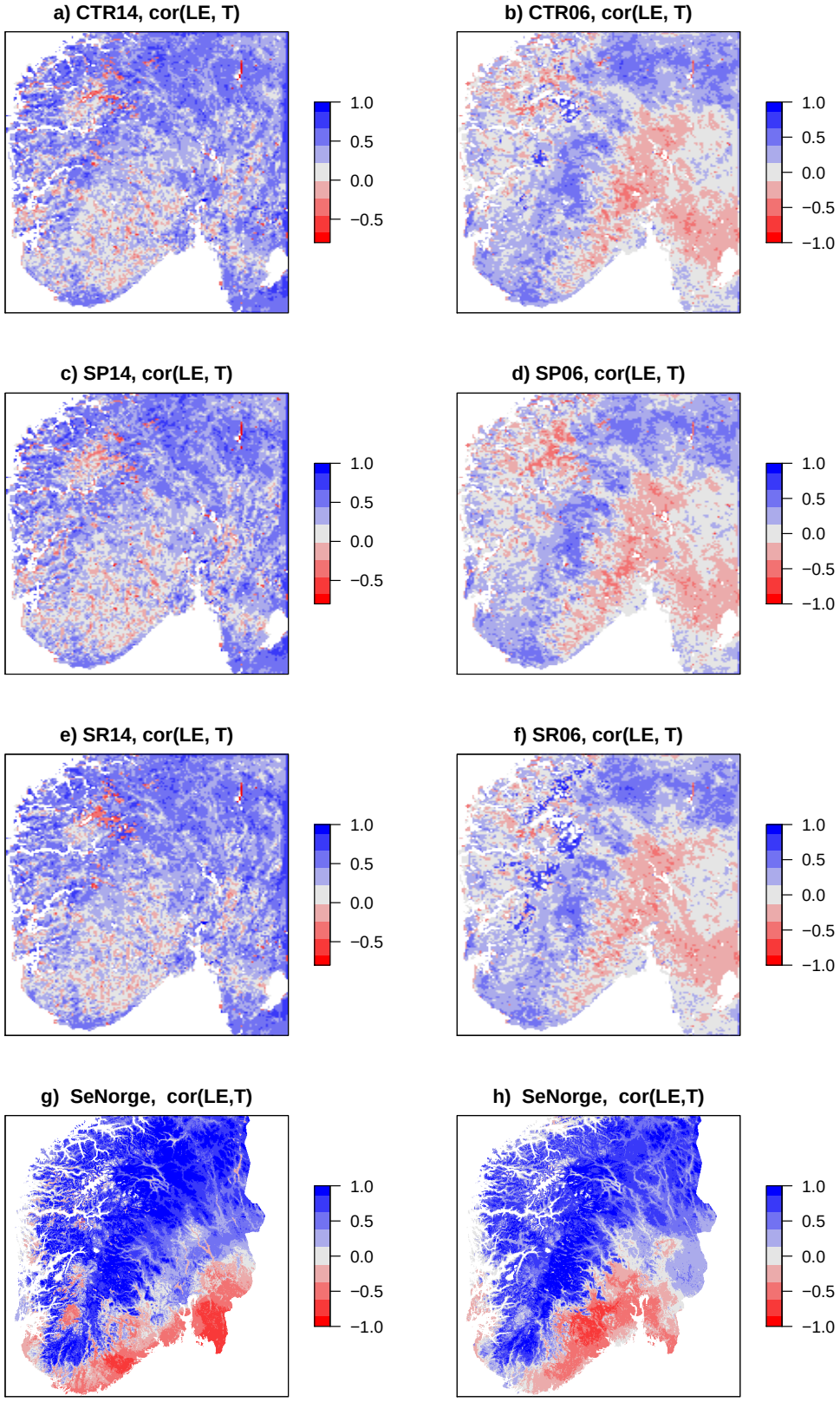

Figure 7: *Atmospheric leg of land–atmosphere coupling (negative correlation, ρ(LE,T), indicates coupling) for the period 15 July–14 August 2014 (left) and 2006 (right). Rows 1–3 show CTR, SP and SR, respectively, from the WRF-Noah-MP runs. SeNorge is shown in the last row. A red color indicates coupling in all plots.*

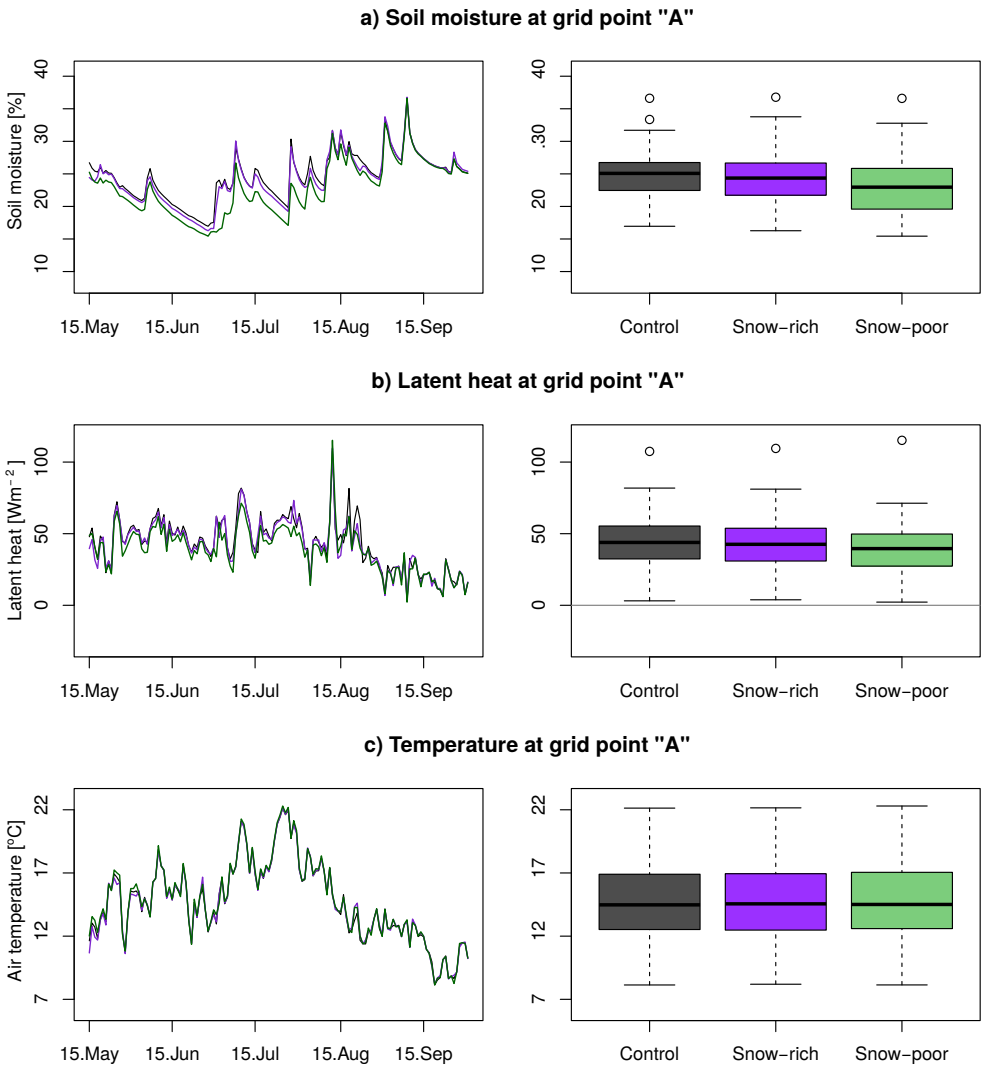

Figure 8: *Model results for the grid cell closest to grid cell "A" (left) and boxplots (right), for a) soil moisture, b) latent heat, and c) air temperature. Daily values are plotted throughout the summer, 15 May–30 September 2014, leaving out three days from the start of the run to let the atmosphere spin up. Boxplots show the temporal distribution of the variable for the control (black box), snow-rich run (purple box), and for the snow-poor run (green box) for the whole time period.*

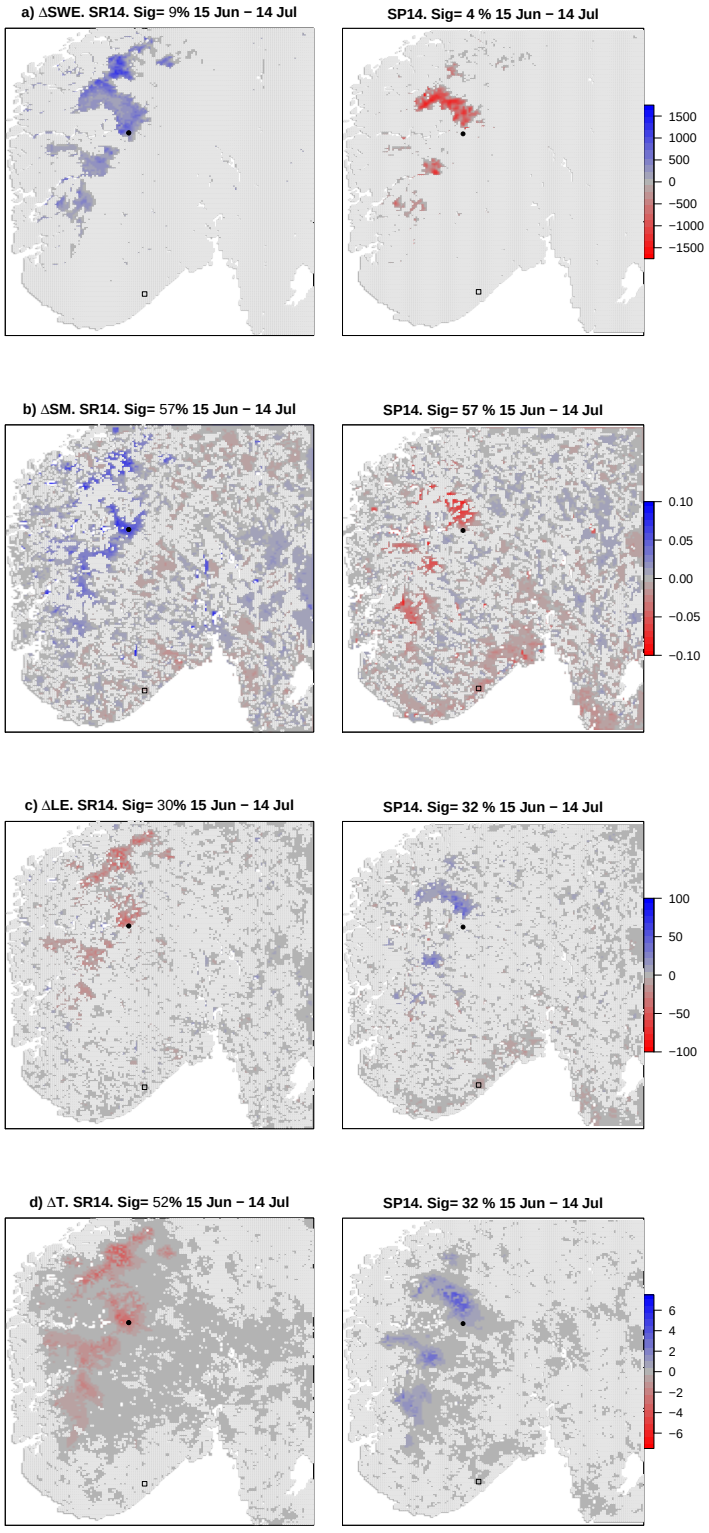

Figure S1: *Similar to Figure 5, but for month two of the simulations (15 June–14 July). This figure continues on the next page.*

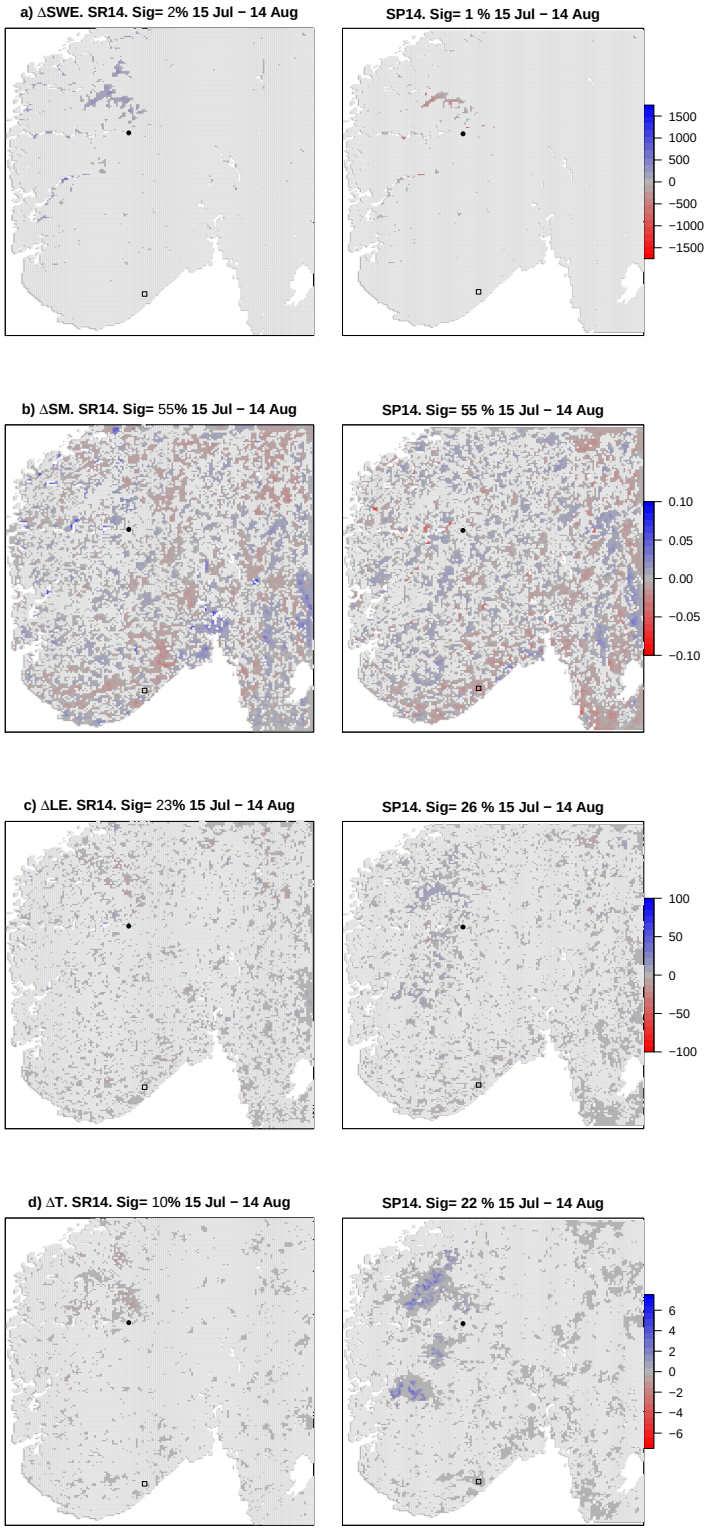

Figure S1: *(cont.) Similar to Figure 5, but for month three of the simulations (15 July–14 August). This figure continues on the next page.*

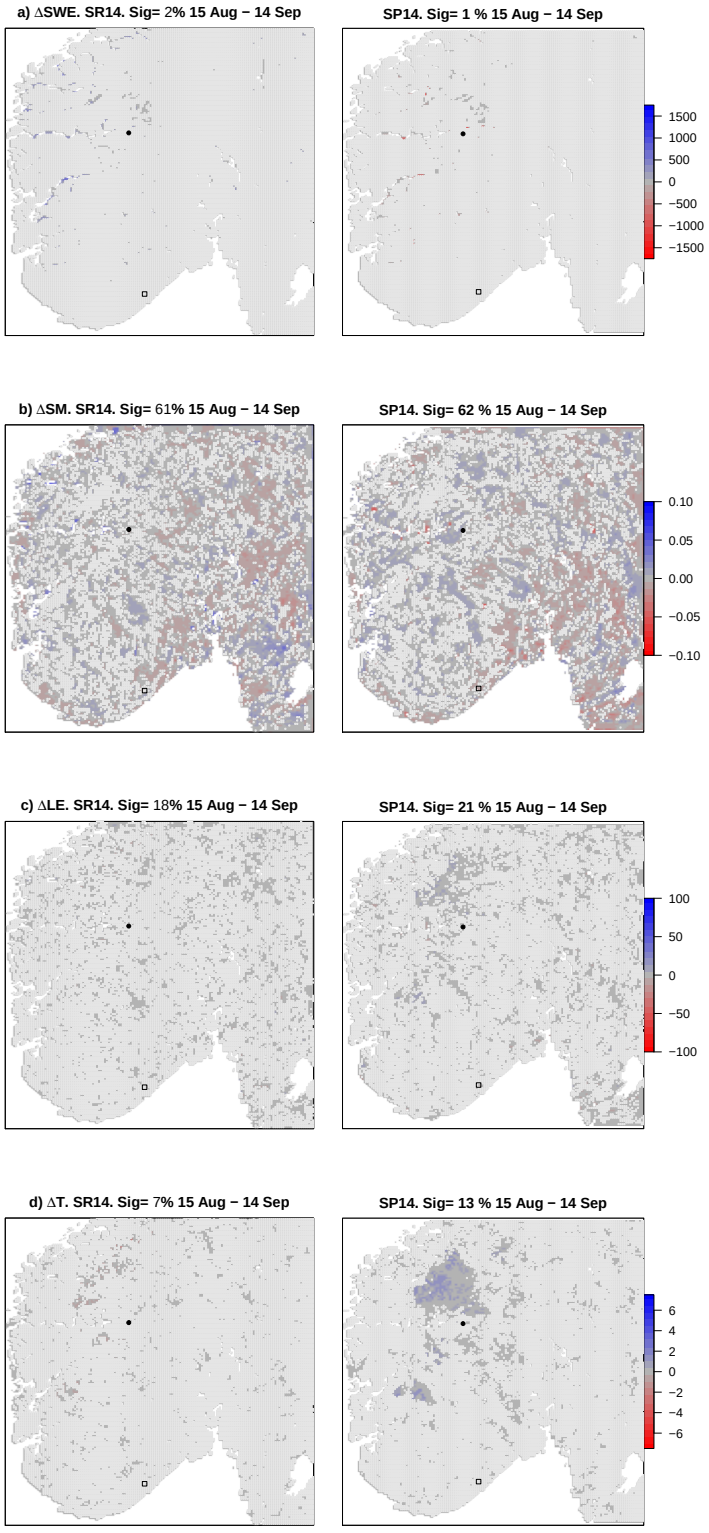

Figure S1: *(cont.) Similar to Figure 5, but for month four of the simulations (15 August–14 September).*

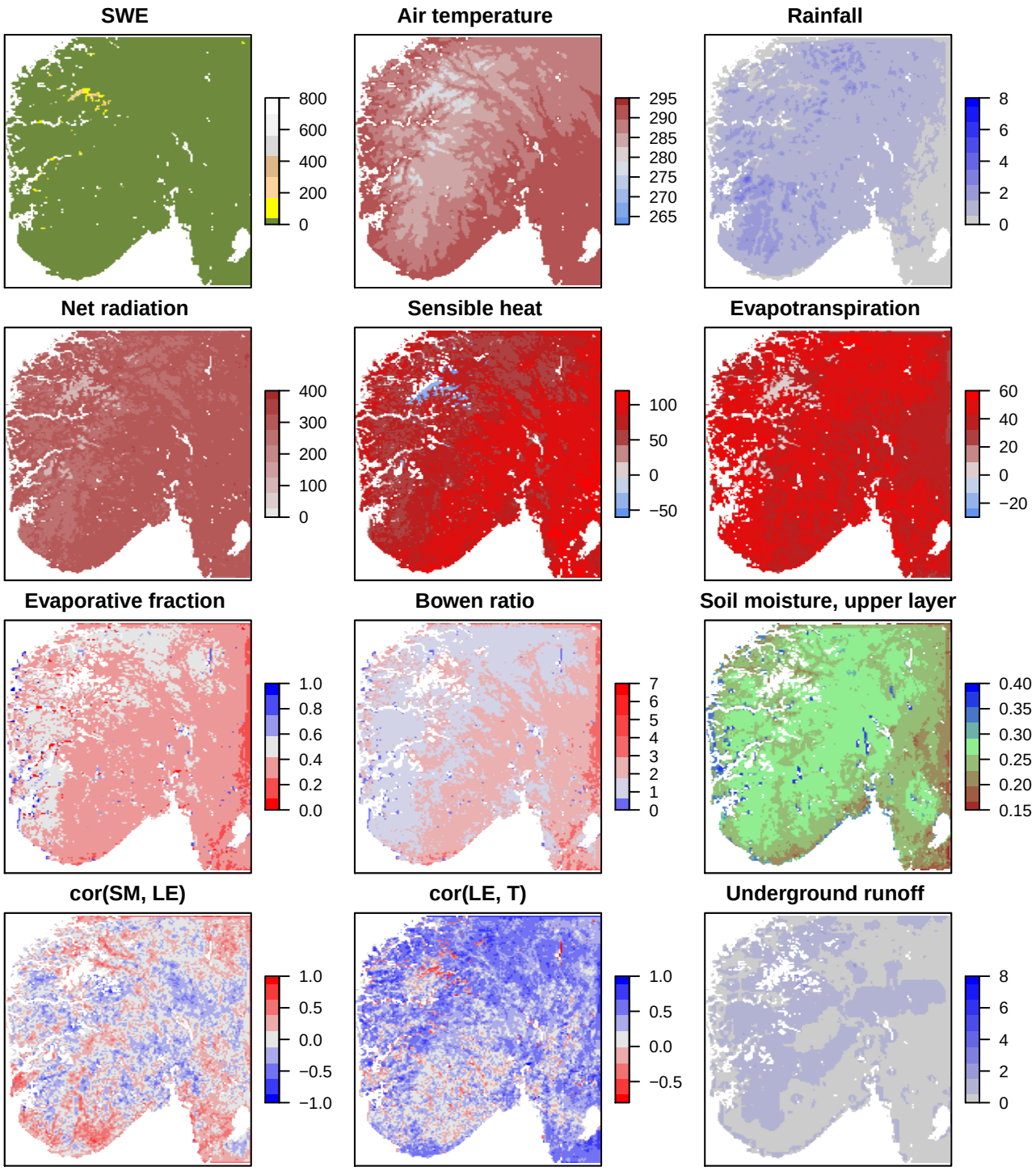

Figure S2: *Monthly average of different variables for 15 July–14 August, using 2014 forcing in the control run (CTR_{14}). cor(SM,LE) denotes the terrestrial leg of land–atmosphere coupling (positive correlation indicates coupling). cor(LE,T) denotes the atmospheric leg of land–atmosphere coupling (negative correlation indicates coupling). The Bowen ratio, B = SH/LE, and the evaporative fraction, EF = LE/(LE+SH), where SH is the sensible heat flux, and LE is the latent heat flux, quantifies the partitioning between sensible and latent heat fluxes.*

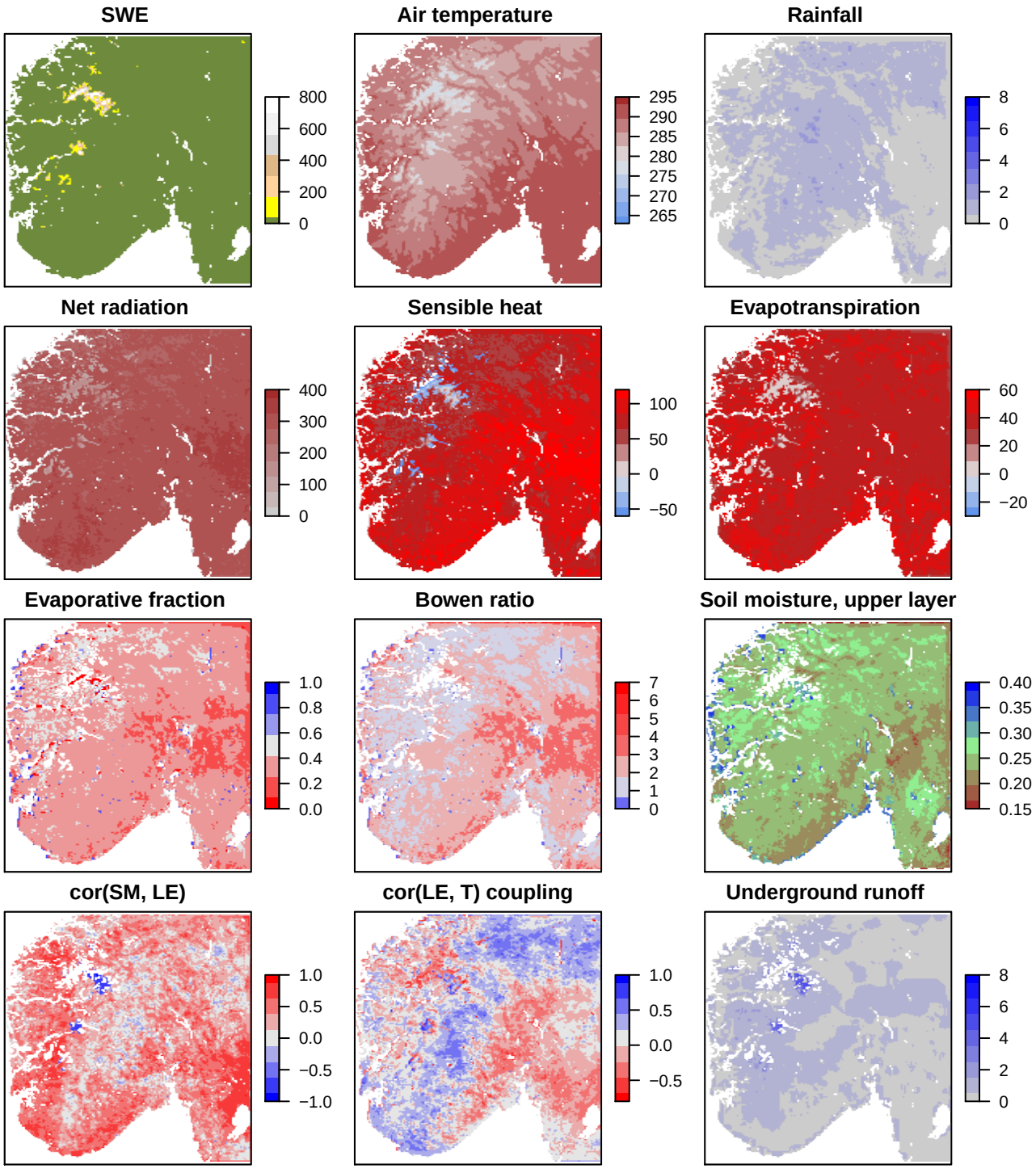

Figure S3: *Monthly average of different variables for 15 July–14 August, using 2006 forcing in the control run (CTR_{06}). cor(SM,LE) denotes the terrestrial leg of land–atmosphere coupling (positive correlation indicates coupling). cor(LE,T) denotes the atmospheric leg of land–atmosphere coupling (negative correlation indicates coupling).*

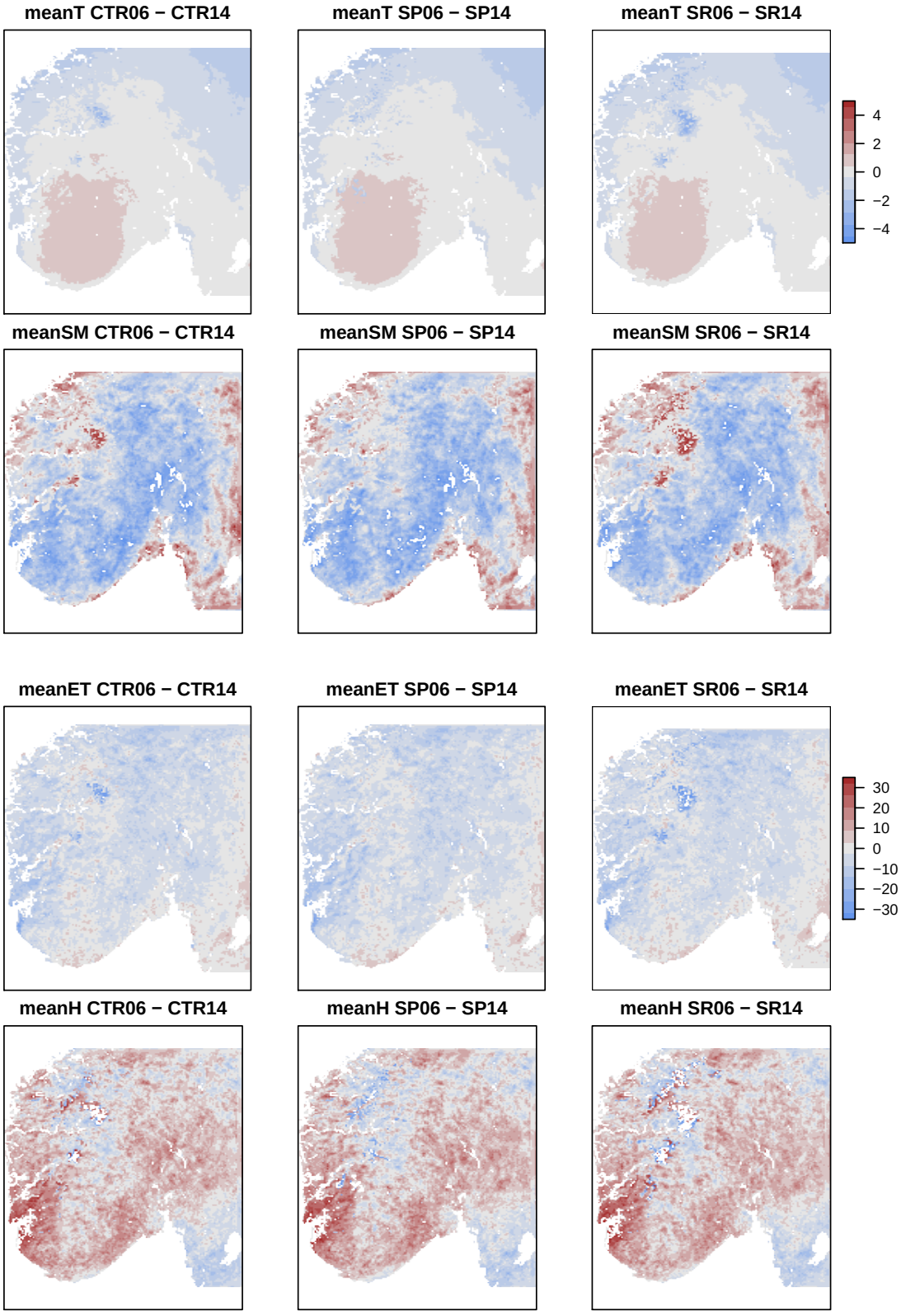

Figure S4: *Differences between model runs (2006 minus 2014), averaged over 15 July–14 August, for air temperature [in °C] (row 1), soil moisture [in %] (row 2, using the same legend as row 1), latent heat [in Wm^2] (row 3) and sensible heat [in Wm^2] (row 4, using the same legend as row 3).*

Appendix

Conference Presentations (oral)

Nilsen, I. B., Fleig, A., Tallaksen, L. M., Hisdal, H. (2013): Regional precipitation and temperature trend patterns in Europe. *94th annual symposium of the Norwegian Geophycisical Society*, 18 September 2013, Geilo, Norway.

Nilsen, I. B., Tallaksen, L. M., Stordal, F., Wiberg, D., van Vliet, M., Xu, C.-Y. (2014): Does NOAH-LSM perform well for extremes, regarding heat fluxes? *Final seminar, Young Scientists Summer Programme, IIASA*, 26 August 2014, International Institute for Applied Systems Analysis (IIASA), Laxenburg, Austria.

Nilsen, I. B., Tallaksen, L. M., Stordal, F., Wiberg, D., van Vliet, M., Xu, C.-Y. (2014): Landoverflatemodellering og varmeflukser under hydrologiske ekstremer (in Norwegian). *95th annual symposium of the Norwegian Geophycisical Society*, 18 September 2014, Oslo, Norway.

Nilsen, I. B., Tallaksen, L. M., Stordal, F., Wiberg, D., van Vliet, M., Xu, C.-Y. (2014): Does NOAH-LSM perform well for extremes, regarding heat fluxes? *PhD conference*, 29–30 September 2014, Bergen, Norway.

Nilsen, I. B., Fleig, A., Tallaksen, L. M., Hisdal, H. (2014): Regional precipitation and temperature trend patterns in Europe. *FRIEND-Water2014: 7th Global FRIEND-Water Conference Hydrology in a Changing World: Environmental and Human Dimensions* 7–10 October 2014, Montpellier, France.

Nilsen, I. B., Stagge, J. H., Tallaksen, L. M. (2015): A Probabilistic approach to attribute warming to changes in atmospheric circulation. *3rd Conference on Modelling Hydrology, Climate and Land Surface Processes*, 7–9 September 2015, Lillehammer, Norway.

Nilsen, I. B., Stagge, J. H., Tallaksen, L. M. (2016): A Probabilistic approach to attribute temperature changes to changes in synoptic types. *European Geosciences Union (EGU) General Assembly 2016*, 17–22 April 2016, Vienna, Austria.

Nilsen, I. B., Erlandsen, H. B., Stordal, F., Xu, C.-Y. and Tallaksen, L. M. (2017): Diagnosing land–atmosphere coupling in a seasonally snow-covered region (South Norway). *4th Conference on Modelling Hydrology, Climate and Land Surface Processes*, 12–14 September 2017, Lillehammer, Norway.

Conference Posters

Nilsen, I. B., Stagge, J. H., Tallaksen, L. M. (2014): Temperature changes in Norway: Recent increases in WFDEI validated against interpolated observations. *European Geosciences Union (EGU) General Assembly 2014*, 27 April–2 May 2014, Vienna, Austria.

Nilsen, I. B., Stagge, J. H., Tallaksen, L. M. (2015): A Probabilistic method of calculating circulation-induced trends. *European Geosciences Union (EGU) General Assembly 2016*, 12–17 April 2015, Vienna, Austria.

Nilsen, I. B., Stagge, J. H., Tallaksen, L. M. (2015): A Probabilistic method of calculating circulation-induced trends. *LATICE seminar*, 9–10 March 2016, Sundvolden, Norway.

Nilsen, I. B., Erlandsen, H. B., Stordal, F., Xu, C.-Y. and Tallaksen, L. M. (2017): Detecting land–atmosphere feedbacks in a seasonally snow-covered region (South Norway). *LATICE seminar*, 15–16 March 2017, Sundvolden, Norway.

Nilsen, I. B., Erlandsen, H. B., Stordal, F., Xu, C.-Y. and Tallaksen, L. M. (2017): Detecting land–atmosphere feedbacks in a seasonally snow-covered region (South Norway). *European Geosciences Union (EGU) General Assembly 2017*, 23–28 April 2017, Vienna, Austria.